ERDC/CHL TR-11-10

Coastal and Hydraulics Laboratory

US Army Corps of Engineers®
Engineer Research and Development Center

Verification and Validation of the Coastal Modeling System

Report 4, CMS-Flow: Sediment Transport and Morphology Change

Alejandro Sánchez, Weiming Wu, Tanya Marie Beck,
Honghai Li, Julie Dean Rosati, Zeki Demirbilek,
and Mitchell Brown

December 2011

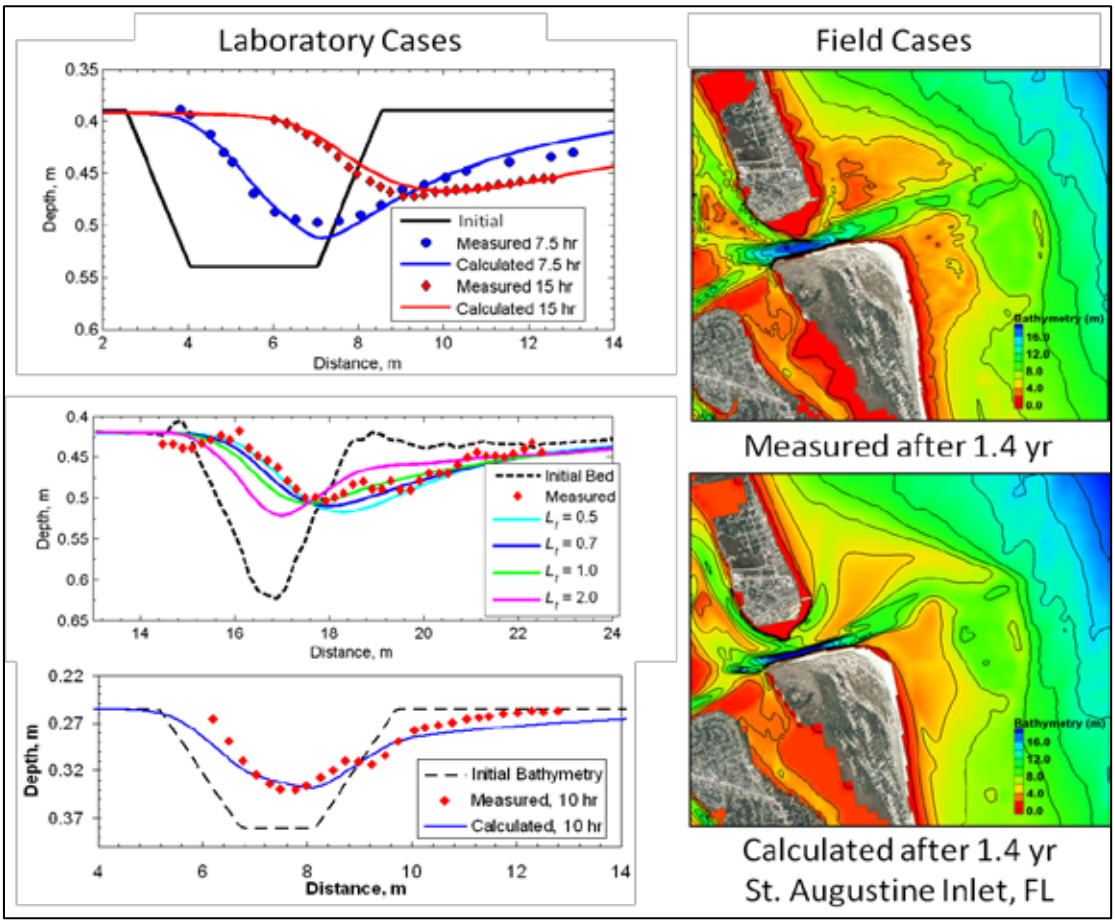

ERDC/CHL TR-11-10
December 2011

Verification and Validation of the Coastal Modeling System

Report 4, CMS-Flow: Sediment Transport and Morphology Change

Alejandro Sánchez, Weiming Wu, Tanya Marie Beck, Honghai Li, Julie Dean Rosati, Zeki Demirbilek, and Mitchell Brown

Coastal and Hydraulics Laboratory,
U.S. Army Engineer Research and Development Center
3909 Halls Ferry Road,
Vicksburg, MS 39180-6199

Report 4 of a series

Abstract: This is the fourth report in the series of four reports, toward the Verification and Validation (V&V) of the Coastal Modeling System (CMS). This report contains details of a V&V study conducted to assess skills of the CMS sediment transport and morphology change for a wide range of problems encountered in coastal applications. The emphasis is on coastal inlets, navigation channels, and adjacent beaches. This evaluation study began by considering simple idealized test cases for checking basic physics and computational algorithms implemented in the model. After these initial fundamental tests, the model was evaluated with several laboratory and field test cases. This report provides description of each test case, model setup, boundary conditions used in different numerical simulations, and assessment of modeling results. The report also includes major findings and guidance for users on how to setup and calibrate the model for practical applications of CMS.

Contents

Figures and Tables

Figures

Tables

Preface

This study was performed by the Coastal Inlets Research Program (CIRP), funded by Headquarters, U.S. Army Corps of Engineers (HQUSACE). The CIRP is administered for Headquarters by the U.S. Army Engineer Research and Development Center (ERDC), Coastal and Hydraulics Laboratory (CHL), Vicksburg, MS, under the Navigation Program of the U.S. Army Corps of Engineers. James E. Walker is HQUSACE Navigation Business Line Manager overseeing CIRP. Jeff Lillycrop, CHL, is the ERDC Technical Director for Navigation. Dr. Julie Rosati, CHL, is the CIRP Program Manager.

CIRP conducts applied research to improve USACE capabilities to manage federally maintained inlets and navigation channels, which are present on all coasts of the United States, including the Atlantic Ocean, Gulf of Mexico, Pacific Ocean, Great Lakes, and U.S. territories. The objectives of CIRP are to advance knowledge and provide quantitative predictive tools to (a) support management of federal coastal inlet navigation projects to facilitate more effective design, maintenance, and operation of channels and jetties, more effective and reduce the cost of dredging, and (b) preserve the adjacent beaches and estuary in a system approach that treats the inlet, beaches, and estuary as sediment-sharing components. To achieve these objectives, CIRP is organized in work units conducting research and development in hydrodynamics, sediment transport and morphology change modeling, navigation channels and adjacent beaches, navigation channels and estuaries, inlet structures and scour, laboratory and field investigations, and technology transfer.

For the mission-specific requirements, CIRP has developed a finite-volume model based on nonlinear shallow water flow equations, CMS-Flow, specifically for inlets, navigation, and nearshore project applications. The governing equations are solved using both explicit and implicit schemes in a finite-volume method on rectangular grids of variable cell sizes (e.g., telescoping grids). The model is part of the Coastal Modeling System (CMS) suite of models intended to simulate nearshore waves, flow, sediment transport, and morphology change affecting planning, design, maintenance, and reliability of federal navigation projects. In this assessment, verification and validation of CMS-Flow sediment transport are performed to determine

capability and versatility of model for Corps projects. The validation of CMS-Flow is performed using real data collected from field and laboratory to determine the reliability of sediment transport and morphology change calculations.

Unless otherwise noted, the following are associated with ERDC-CHL, Vicksburg, MS. This report was prepared by Alejandro Sánchez and Dr. Zeki Demirbilek, Harbors Entrances and Structures Branch; Tanya M. Beck, Dr. Honghai Li, and Mitchell Brown, Coastal Engineering Branch; Dr. Julie D. Rosati, Coastal Processes Branch; and Dr. Weiming Wu, The University of Mississippi. The work described in the report was performed under the general administrative supervision of Dr. Jackie Pettway, Chief of Harbors Entrances and Structures Branch; Dr. Jeffrey Waters, Chief of Coastal Engineering Branch; Dr. Ty V. Wamsley, Chief of Coastal Processes Branch; Dr. Rose M. Kress, Chief of Navigation Division; and Bruce A. Ebersole, Chief of Flood Damage Reduction Division. Dr. Earl Hayter and Mark Gravens reviewed the report, and Donnie F. Chandler, ERDC Editor, ITL, reviewed and edited the report. José Sánchez and Dr. William D. Martin were respectively Deputy Director and Director of CHL during the study and preparation of the report.

COL Kevin J. Wilson was ERDC Commander. Dr. Jeffery P. Holland was ERDC Director.

Unit Conversion Factors

Multiply	By	To Obtain
cubic yards	0.7645549	cubic meters
degrees (angle)	0.01745329	radians
feet	0.3048	meters
knots	0.5144444	meters per second
miles (nautical)	1,852	meters
miles (U.S. statute)	1,609.347	meters
miles per hour	0.44704	meters per second
pounds (force)	4.448222	newtons
pounds (force) per foot	14.59390	newtons per meter
pounds (force) per square foot	47.88026	pascals
square feet	0.09290304	square meters
square miles	2.589998 E+06	square meters
tons (force)	8,896.443	newtons
tons (force) per square foot	95.76052	kilopascals
yards	0.9144	meters

1 Introduction

1.1 Overview

The Coastal Modeling System (CMS) is an integrated numerical modeling system for simulating nearshore waves, currents, water levels, sediment transport, and morphology change (Militello et al. 2004; Buttolph et al. 2006; Lin et al. 2008; Reed et al. 2011). The system is designed for coastal inlets and navigation applications including channel performance and sediment exchange between inlets and adjacent beaches. Modeling provides planners and engineers with essential information for improving the usage of USACE Operation and Maintenance Funds. The Coastal Inlets Research Program (CIRP) is developing, testing, improving, and transferring the CMS to Corps Districts and industry, and assisting users in engineering studies. The overall framework of the CMS and its components are presented in Figure 1.

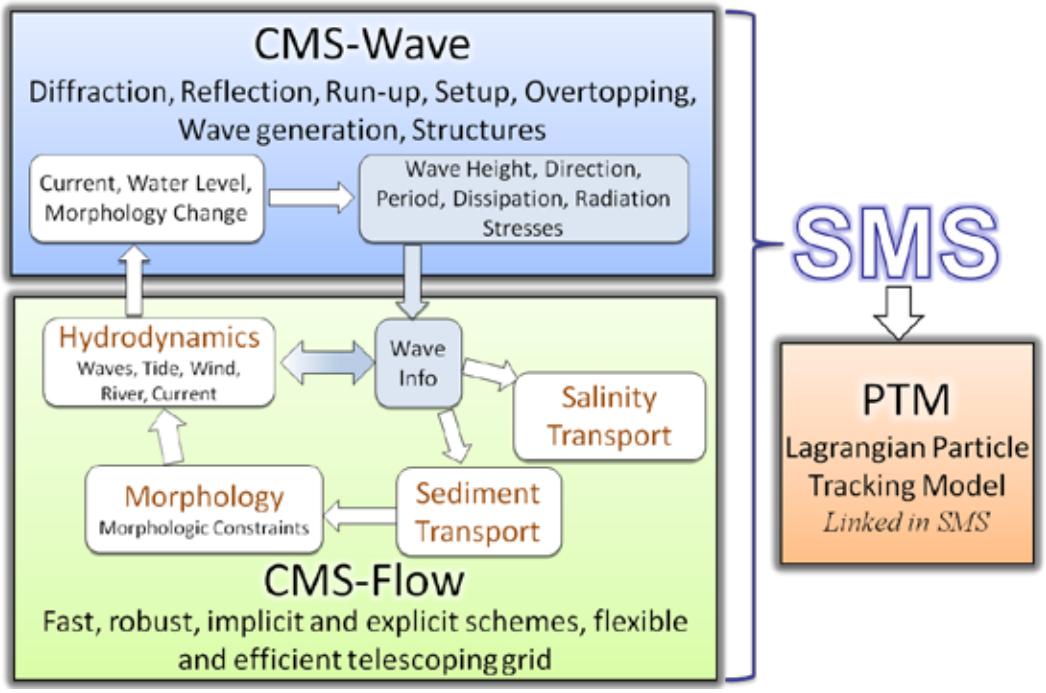

Figure 1. Coastal Modeling System framework and its components.

CMS-Flow is a two-dimensional (2-D), depth-averaged nearshore circulation, salinity, sediment transport, and morphology change model. CMS-Flow calculates depth-averaged currents and water levels, and includes physical processes such as advection, turbulent mixing, combined

wave-current bottom friction, wind, wave, river, tidal forcing, Coriolis force, and the influence of coastal structures (Buttolph et al. 2006; Sánchez and Wu 2011a). CMS-Wave is a spectral wave transformation model. It solves the wave-action balance equation using a forward marching Finite Difference Method (Mase et al. 2005; Lin et al. 2008). The model includes physical processes such as wave shoaling, refraction, diffraction, reflection, wave-current and wave-wave interaction, wave breaking, whitecapping, wind wave generation, and coastal structures. The CMS takes advantage of the Surface-water Modeling System (SMS) interface (Zundel 2006) versions 8.2 through 11.1 for grid generation, model setup, plotting, and post-processing of modeling results. The SMS also provides a link between the CMS and the Langragian Particle Tracking Model (PTM) (MacDonald et al. 2006).

The CMS sediment transport model is designed for studying channel and jetty performance and alternatives, nearshore sediment placement, and coastal processes. Some examples of applications of the CMS sediment transport model are presented in Batten and Kraus (2006), Wamsley et al. (2006), Li et al. (2009), Li et al. (2011), Beck and Kraus (2010), Byrnes et al. (2010), Rosati et al. (2011), Reed and Lin (2011), and Wang et al.(2011).

1.2 Purpose of study

When a numerical model is developed, it should be verified and validated before it is applied in engineering practice. Verification is the process of determining the accuracy of which the governing equations of a specific model are being solved. It checks the numerical implementation of the governing equations. Validation is the process of determining the degree to which a model is an accurate representation of real world physics and processes from the perspective of the intended uses of the model. Another often used term in model application is calibration, which is the process of determining the unknown model parameters or variables that represent physical quantities. Almost all nearshore models for hydrodynamics, waves, and sediment transport have calibration parameters such as bottom friction and sediment transport scaling factors. The development of appropriate values of these parameters for different problems is still an active area of research. Many of the calibration parameters are due to simplification and parameterization of the physics. Even a well verified and validated model may still need to be calibrated for different practical problems.

This report provides details of a Verification and Validation (V&V) study conducted by CIRP to evaluate the capabilities of the CMS. The V&V study is divided into four separate reports:

1. Summary Report (Demirbilek and Rosati 2011),
2. CMS-Wave (Lin et al. 2011),
3. CMS-Flow: Hydrodynamics (Sánchez et al. 2011), and
4. CMS-Flow: Sediment Transport and Morphology Change (present report).

These reports describe detailed aspects of the V&V evaluations, applications, and model performance skills. For details of V&V protocol, see Report 1 in this series. In the present Report 4, the numerical implementation of advection and diffusion is verified for a simple one-dimensional (1-D) analytical test case of scalar transport. Then, the model is validated using six laboratory experiments and three field studies. One objective of the V&V study is to determine appropriate ranges for sediment transport parameters for different applications and to establish a basis for user guidance. Future improvements are identified to enhance CIRP model's unique features and computational capabilities for practical applications. This Report 4 represents the first of a series of sediment transport V&V reports and is not intended to be comprehensive. Additional cases, and extended results and discussion of the test cases provided here, will be posted on the CIRP website http://cirp.usace.army.mil/CMS.

1.3 CMS sediment transport and morphology change

In CMS, non-cohesive sediment transport is modeled using an Eulerian approach in which the sediment is represented by concentration rather than discrete particles or groups of particles (parcels). Some important features of the CMS sediment transport model are:

1. Three sediment transport model options,
2. Four transport formulas for combined waves and currents,
3. Transport over hard bottoms,
4. Hiding and exposure,
5. Bed material sorting and gradation,
6. Bed slope effects on transport, and
7. Avalanching.

Sediment transport is calculated in CMS-Flow on the same grid as the hydrodynamics and salinity transport. The coupling procedure between

waves, hydrodynamics, and sediment transport is illustrated in Figure 1. In this coupling procedure (referred to as semi-coupling), waves, hydrodynamics, and sediment transport are computed consecutively with information passed to one another. Fully coupled models that solve waves, hydrodynamics, and sediment transport simultaneously are not applied usually for practical engineering due to their excessive computational costs.

There are three sediment transport models currently available in CMS:

1. Equilibrium Total load (ET),
2. Equilibrium Bed load and Non-Equilibrium Suspended load (EBNES), and
3. Non-Equilibrium Total load transport (NET).

The main difference between the three models is the assumption of the local equilibrium transport for bed and suspended loads. The recommended transport model for coastal applications is the NET but the other models are provided since they were implemented in previous versions of the CMS. There are also two time marching schemes:

1. Explicit
2. Implicit.

All three sediment transport models are available with the explicit time marching scheme, while only the NET is currently available with the implicit time marching scheme. The total-load transport formula reduces to the bed-load transport formula for purely bed-load transport, and to the suspended-load transport formula for purely suspended-load transport. The NET includes a correction factor which accounts for the vertical non-uniform profiles of sediment concentration and current velocity Sánchez and Wu (2011b).

For each of these sediment transport models, an empirical formula is chosen to calculate the transport capacity or equilibrium transport rate. There are four sediment transport capacity formulas in CMS:

1. Lund-CIRP (Camenen and Larson 2005, 2007, 2008),
2. Watanabe (1987),
3. Soulsby-van Rijn (Soulsby 1997),
4. van-Rijn (van Rijn 1984a,b; 2007a,b).

The bed- and suspended-load transport rates from these formulas may be adjusted using scaling factors to calibrate the transport rates to field or laboratory measurements. The transport capacity formula is perhaps the most important aspect of the sediment transport model because it determines where and how much sediment is transported and, in turn, erosional and depositional patterns.

CMS also offers options to simulate sediment transport as uniform (single grain size) or non-uniform (multiple grain sizes). In the case of single-sized sediment transport, the option is available to consider a simple hiding and exposure correction through the critical Shields parameter, by assuming that the spatial distribution of the bed material composition is constant in time. This approach is reasonable for sites in which the bed morphology change is due mostly to a narrow sediment size range with the presence of other much coarser (shell hash) or finer material not having a significant contribution to the bed change, at least in the area of interest. For further details on this approach the reader is referred to Sánchez and Wu (2011a).

For applications in which the bed sediments are well graded, the use of a multi-fraction approach is necessary. This approach assumes that the total sediment transport is equal to the sum of the transport of discrete sediment sizes classes (Wu 2007). For each size class, the transport, bed material sorting, and bed change equations are solved simultaneously at each time step (semi-coupling). This approach allows the use of large computational time steps while still maintaining a strong coupling between the bed material composition and the transport equation. The bed is divided into discrete vertical layers and the fractional composition of each layer is tracked in time. The multiple-size approach is more realistic than the single-size approach. However, it is more complex, computationally intensive, and requires more input data. For further details on the multi-fraction approach of CMS see Sánchez and Wu (2011b).

1.4 Report organization

This report is organized into five chapters. Chapter 1 presents the motivation, definitions, and an overview of the CMS sediment transport and morphology change V&V study. Chapter 2 discusses verification of sediment transport calculations with CMS as compared to 1-D analytical solutions of the advection-diffusion equation (Category 1). Chapters 3 and 4 present the calibration and validation of CMS with comparison of model calculations to

laboratory (Category 2) and field (Category 3) data, respectively. In Chapters 2-4, test cases are identified by Category "C" and Example number "Ex" as in C1-Ex1, etc. Chapter 5 summarizes the study and discusses future work.

2 Analytical Solutions

2.1 Overview

The purpose of this chapter is to document comparison of sediment transport calculations by CMS with the analytical solutions available in the literature. The implemented numerical methods for advection and diffusion are verified with a one-dimensional analytical test case of the transport of a Gaussian shaped scalar quantity. Tests are conducted with and without the diffusion term using different grid resolutions and time steps to study the model result sensitivity. Future tests will include 2-D advection and diffusion with source terms.

2.2 Test C1-Ex1: Scalar transport

2.2.1 Purpose

The CMS is applied to a one-dimensional (1-D) problem of scalar transport in an idealized rectangular domain to analyze the model performance in simulating the processes of advection and diffusion, and assess numerical diffusion in the model as a function of time step and grid resolution.

2.2.2 Description

For a 1-D rectangular channel, the depth-averaged scalar transport equation is given by

$$\frac{\partial(h\phi)}{\partial t}+\frac{\partial(hU\phi)}{\partial x}=\frac{\partial}{\partial x}\left(\Gamma h\frac{\partial\phi}{\partial x}\right)-kh\phi \tag{1}$$

where t is the time, x is the distance along the channel, h is the total water depth, ϕ is a depth-averaged scalar quantity (e.g. sediment concentration, salinity), Γ is the diffusion coefficient, and k is a decay coefficient. Assuming a constant water depth, current velocity, and diffusion coefficient, the analytical solution to the above problem for an initial Gaussian shaped scalar field can be calculated easily (Chapra 1997).

$$\phi(x,t)=\frac{M}{2\sqrt{\pi(\Gamma t+C)}}\exp\left[-\frac{\left(x-x_0-Ut\right)^2}{4(\Gamma t+C)}-kt\right] \tag{2}$$

where x_0 is the location of the initial profile center, M is a constant which controls the magnitude of the initial profile, and C is also a constant which controls the width of the initial profile. The analytical solution is compared to the calculated results for advection only; combined advection and diffusion; and advection, diffusion, and a sink.

2.2.3 Model setup

The test considered a wide rectangular flume 10 km long and 30 m wide. Two grids were set up with constant resolutions of 1 and 10 m, and calculations were made with two different time steps of 1 and 10 min. A summary of the selected model parameters are listed in Table 1. The second-order Hybrid Linear/Parabolic Approximation (HLPA) scheme of Zhu (1991) was used for the advection term. Choi et al. (1995) found that the HLPA scheme has similar accuracy to the third-order SMARTER and LPPA schemes but is simpler and more efficient. Results using the first-order upwind and exponential schemes are also provided for reference. The diffusion term was discretized with the standard second-order central difference scheme. The temporal term was discretized with the first-order backward difference scheme. The same numerical methods employed here are implemented in CMS-Flow for the momentum, sediment, and salinity transport equations.

Table 1. CMS-Flow setup for the scalar transport test cases.

Parameter	Value
Solution scheme	Implicit
Simulation duration	24 hr
Ramp period duration	0.0
Grid resolution, Δx	10, 50 m
Time step, Δt	1, 10 min
Advection scheme	HLPA, Upwind, and Exponential
Current velocity	0.05 m/sec
Water depth	2.0 m
Diffusion coefficient	0.0, 3.0 m^2/sec
Constant M	1800
Constant *C*	259,200 m^2

2.2.4 Results and discussion

2.2.4.1 Advection only

For this case, the diffusion and decay coefficients were set to zero. The calculated and analytical scalar profiles at times 0 and 24 hr are presented in Figure 2. The corresponding goodness-of-fit statistics are presented in Table 2. The analytical scalar profile at 24 hr is equal to the initial profile displaced by 4.32 km. The first-order upwind produced significantly more numerical dissipation than the second-order HLPA scheme. The HLPA scheme was found to increase the solver convergence rate significantly, leading to shorter computational times by about 37 percent compared to the simpler and less computationally intensive upwind scheme.

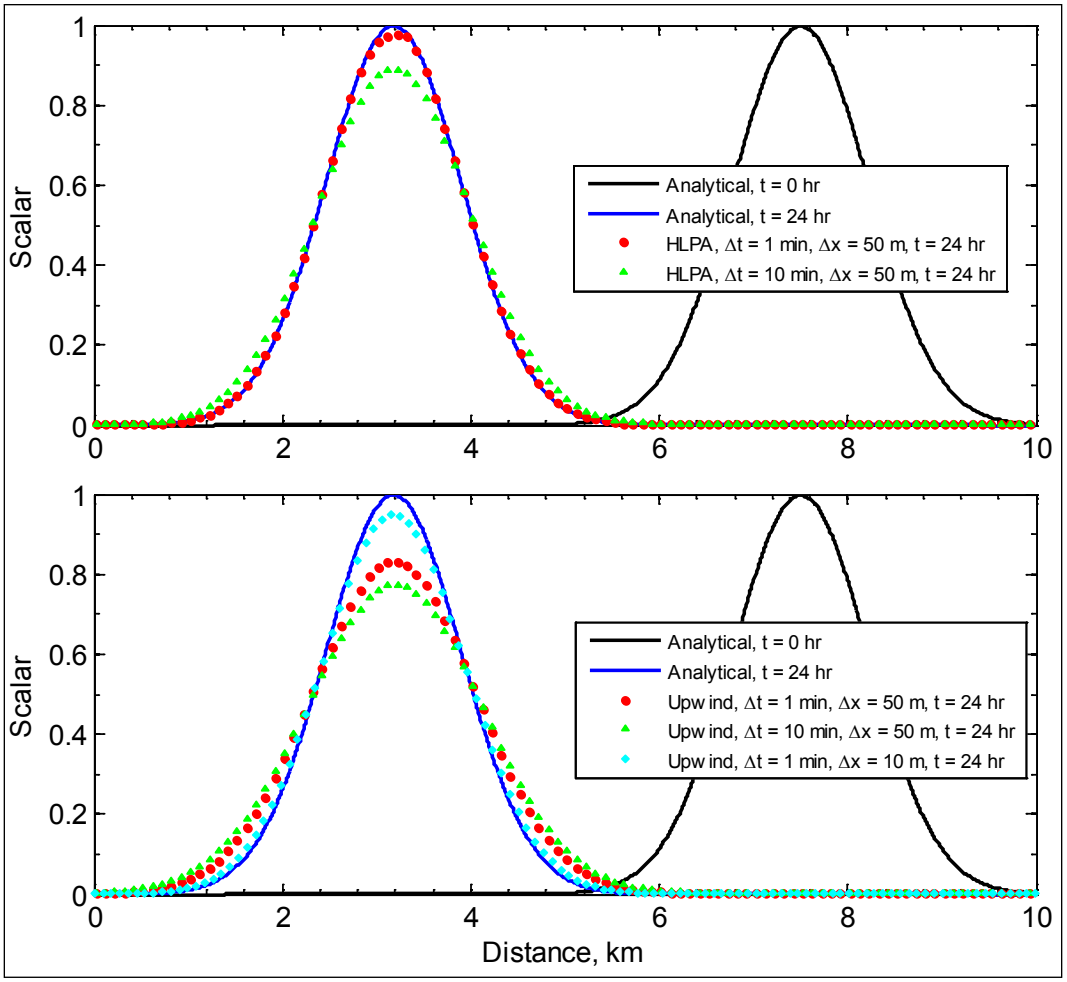

Figure 2. Analytical and calculated scalar profiles for the advection only case. Current is from left to right.

Table 2. Goodness-of-fit statistics* for the advection test case.

	Run				
Setting/Statistic	1	2	3	4	5
Advection scheme	HLPA	HLPA	Upwind	Upwind	Upwind
Resolution, m	50	50	50	50	10
Time step, min	1	10	1	10	1
NRMSE, %	0.49	3.39	5.39	7.36	1.58
NMAE, %	0.34	2.05	3.30	4.54	1.00
R^2	0.999	0.993	0.983	0.965	0.999

*defined in Appendix A

2.2.4.2 Advection and diffusion

The diffusion coefficient was set to 3 m^2/sec, which is representative of sediment and salinity diffusion coefficients for coastal applications. The decay coefficient was set to zero. The analytical and calculated scalar profiles at times 0 and 24 hr are shown in Figure 3 for the HLPA and exponential schemes. Table 3 displays the correlation coefficients, RMSEs, and NRMSEs between the analytical solution and the CMS calculations. Compared to the previous case of advection only, the CMS results show better correlation and smaller errors with both the advection and diffusion terms included. Physical diffusion tends to smooth out the scalar distribution, reducing the horizontal gradients and thus numerical dissipation. In the case of the exponential scheme, a small phase lag is noticeable which decreases with the smaller time step. Similar results were obtained by Chapra (1997). When diffusion is present, the differences between first and second order advection schemes become less significant. The NMAEs for HLPA and upwind schemes were 0.36 and 0.73 percent respectively, using a time step of 1 min and grid size of 50 m (Table 3). For a grid size of 50 m and time step of 1 min, the NMAEs for HLPA and exponential schemes were 0.36 and 0.73 percent, respectively, for the case of advection and diffusion (Table 3).

2.2.4.3 Advection, diffusion and sink

As in the previous test case, the diffusion coefficient was set to 3 m^2/sec, which is representative of the sediment and salinity diffusion coefficients for coastal applications. The decay coefficient was set as 0.864 day^{-1} to test the numerical implantation.

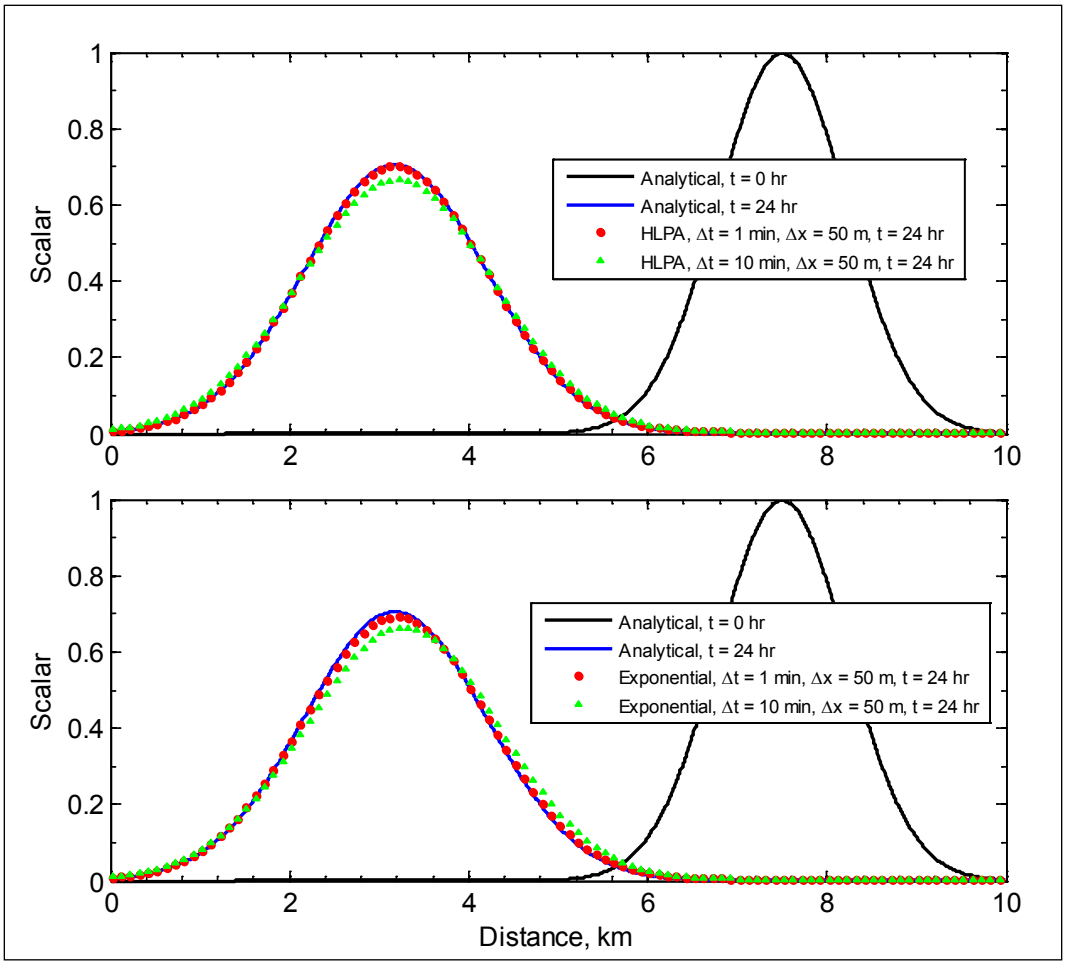

Figure 3. Analytical and calculated scalar profiles for the case of advection and diffusion. Current is from left to right.

Table 3. Goodness-of-fit statistics* for the advection-diffusion test case.

	Run			
Setting/Statistic	6	7	8	9
Advection scheme	HLPA	HLPA	Exponential	Exponential
Resolution, m	50	50	50	50
Time step, min	1	10	1	10
NRMSE, %	0.40	2.19	0.87	3.15
NMAE, %	0.36	1.64	0.73	2.22
R^2	0.999	0.998	0.999	0.994

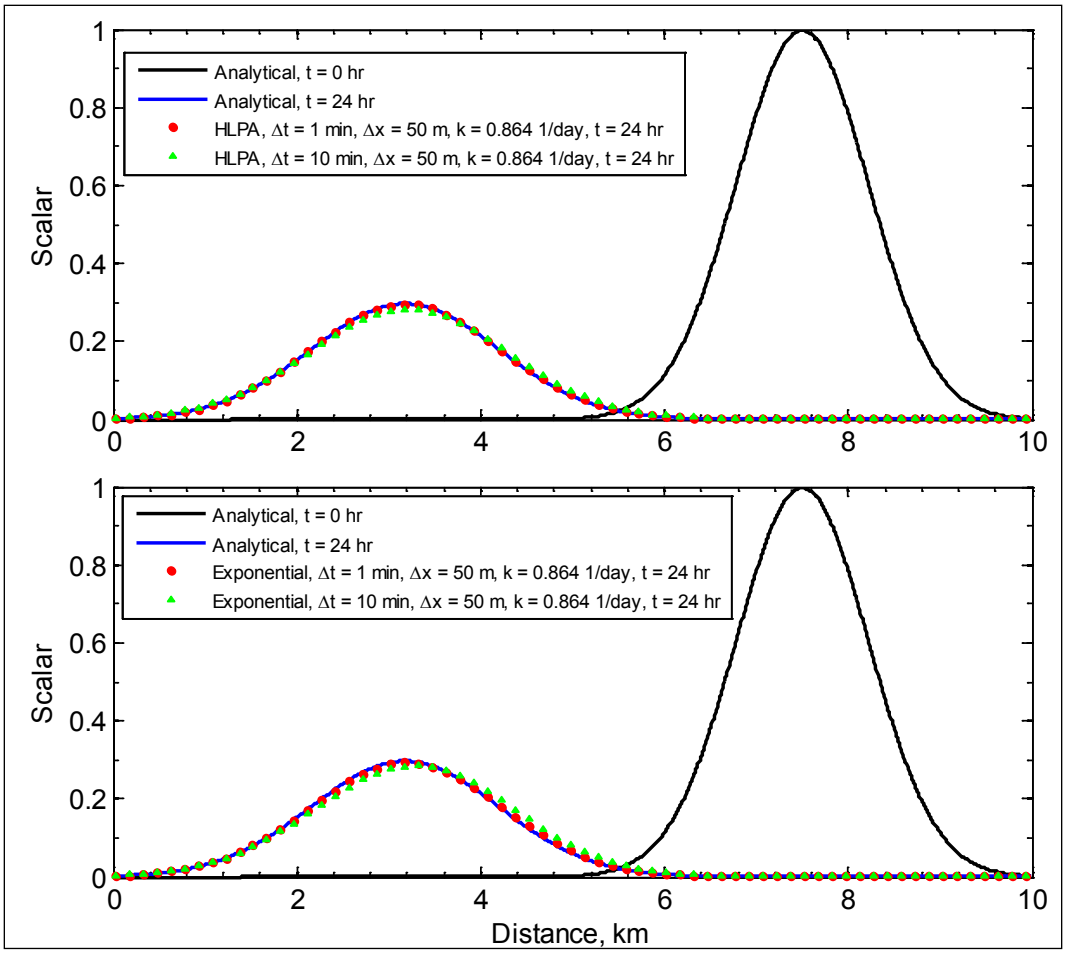

Figure 4. Analytical and calculated scalar profiles for the case of advection, diffusion, and decay. Current is from left to right.

Figure 4 shows the analytical and calculated scalar profiles at 0 and 24 hr. The corresponding goodness-of-fit statistics are presented in Table 4, which are similar to the previous advection and diffusion test case. Differences between first- and second-order advection schemes are less significant compared to the advection-only case due to the fact that physical diffusion tends to smooth out the scalar profile, reducing the horizontal gradients and numerical dissipation.

2.2.5 Conclusions

Depth-averaged scalar transport calculations by the CMS were verified for the case of an idealized channel with constant water depth, current velocity, diffusion coefficient, and decay coefficient. The tests were conducted with and without the diffusion and sink terms. The best model results were obtained with the second-order HLPA advection. Computed results show

that simulations with large time steps and coarse mesh could generate extra numerical dissipation and result in excessive smoothing of the scalar field, and thus underestimate peak scalar values. To solve the transport problems with sharp gradients, a fine grid resolution and small time step are necessary.

Table 4. Goodness-of-fit statistics* for advection-diffusion-decay test case.

	Run			
Setting/Statistic	10	11	12	13
Advection scheme	HLPA	HLPA	Exponential	Exponential
Resolution, m	50	50	50	50
Time step, min	1	10	1	10
NRMSE, %	0.40	2.29	0.93	3.45
NMAE, %	0.36	1.71	0.77	2.42
R^2	0.999	0.997	0.999	0.991

2.2.6 Recommendations

Caution should be taken in selecting the proper time step for a scalar transport simulation. Small time steps and finer grid resolutions can reduce numerical dissipation. It is possible to use a higher-order discretization for the temporal term to improve the results. However, the advantages of the higher-order approach are expected to be minor. There always is a compromise between numerical accuracy and computational cost. For most practical coastal sediment transport applications, the differences between first- and second-order advection schemes have been found to be insignificant, indicating that numerical dissipation is relatively small compared to physical diffusion. In addition, errors induced by transport capacity formulas, estimates of adaptation length, bathymetry, etc., are much greater and, therefore, it is hard to justify the use of high-order methods in morphodynamic models.

3 Laboratory Studies

3.1 Overview

Cases presented in this chapter compare CMS calculations to six laboratory studies of sediment transport and morphology change. Three cases consider channel infilling and migration:

1. In steady flows (Test C2-Ex1),
2. With waves parallel to the direction of flow (Test C2-Ex2), and
3. With waves perpendicular to the flow (Test C2-Ex3).

The other three cases are used to evaluate CMS capabilities for:

1. Combined wave-current transport in surf zone (Test C2-Ex4),
2. Non-erodible hard bottom (Test C2-Ex5), and
3. Non-uniform sediment deposition (Test C2-Ex6).

3.2 Test C2-Ex1: Channel infilling and migration: steady flow only

3.2.1 Purpose

The CMS was applied to a laboratory flume study of channel infilling and migration due to a steady flow perpendicular to the channel axis. Model performance was evaluated by comparing measured and computed bed elevations of the channel cross-sections. Three channel cross-sections with slopes from 1:10 to 1:3 were simulated to test the limits of the depth-averaged model. Specific model features tested were:

1. Single-sized non-equilibrium total-load sediment transport,
2. Equilibrium inflow concentration boundary condition, and
3. Zero-gradient outflow boundary condition.

3.2.2 Experimental setup

Three laboratory experiments of channel infilling and migration were carried out at the Delft Hydraulics Laboratory (DHL 1980) in a rectangular flume (length = 30 m, depth = 0.7 m, and width = 0.5 m) with a medium sand (d_{50} = 0.16 mm, d_{90} = 0.2 mm). In these tests, the mean flow velocity and water depth at the inlet were 0.51 m/sec and 0.39 m, respectively. The

initial channel cross-sections had side slopes of 1:10, 1:7 and 1:3. Sediment was supplied at a rate of 0.04 kg/m/sec at the inlet to avoid erosion. The upstream bed and suspended load transport rates were estimated at 0.01 and 0.03 kg/m/sec, respectively.

3.2.3 Model setup

The laboratory study was simulated as a 1-D problem and the flume wall effects were ignored in the simulation for simplicity. The computational grid consisted of 3 rows and 220 columns (see Figure 5) with constant resolution of 0.1 m. The computational time step was 1 min. A flux boundary was specified for the upstream boundary with an equilibrium sediment concentration. Water level and zero concentration gradient boundary conditions were specified at the downstream boundary. Bed and suspended load scaling factors were adjusted to match the measured inflow transport rates and were estimated at 1.2 and 0.5 kg/m/sec, respectively. The Lund-CIRP transport formula (Camenen and Larson 2005, 2007, 2008) was used for all three cases. The transport grain size was set to median grain size (d_{50} = 0.16 mm), and no hiding and exposure were considered in the present simulations. The bed slope coefficient was set to 1.0. Sensitivity analysis shows that the model results were not sensitive to bed slope coefficients between 0.1 and 2.0. The bed porosity was estimated at 0.35. Representative settling velocity was 0.013 m/sec. A summary of selected model parameters is shown in Table 5. The total-load adaptation length was calibrated to 0.75 m using the measured bed elevations for Case 1, and then was applied in cases of side slopes 1:7 and 1:3 (Cases 2 and 3, respectively) to validate the model.

3.2.4 Results and discussion

Cases 1, 2, and 3 correspond to the channels with side slopes equal to 1:10, 1:7 and 1:3, respectively. Since the depth-averaged CMS is expected to

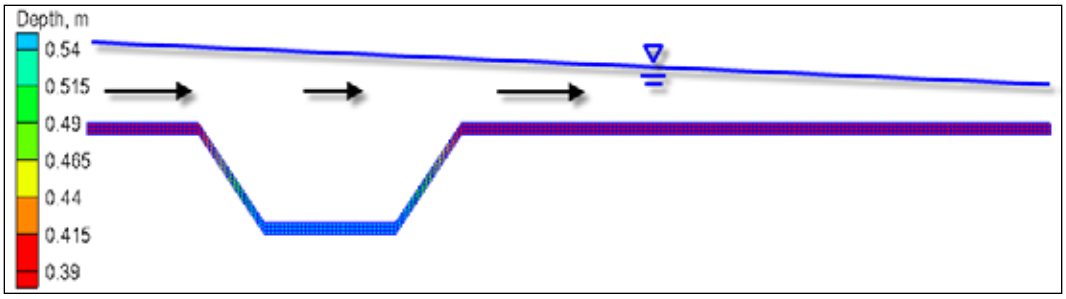

Figure 5. Computational grid for the DHL (1980) experiment test case

Table 5. CMS-Flow parameter settings for DHL (1980) experiment test case.

Parameter	Value
Flow time step	1 min
Simulation duration	15 hr
Ramp period duration	0.1 hr
Water density	1,000 kg/m^3
Manning's coefficient	0.025 sec/m$^{1/3}$
Wall friction	Off
Transport grain size	0.16 mm
Bed slope coefficient	1.0
Sediment porosity	0.35
Sediment density	2,650 kg/m^3
Suspended load scaling factor	1.2
Bed load scaling factor	0.5
Morphologic acceleration factor	1.0
Total load adaptation length	0.75 m

perform best for the cases without three-dimensional (3-D) flows caused by the steeper side slopes, Case 1 was chosen for calibration. Case 1 also has the most data of the three cases since bed elevations were measured at two elapsed times

3.2.4.1 Calibration

The only calibration parameter used was the total-load adaptation length which was estimated at 0.75 m. Computed and measured still-water depths for Case 1 are compared in Figure 6. The goodness-of-fit statistics for calculated water depth in Case 1 are given in Table 6. The Brier Skill Score (BSS) values indicate excellent model performance; however, it is recognized that these results were calibrated to best represent the measurements.

3.2.4.2 Validation

Computed and measured still-water depths for Cases 2 and 3 are compared in Figures 7 and 8. The corresponding goodness-of-fit statistics are given in Table 7. The model performance for Cases 2 and 3 was not as good as for Case 1, possibly due to flow separation on the upstream channel side caused by the steeper slopes of Case 3 and perhaps Case 2.

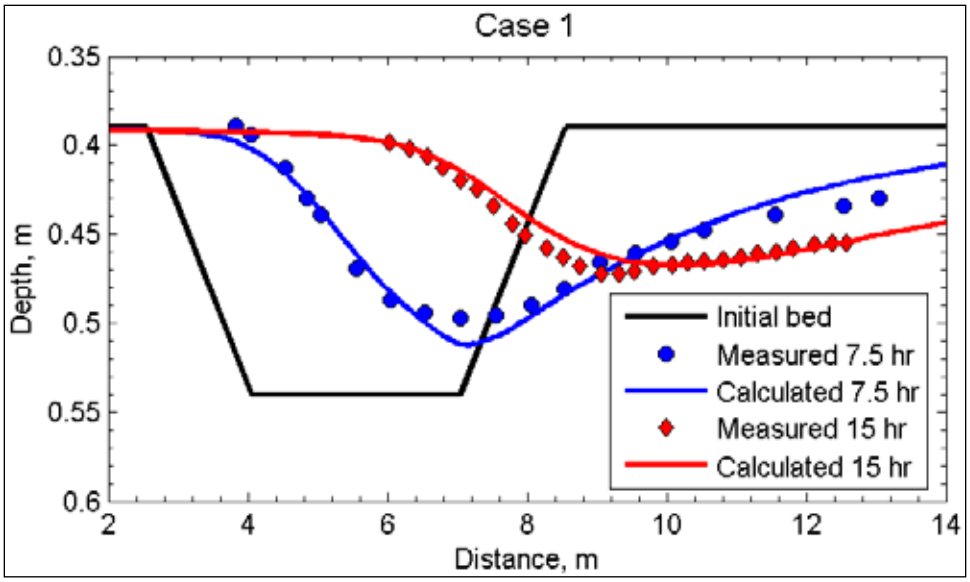

Figure 6. Measured and calculated bed elevations for Case 1 of DHL (1980).

Table 6. Water depth goodness-of-fit statistics* for Case 1 of DHL (1980).

Case	Time, hr	BSS	NRMSE, %	NMAE, %	R^2	Bias, m
1	7.5	0.905	7.09	5.92	0.956	0.0010
	15	0.932	7.75	5.77	0.955	-0.0031

*defined in Appendix A

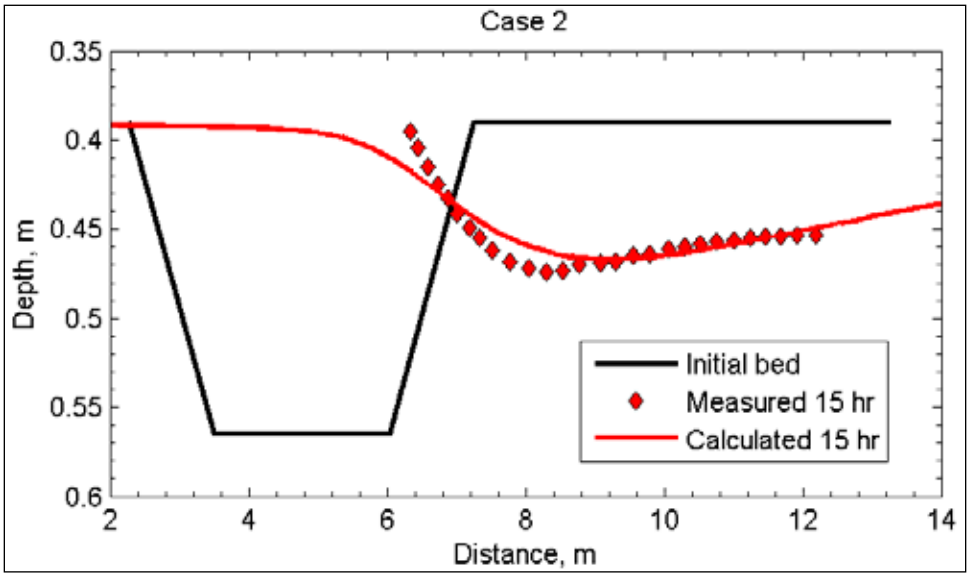

Figure 7. Measured and calculated bed elevations for Case 2 of DHL (1980).

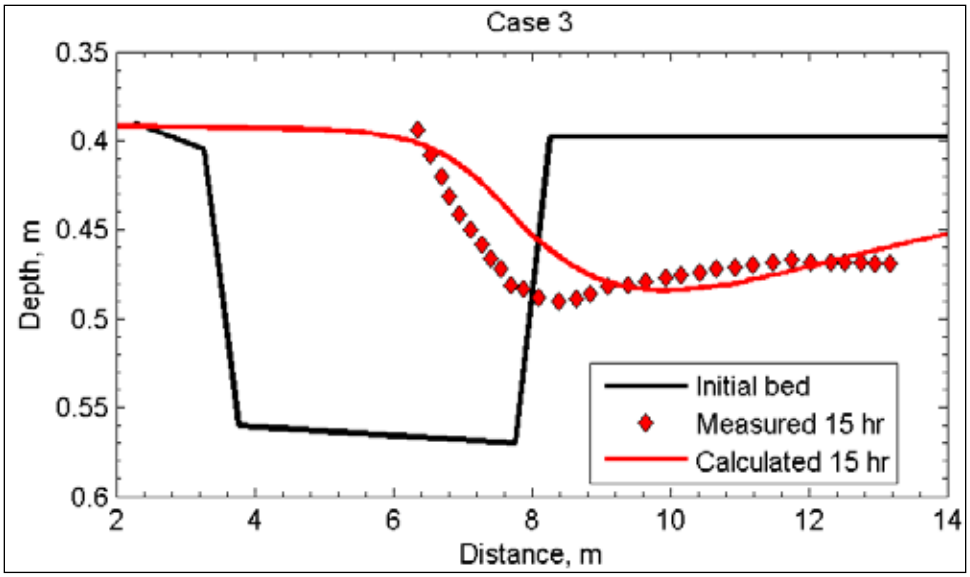

Figure 8. Measured and calculated bed elevations for Case 3 of DHL (1980).

Table 7. Water depth goodness-of-fit statistics* for Cases 2 and 3 of DHL (1980).

Case	Time, hr	BSS	NRMSE, %	NMAE, %	R^2	Bias, m
2	15	0.888	10.21	7.55	0.880	-0.0005
3	15	0.795	20.19	15.36	0.623	-0.0098

*defined in Appendix A

When flow separation occurs, it is expected to cause a steepening of the upstream profile by hindering the downstream (downslope) movement of sediment at the upstream channel side. The presence of flow separation for Cases 2 and 3 is supported by the steep measured bathymetry. Since the CMS is a depth-averaged model, flow separation will cause significant errors in the computed morphology change. In general, flow separation is greatest at an incident current angle of 90 deg with respect to the channel axis and reduces as the angle decreases. Since most navigation channels at coastal inlets are approximately aligned with flow, flow separation may not be a major source of error in field applications. In applications with flow separation or other three-dimensional (3-D) flow patterns, a corresponding 3-D flow and sediment transport model may be necessary.

3.2.5 Conclusions and recommendations

The CMS was applied to three laboratory cases of channel infilling and migration caused by steady flow. The model was calibrated using one case and validated using the other two cases. A good agreement was obtained

between computed and measured water depths, as indicated by the goodness-of-fit statistics in Tables 6 and 7. The best results were obtained for the mild (1:10) channel slope test case. Measured bed elevations for the channels with side slopes of 1:7 and 1:3 indicated flow separation which is not accounted for in the present depth-averaged model.

3.3 Test C2-Ex2: Channel infilling and migration: waves parallel to flow

3.3.1 Purpose

The CMS was applied to a laboratory case to study channel infilling and migration with collinear steady flow and regular waves. Specific model features tested were:

1. Inline wave-current-sediment coupling,
2. The single-sized non-equilibrium total-load sediment transport model, and
3. Sediment boundary conditions.

The model performance was tested using measured water depths and a sensitivity analysis was done for the transport formula, total-load adaptation length, and bed slope coefficient.

3.3.2 Experimental setup

Van Rijn (1986) reported results from a laboratory experiment on the evolution of channel morphology in a wave-current flume caused by cross-channel flow and waves parallel to the flow. The flume was 17-m long, 0.3-m wide and 0.5-m deep. A pumping system was used to generate a steady current in the flume. The inflow depth-averaged velocity and water depth were 0.18 m/sec and 0.255 m, respectively. A circular weir was used to control the upstream water depth. Regular waves with a height of 0.08 m and period of 1.5 s were generated by a simple wave paddle. The bed material consisted of fine well sorted sand with d_{50} = 0.1 mm and d_{90} = 0.13 mm. Sand was supplied at a rate of 0.0167 kg/m/sec at the upstream end to maintain the bed elevation. A summary of the experiment hydrodynamic and wave conditions is presented in Table 8.

Table 8. Hydrodynamic and wave conditions for the van Rijn (1986) test case.

Variable	Value
Upstream water depth	0.255 m
Upstream current velocity	0.18 m/sec
Wave height (regular)	0.08 m
Wave period (regular)	1.5 sec
Incident wave angle with respect to flow	0 deg
50th percentile (median) grain size, d_{50}	0.1 mm
90th percentile grain size, d_{90}	0.13 mm

3.3.3 Model setup

For simplicity, the case was simulated as a 1-D problem by neglecting the flume wall effects. The computational grid had a constant resolution of 0.1 m, and was 3 cells wide (minimum for CMS) and 140 cells long (Figure 9). Water flux and equilibrium sediment concentration was specified at the upstream boundary, and a water level and zero-concentration-gradient boundary was specified at the downstream end. Zero current velocity and water levels were specified as the initial condition (cold start). A summary of the relevant CMS-Flow and CMS-Wave settings is provided in Tables 9 and 10. The Lund-CIRP (Camenen and Larson2005, 2007, 2008), Soulsby-van Rijn (Soulsby 1997) (referred to as Soulsby for short), and van Rijn (van Rijn 1984ab; 2007b) transport formulas were used. Bed and suspended load transport scaling factors in Table 9 were adjusted to match the measured inflow sediment supply rate. Results are presented for a range of adaptation lengths and bed slope coefficients.

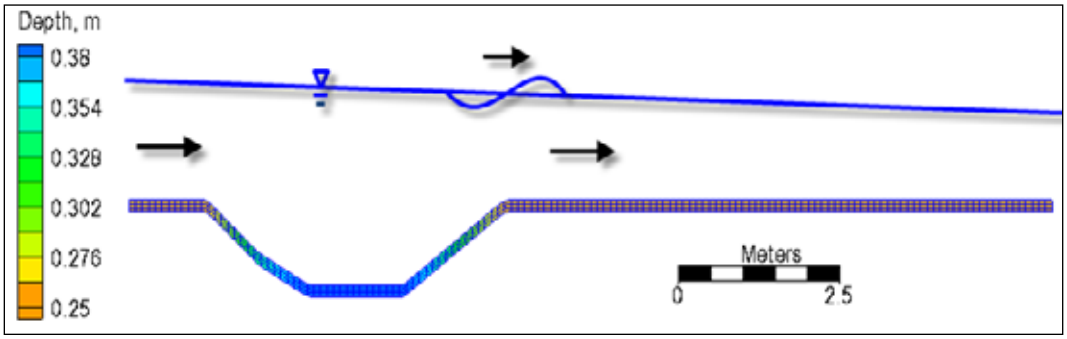

Figure 9. CMS computational grid for the van Rijn (1986) test case.

Table 9. CMS-Flow settings for the van Rijn (1986) test case.

Parameter	Value
Solution scheme	Implicit
Time step	2 min
Simulation duration	10 hr
Ramp period duration	0.5 hr
Inflow discharge	0.0138 m^3/sec
Outflow water level	-0.002 m
Manning coefficient	0.025 sec/$m^{1/3}$
Wall friction	Off
Water density	1000 kg/m^3
Transport grain size	0.1 mm
Sediment transport formula	Lund-CIRP, Soulsby-van Rijn, and van Rijn
Bed and suspended load scaling factors	0.9 (Lund-CIRP) 2.7 (Soulsby-van Rijn), and 2.0 (van Rijn)
Morphologic acceleration factor	1.0
Sediment porosity, p_m	0.3, 0.35, 0.4
Sediment density	2,650 kg/m^3
Sediment fall velocity	0.007 m/sec
Bed slope coefficient, D_s	0, 1, 5
Total-load adaptation length, L_t	0.5, 1, 2, 5, and 10 m

Table 10. CMS-Wave settings for the van Rijn (1986) test case.

Parameter	Value
Wave height (regular)	0.08 m
Wave period (regular)	1.5 sec
Incident wave angle with respect to flow	0.0 °
Bottom friction	Off
Steering interval	0.5 hr

3.3.4 Results and discussion

The computed bed elevations after 10 hr for different transport formulas, adaptation lengths, bed slope coefficients, and porosities are shown in

Figures 10-13. The corresponding water depth goodness-of-fit statistics are provided in Tables 11-14. The results are consistent with those obtained by Sánchez and Wu (2011a) using a previous version of the CMS. The model reproduces the general trends of the morphology change including the upstream bank migration, channel infilling, and downstream bank erosion.

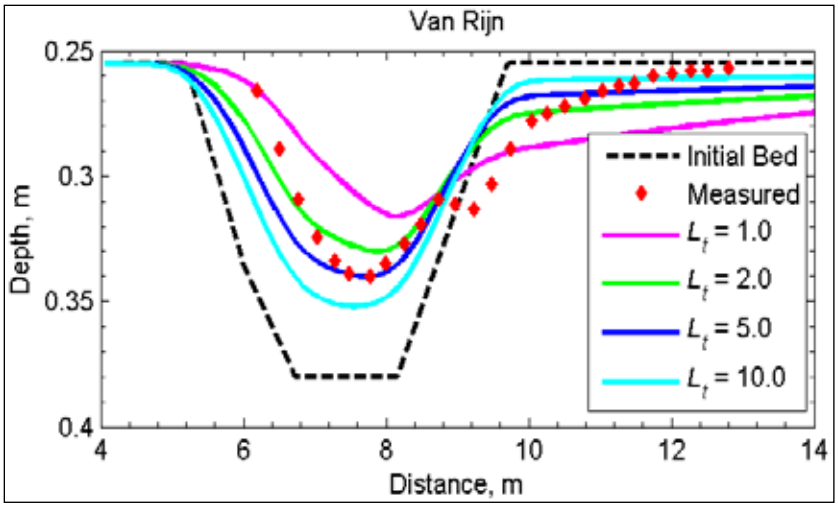

Figure 10. Measured and calculated water depths at 10 hr using the van Rijn transport formula and total-load adaptation lengths between 1 and 10 m.

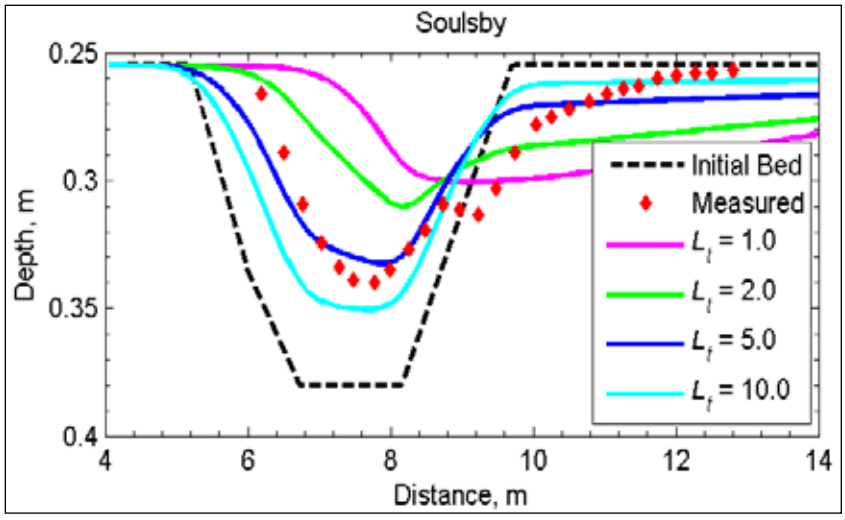

Figure 11. Measured and calculated water depths at 10 hr using the Soulsby-van Rijn transport formula and total-load adaptation lengths between 1 and 10 m.

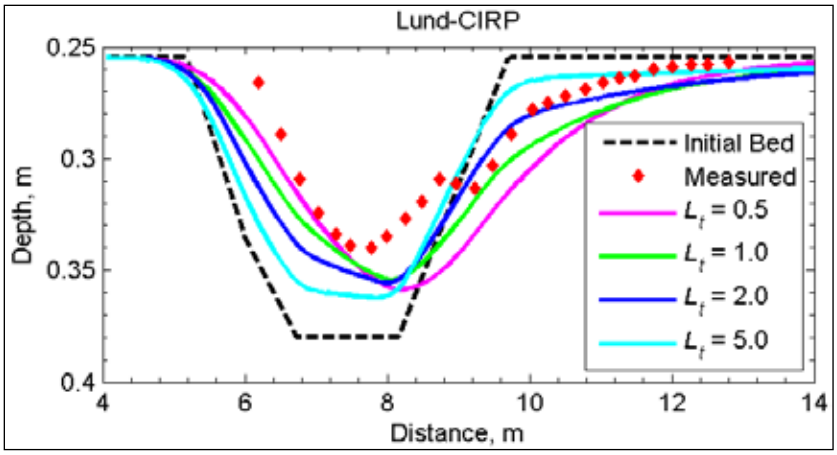

Figure 12. Measured and calculated water depths at 10 hr using the Lund-CIRP transport formula and total-load adaptation lengths between 0.5 and 5 m.

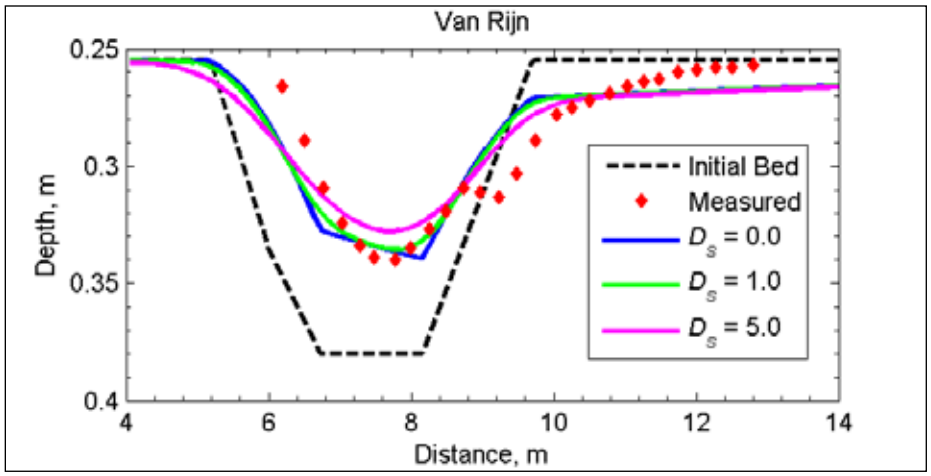

Figure 13. Measured and calculated water depths at 10 hr using the van Rijn transport formula and total-load adaptation length of 5.0 m and bed slope coefficient between 0 and 5.

Table 11. Water depth goodness-of-fit statistics* using the van Rijn transport formula and varying total-load adaptation length.

Total-load Adaptation Length, m	BSS	NRMSE %	NMAE %	R^2	Bias m
1.0	0.453	23.50	20.78	0.700	-0.0008
2.0	0.686	13.50	11.15	0.876	0.0002
5.0	0.627	16.05	11.57	0.807	0.0015
10.0	0.471	22.73	17.46	0.766	0.0037

*defined in Appendix A

Table 12. Water depth goodness-of-fit statistics* using the Soulsby transport formula and varying total-load adaptation length.

Total-load Adaptation Length, m	BSS	NRMSE %	NMAE %	R^2	Bias m
1.0	-0.025	0.4407	0.3813	0.070	-0.0051
2.0	0.346	0.2812	0.2494	0.461	-0.0048
5.0	0.667	0.1433	0.1111	0.836	-0.0012
10.0	0.486	0.2210	0.1693	0.763	0.0026

*defined in Appendix A

Table 13. Water depth goodness-of-fit statistics using the Lund-CIRP transport formula and varying adaptation length.

Total-load Adaptation Length, m	BSS	NRMSE %	NMAE %	R^2	Bias m
0.5	0.458	0.2396	0.2042	0.909	0.0170
1.0	0.548	0.1998	0.1765	0.938	0.0147
2.0	0.514	0.2147	0.1671	0.866	0.0124
5.0	0.327	0.2973	0.2193	0.744	0.0098

*defined in Appendix A

Table 14. Water depth goodness-of-fit statistics* using the van Rijn transport formula as a function of varying bed slope coefficient.

Bed slope Coefficient	BSS	NRMSE %	NMAE %	R^2	Bias m
0.0	0.648	15.13	11.49	0.816	0.0012
1.0	0.669	14.25	10.59	0.834	0.0008
5.0	0.694	13.17	10.70	0.880	-0.0005

*defined in Appendix A

3.3.4.1 Transport formula and adaptation length

Among the three transport formulas, the van Rijn transport formula produced the best agreement as compared with measurements. The van Rijn and Soulsby transport formulas produced relatively similar results and were the best for a total-load adaptation length L_t = 5 m, while the Lund-CIRP formula provided the best results with L_t = 0.5 and 1 m, consistent with other similar experiments of channel infilling and migration. Of the three formulas tested, the Soulsby formula was the most sensitive to L_t and

produced a negative BSS (see Appendix A for definition) for L_t =1.0 m and less. The Lund-CIRP formula was the least sensitive to L_t.

The differences in the best fit L_t for different transport formulas are due to differences in the transport capacities over the channel trough. The upstream concentration capacities were equal for all formulas since the bed and suspended load scaling factors were adjusted to match the measured sediment supply rate. These scaling factors were 2.0, 2.7, and 0.9 for the van Rijn, Soulsby, and Lund-CIRP transport formulas, respectively (see Table 9). Over the trough, the van Rijn, Soulsby, and Lund-CIRP formulas predicted concentration capacities equal to 0.051, 0.002, and 0.232 kg/m^3, respectively. The van Rijn and Soulsby formulas estimated much smaller concentration capacities in the channel trough and produced greater channel infilling and migration than the Lund-CIRP formula. The van Rijn and Soulsby transport formulas also required larger transport scaling factors to match sediment supply rate (see Table 9). The adaptation length should be independent of the transport formula, yet the results show that errors from the transport formula may lead to different calibrated adaptation lengths. These results emphasize the importance of having an accurate transport formula.

3.3.4.2 Bed slope coefficient

The bed slope coefficient D_s is usually not an important calibration parameter for field applications. It has a default value of 1.0. Increasing the bed slope coefficient has the net effect of moving sediment downslope and smoothing the bathymetry. For this laboratory experiment case, the fraction of bed load upstream of the channel was approximately 8 to 17 percent. Although the best goodness-of-fit statistics were obtained from D_s = 5.0, it is clear from Figure 13 that this produced excessive smoothing as compared to D_s = 1.0. When the bed slope coefficient is turned off (D_s = 0.0), the calculated bed profile preserves the sharp corners from the initial profile but this is an unrealistic trend.

3.3.5 Conclusions and recommendations

The CMS was applied to a laboratory experiment case of channel infilling and migration under steady flow and regular waves perpendicular to the channel axis (parallel to the flow). The non-equilibrium total-load sediment transport model was able to reproduce the overall morphologic behavior. A sensitivity analysis was conducted for three transport formulas, varying

total-load adaptation lengths and bed slope coefficients. The results show the importance of having an accurate sediment transport formula and how errors in the transport formula may lead to different calibration parameters. The bed slope coefficient is shown to be of secondary importance compared to the transport formula and adaptation length. For practical applications, running multiple simulations using different transport formulas and other model settings is recommended to assess the sensitivity of modeling results.

3.4 Test C2-Ex3: Channel infilling and migration: waves perpendicular to flow

3.4.1 Purpose

The CMS was applied to a laboratory case of channel infilling and migration with steady flow and random waves. The case is similar to the previous one except that the waves were parallel to the channel axis (perpendicular to flow). Specific model features tested in this case were:

1. Inline wave-current-sediment coupling,
2. Single-sized non-equilibrium total-load transport model, and
3. Sediment boundary conditions.

The model performance was evaluated using measured water depths and a sensitivity analysis was performed for the total-load adaptation length.

3.4.2 Experiment

Van Rijn and Havinga (1995) conducted a laboratory experiment on the channel morphology change under steady cross-channel flow with waves perpendicular to the flow. The flume was approximately 4 m wide and had 1:10 side slopes. The depth-averaged current velocity and water depth at the inlet were 0.245 m/sec and 0.42 m, respectively. Random waves (JONSWAP form) were generated at a 90 deg angle to the flow and had a significant wave height of 0.105 m and peak wave period of 2.2 sec. The suspended sediment transport rate was measured to be at 0.022 kg/m/sec. Table 15 summarizes the experimental conditions.

Table 15. General conditions for van Rijn and Havinga (1995) experiment.

Parameter	Value
Upstream current velocity	0.245 m/sec
Upstream water depth	0.42 m
Significant wave height	0.105 m
Peak wave period	2.2 sec
Wave direction	90°
Upstream suspended transport rate	0.022 kg/m/sec
Median grain size	0.1 mm

3.4.3 Model setup

For simplicity, the case was simulated as a 1-D problem by ignoring the flume wall effects. The same computational grid used for CMS-Flow and CMS-Wave is shown in Figure 14 with the colors representing the initial bathymetry. The grid had 390 active computational cells and a constant resolution of 0.1 m. A water flux boundary condition was used at the upstream boundary (left side) and a water level boundary at the downstream boundary (right side). The initial condition was specified as zero for water level and current velocity over the whole grid. Equilibrium sediment concentration was specified at the inflow boundary and a zero-gradient boundary condition at the outflow boundary.

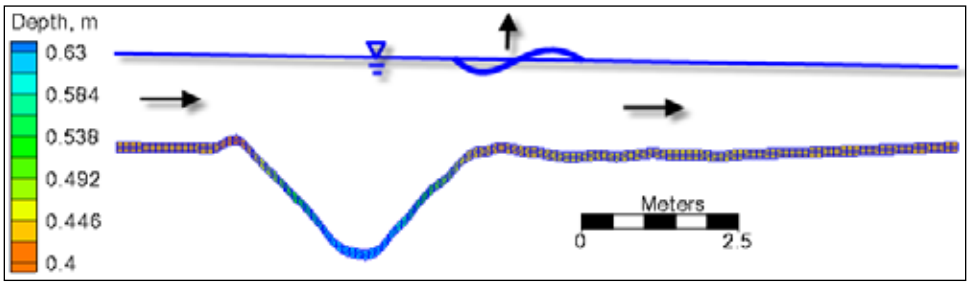

Figure 14. CMS computational grid for the van Rijn and Havinga (1986) test case.

Table 16 shows CMS setup parameters. Default CMS values were used wherever possible. The Manning's coefficient was estimated as 0.02 sec/m$^{1/3}$ by fitting a lognormal distribution to the measured current velocity profile. The suspended-load scaling factor was adjusted based on the measured inflow transport rate and set to 0.67, which is within the generally accepted range of 0.5 to 2.0. Since no measurements for bed load were available, the bed-load transport capacity was not modified. The

transport grain size was set to median grain size so that no hiding and exposure was considered in the simulation. Model result sensitivity to the adaptation length L_t was tested for the values of 0.5, 0.7, 1, and 2 m, as shown in Table 16.

3.4.4 Results and discussion

Figure 15 shows a comparison of the measured and computed bed elevations after 23.5 hr for each adaptation length evaluated. The results are consistent with those obtained by Sánchez and Wu (2011a) with a previous version of the CMS. The model reproduces the overall measured trend of the channel migration and infilling. However, the computed bathymetry is much smoother than the measured bathymetry. This is due to the fact that the model does not simulate the small-scale bed forms.

Table 16. CMS-Flow input settings for the Van Rijn and Havinga (1995) test case.

Setting	Value
Solution scheme	Implicit
Simulation duration	24 hr
Ramp period duration	30 min
Time step	1 min
Manning's coefficient	0.02 sec/m$^{1/3}$
Steering interval	3 hr
Transport grain size	0.1 mm
Transport formula	Lund-CIRP
Bed load scaling factor	1.0
Suspended load scaling factor	0.67
Morphologic acceleration factor	1.0
Sediment fall velocity	0.6 mm/sec
Bed porosity	0.4
Bed slope coefficient	1.0
Total-load adaptation length, L_t	0.5, 0.7, 1, 2 m

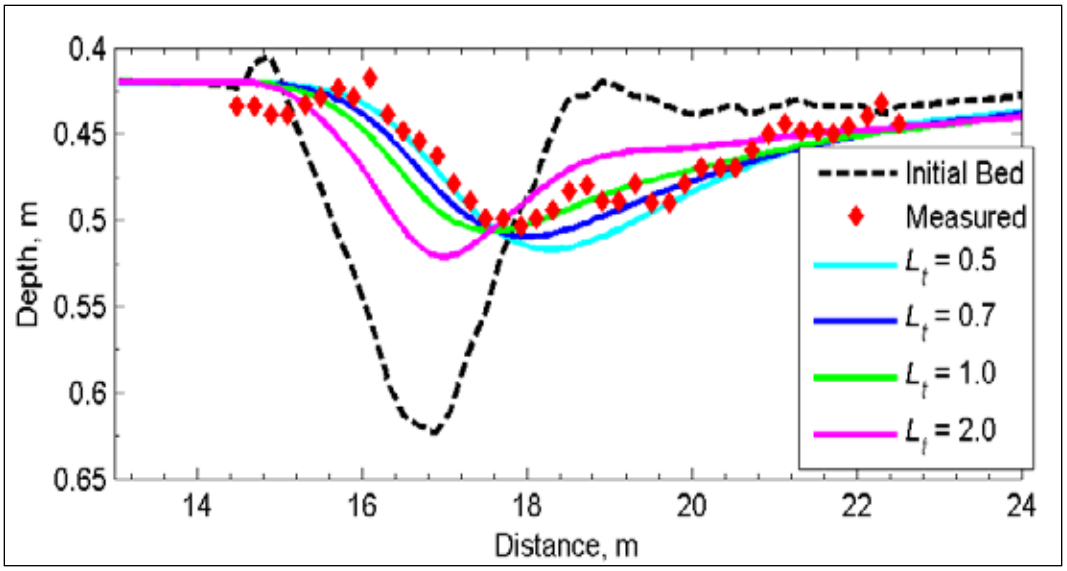

Figure 15. Measured and calculated bathymetry at 23.5 hr with varying total-load adaptation lengths between 0.5 and 2.0 m.

Based on the goodness-of-fit statistics shown in Table 17, the model performance is relatively good. For this case, adaptation lengths of 0.5, 0.7, and 1 m gave similar results. The results show that the model results can be sensitive to the adaptation length. However, once this parameter is calibrated, relatively accurate results may be obtained. This parameter is difficult to estimate because it depends on the vertical structure of currents, sediment concentration, and turbulence, which are difficult to assess with a depth-averaged model.

Table 17. Water depth goodness-of-fit statistics* for the Van Rijn and Havinga (1995) experiment.

Total-load Adaptation Length, m	BSS	NRMSE, %	NMAE, %	R^2	Bias, m
0.5	0.978	15.60	12.55	0.897	0.0071
0.7	0.983	13.85	12.02	0.876	0.0063
1.0	0.976	16.37	12.91	0.754	0.0054
2.0	0.917	30.49	22.91	0.252	0.0039

*defined in Appendix A

3.4.5 Conclusions and recommendations

The CMS model performance in simulating channel infilling and migration was assessed with a laboratory flume experiment case under random waves and steady flow. The waves in this case were perpendicular to the direction

of the flow. Coupled waves, currents, and non-equilibrium sediment transport were simulated with the inline CMS (single code), and computed water depths were compared to measurements. The goodness-of-fit statistics for the water depths indicates good model performance for total-load adaptation lengths from 0.5 to 1.0 m. For practical applications it is important to calibrate the adaptation length using measured morphology changes. Future research will be directed towards better understanding and predicting the adaptation length for a wide variety of conditions.

3.5 Test C2-Ex4: Large-scale sediment transport facility

3.5.1 Purpose

Data from the Large-Scale Sediment Transport Facility provide detailed measurements of wave height, water level, longshore current speed, and sediment transport (bed- and suspended-load) within a controlled laboratory environment. Application of the CMS to this test case demonstrated the model capability of calculating the cross-shore distribution of wave height, longshore current, and sediment transport from the wave breaker zone inshore.

3.5.2 Experimental setup

The Large-Scale Sediment Transport Facility (LSTF) at ERDC (see Figure 16) is capable of simulating oblique (6.5 deg incident angle) regular and random waves, and a uniform longshore current. The longshore current is recirculated from the downdrift end to the updrift end of the LSTF by adjusting a series of 20 pumps in the cross-shore direction, therefore simulating an infinite beach. The test case discussed here represented a natural beach with a uniform longshore current. The experiment was 160 min long and measured the cross-shore distribution of significant wave height, water level, current speed, and suspended-sediment transport. All comparisons here are for Case 1, in which a longshore current was induced by oblique random waves and the pumps were adjusted to match the measured longshore current. Table 18 summarizes the setup for LSTF Case 1.

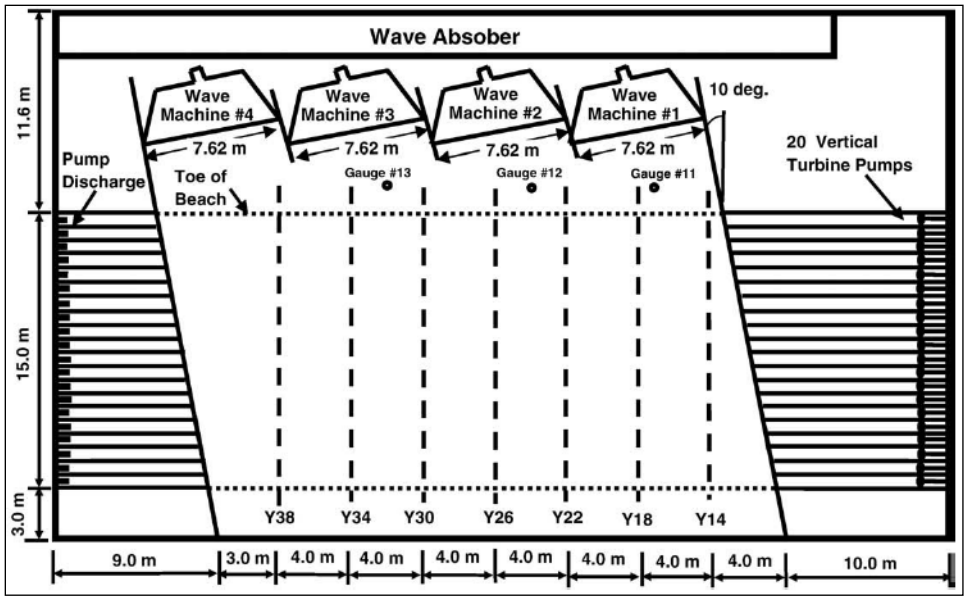

Figure 16. LSTF configuration (Gravens and Wang 2007).

Table 18. Wave and hydrodynamic conditions for LSTF Test Case 1.

Variable	Value
Offshore significant wave height, H_s	0.228 m
Peak period, T_p	1.465 sec
Incident wave angle, Θ_o	6.5°
Water level, η_0	-0.001 m

3.5.3 Model setup

The computational domain was generated based on the interpolation of measured beach profiles from profile Y14 to Y34 (see Figure 16). A constant grid resolution of 0.2 and 0.4 m was used in the cross-shore and longshore directions, respectively. A TMA spectrum was assumed at the offshore boundary with the parameter values γ = 3.3, and n = 100. The offshore water level during the experiment was not equal to the Still Water Level (SWL) because of the wave setup. The offshore water level was approximated for each experiment based on the most offshore water level gauge. Tables 19 and 20 summarize the CMS-Flow and CMS-Wave settings, respectively.

Table 19. CMS-Flow settings for the LSTF test cases.

Setting	Value
Solution scheme	Implicit
Time step	1 min
Wetting and drying depth	0.001 m
Simulation duration	3.0 hr
Ramp duration	2.5 hr
Manning coefficient	0.016 sec/$m^{1/3}$
Transport grain size	0.15 mm
Transport formula	Lund-CIRP, van Rijn, and Soulsby-van RIjn
Sediment porosity	0.4
Morphologic acceleration factor	0.0 (no bed change)

Table 20. CMS-Wave settings for the LSTF test cases.

Setting	Value
Wave breaking	Battjes and Janssen (1978)
Bottom friction	Off
Steering interval	0.25 hr
Roller	On
Roller dissipation coefficient	0.1
Roller efficiency factor	1.0

3.5.4 Results and discussion

Calculated wave heights, depth-averaged current velocities, and water levels are compared with the LSTF center line profile measurements in Figures 17 through 19. Table 21 summarizes the goodness-of-fit statistics for hydrodynamics in Case 1. Wave heights and water levels have normalized errors of 3 to 4 percent and 10 to 12 percent, respectively. Similar results were obtained by Nam et al. (2009). Longshore current calculations have larger errors ranging from 18 to 24 percent. The calculated peak longshore current is slightly offshore from the measured peak. Reducing the roller dissipation coefficient may improve these estimates by moving the peak longshore current closer to the shoreline. Another reason is that the location of the second breaker zone, located at approximately 6 to 7 m from the shoreline, is predicted slightly further offshore, causing the a longshore current peak which is also further offshore.

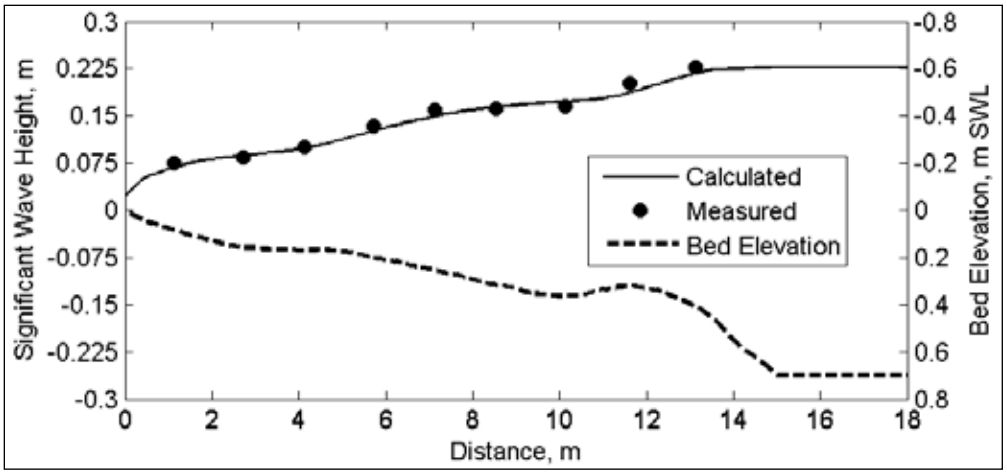

Figure 17. Measured and computed significant wave heights for LSTF Case 1.

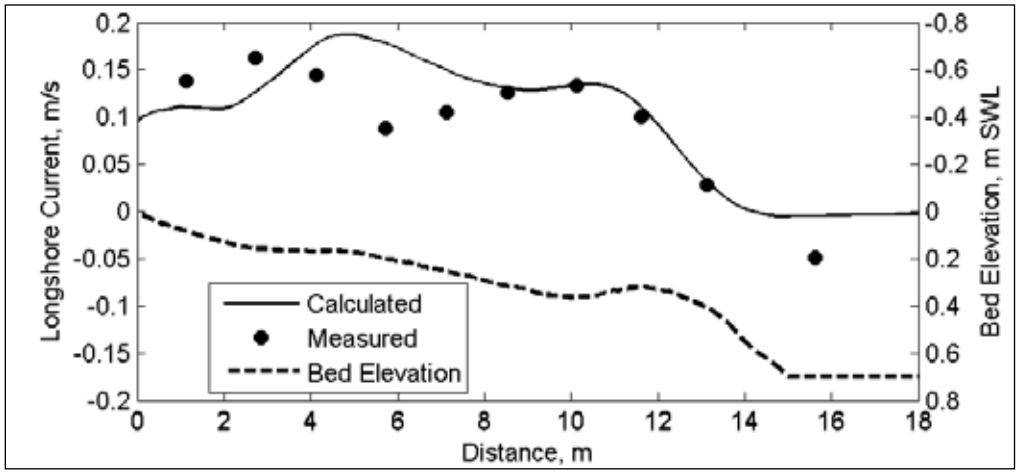

Figure 18. Measured and computed longshore currents for LSTF Case 1.

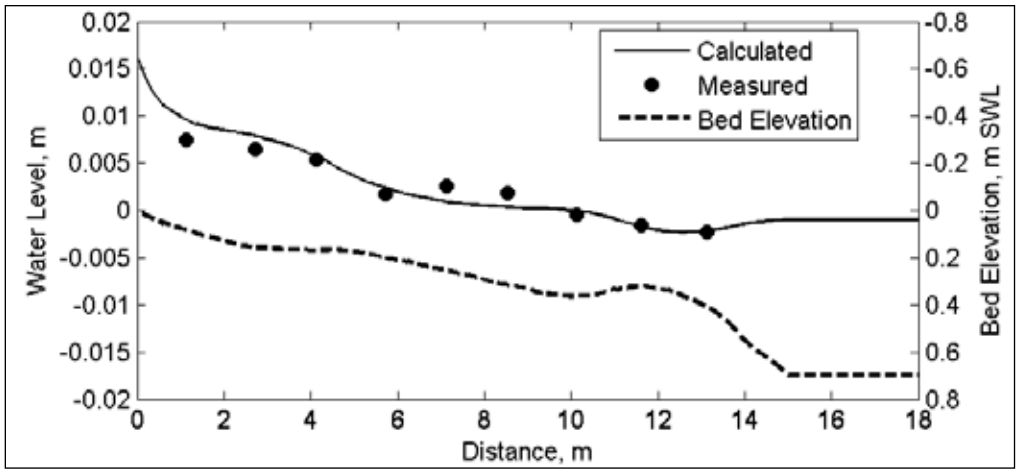

Figure 19. Measured and computed mean water levels for LSTF Case 1.

Table 21. Goodness-of-fit statistics* for waves, water levels and longshore currents in LSTF Case 1.

	H_s	Water Level	Longshore Current
NRMSE, %	3.63	12.18	24.09
NMAE, %	3.15	9.86	18.09
R^2	0.982	0.934	0.665
Bias, m, m/sec	-0.005	0.0001	0.017

*defined in Appendix A

Figures 20 through 22 show comparisons between calculated and measured suspended sediment transport in the longshore direction using three sediment transport formulas: Lund-CIRP (Figure 20), Soulsby-van Rijn (Figure 21), and van Rijn (Figure 22). The measurements show three peaks in the sediment transport magnitudes, one near the offshore bar, another in the middle of the profile where there is a very slight inshore bar, and the greatest value at the swash zone. All three formulations predict well the locations of the two offshore peaks but underestimate the sediment transport near the shoreline. This is due to the fact that the swash zone is not included in the present CMS. Nam et al. (2009) found similar results without the swash zone transport and also obtained significantly improved results by including the swash zone sediment transport. The swash zone sediment transport not only increases the transport in the swash zone but also in the surf zone by acting as a concentration boundary condition to the transport equation in the surf zone.

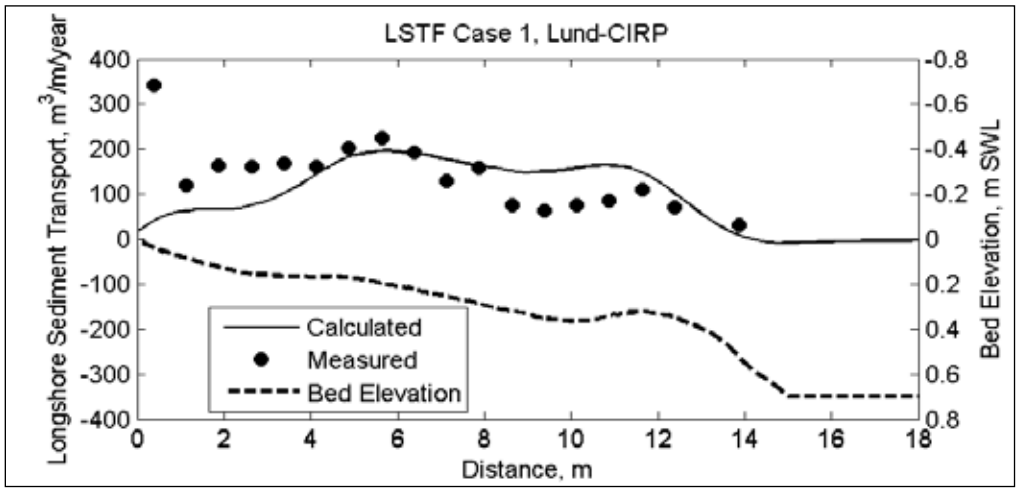

Figure 20. Measured and computed longshore sediment transport rates in LSTF Case 1 using the Lund-CIRP formula.

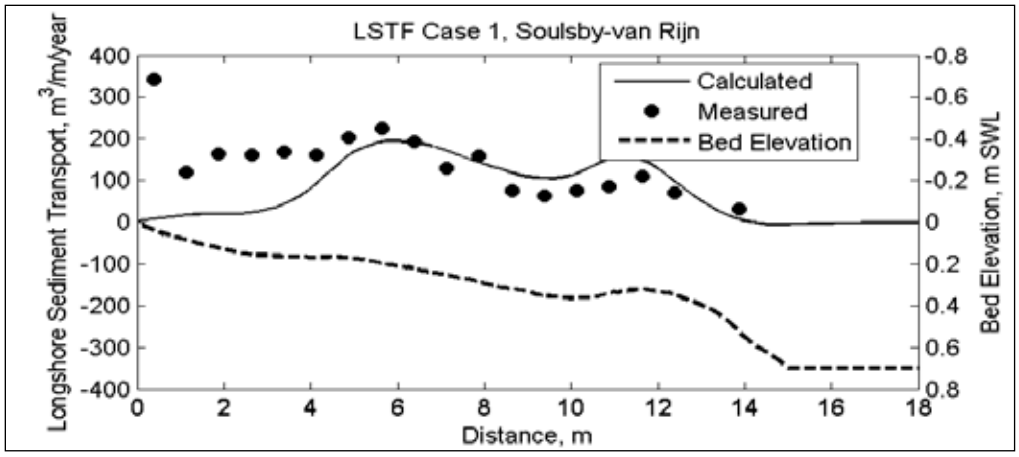

Figure 21. Measured and computed longshore sediment transport rates in LSTF Case 1 using the Soulsby-van Rijn formula.

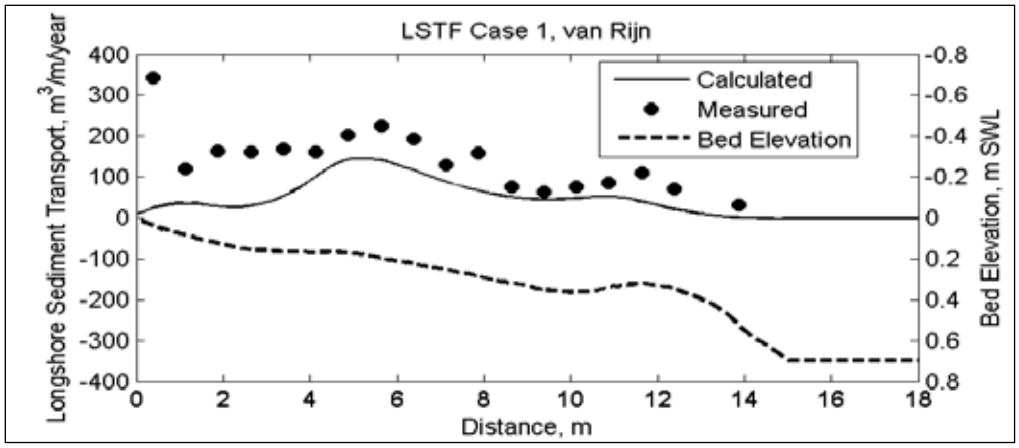

Figure 22. Measured and computed longshore sediment transport rates in LSTF Case 1 using the van Rijn formula.

In the present version of CMS, the wave height and current velocity will always tend to go to zero towards the shoreline, leading to an underprediction of the transport. The Lund-CIRP and Soulsby-van Rijn formulas predict well the magnitude of the transport while the van Rijn formula underpredicts the transport by a factor of about two. It is interesting to note that, even though the location of the peak longshore current is not well predicted, the location of the peak longshore sediment transport is well predicted.

Table 22 summarizes the goodness-of-fit statistics for the sediment transport calculations. All formulas have a negative bias, meaning that they all underpredict the magnitude of the mean sediment transport. Errors range from 22 to 26 percent, 26 to 33 percent, and 35 to 40 percent for the Lund-CIRP, Soulsby-van Rijn, and van Rijn formulations, respectively.

Table 22. Sediment transport goodness-of-fit statistics* for LSTF Case 1.

Statistic	Lund-CIRP	Soulsby-van Rijn	van Rijn
NRMSE, %	25.88	32.02	33.77
NMAE, %	21.99	26.01	29.81
R^2	0.164	0.097	0.567
Bias, $m^3/m/year$	2.79	-23.38	-66.80

*defined in Appendix A

3.5.5 Conclusions and recommendations

The CMS was applied to LSTF Case 1 to compare with measured wave height, longshore current speed, water level, and sediment transport rate. Hydrodynamic comparisons were good, with errors of 3 to 4 percent and 9 to 12 percent for wave height and water level, respectively. Calculated longshore current speed agreed with measurements near the breaker line and into the surf zone, but the calculated peak current speed was offshore from the measurements, resulting in errors ranging from 18 to 24 percent. Calculations of sediment transport were conducted using three different formulas available in CMS. All formulas had a negative bias, meaning that they all underpredicted the magnitude of the mean sediment transport. Errors ranged from 22 to 26 percent, 26 to 32 percent, and 30 to 34 percent for the Lund-CIRP, Soulsby-van Rijn, and van Rijn formulas, respectively. Sediment transport calculations using the Lund-CIRP and Soulsby-van Rijn were in better agreement from the breaker zone to mid-way through the surf zone. All formulas underpredicted sediment transport near the shoreline due to the lack of swash zone processes, which are presently being implemented in CMS. When calibrating the net longshore sediment transport from CMS to estimates from sediment budgets, it is important to take into account that the CMS will tend to underpredict the longshore sediment transport due to the missing swash zone processes. As the LSTF experiments show, the longshore sediment transport in the swash zone can be significant and even larger than that in the surf zone. These tests demonstrate that CMS can be applied to calculate nearshore hydrodynamics and sediment transport within the calculated error bounds.

3.6 Test C2-Ex5: Clear water jet erosion over a hard bottom

3.6.1 Purpose

The CMS was applied to a laboratory case of a clear water jet in a rectangular flume with a sandy bed layer over a hard bottom. The experiment is good for testing the sediment transport model under strong erosion conditions in the presence of a hard bottom.

3.6.2 Experimental setup

Thuc (1991) carried out a movable bed laboratory experiment in a rectangular flume 5-m long and 4-m wide, with a narrow 0.2-m-wide inlet and a 3-m-wide outlet. The initial water depth was 0.15 m, with a 0.16-m layer of sand (d_{50} = 0.6 mm) over a concrete bottom. The estimated sand settling velocity is 0.013 m/sec. Hydrodynamic and sediment parameters for the experiment are summarized in Table 23.

Table 23. Hydrodynamic and sediment conditions for the Thuc (1991) experiment case.

Parameter	Value
Inflow depth-averaged current velocity	0.6 m/sec
Initial water depth	0.15 m
Bed median grain size	0.6 mm
Representative sediment fall velocity	0.013 m/sec
Bed layer thickness	0.16 m

3.6.3 Model setup

The transport equation which best fit the measurements was the Soulsby-van Rijn (Soulsby 1997). No measurements of bed- or suspended-load were available. It was found that the best morphologic results were obtained with bed- and suspended-load scaling factors of 2.0, which are within the typical accepted range of 0.5 to 2.0. The total-load adaptation length was calculated based on a weighted averaged of the bed and suspended-load adaptation lengths. The suspended-load adaptation length was calculated using the Armanini and di Silvio (1986) formula. The bed-load adaptation length was set to the local water depth. The bed slope coefficient was set to 0.5. Sensitivity analysis showed that the results were not sensitive to the bed slope coefficient. The parameters used are listed in Table 24. The model setup and results shown here are the same as those presented in Wu et al. (2010).

Table 24. Hydrodynamic and sediment parameters for the Thuc (1991) experiment case.

Parameter	Value
Solution scheme	Implicit
Time step	30 s
Simulation duration	4.25 hr
Ramp period duration	0.01 hr
Manning's coefficient	0.03 sec/$m^{1/3}$
Transport grain size	0.6 mm
Sediment fall velocity	0.013 m/sec
Sediment density	2,650 kg/m^3
Sediment porosity	0.4
Bed and suspended load scaling factors	2.0
Morphologic acceleration factor	1.0
Sediment inflow loading factor	0.0 (clear water)
Total load adaptation coefficient method	Weighted average of bed and suspended load adaptation lengths
Suspended load adaptation coefficient method	Armanini and di Silvio (1986)
Bed load adaptation length	Equal to local water depth
Avalanching	On

The computational grid (see Figure 23) had a constant resolution in the x-direction of 0.1 m and a variable resolution in the y-direction between 0.0333 and 0.1333 m. The computational mesh consisted of 62 rows and 69 columns. The computational time step was 30 sec. A water flux boundary was applied at the upstream end and a water level boundary was applied to the downstream end. The initial water level and current velocities were set to zero for the whole domain (cold start).

3.6.4 Results and discussion

Figure 24 shows the calculated flow pattern in the domain and bed change contours around the inflow region at the center part of the basin after an elapsed time of 4 hr. Similar results were obtained by Min Duc et al. (2004) and Wu (2004). Erosion occurred due to the inflow of clear water, and the eroded sediment moved downstream and deposited forming a dune feature which migrated slowly downstream. The results show good symmetry about the centerline. Figure 25 compares the measured and calculated bed changes along the longitudinal centerline at 1 and 4 hr. The calculated erosion and deposition depths are in good agreement with the measured data, in particular at time 4 hr. The goodness-of-fit statistics for the computed water depth is shown in Table 25.

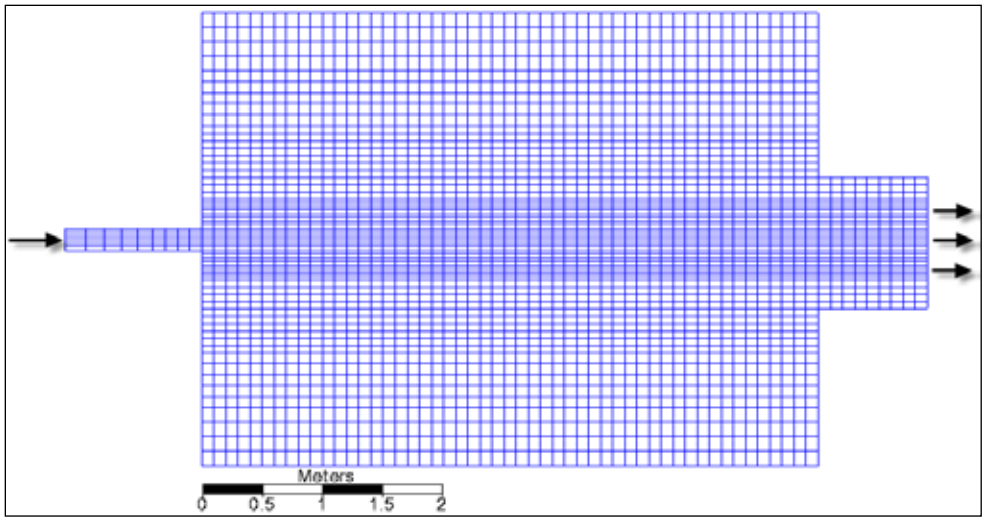

Figure 23. Computational grid for the Thuc (1991) experiment case.

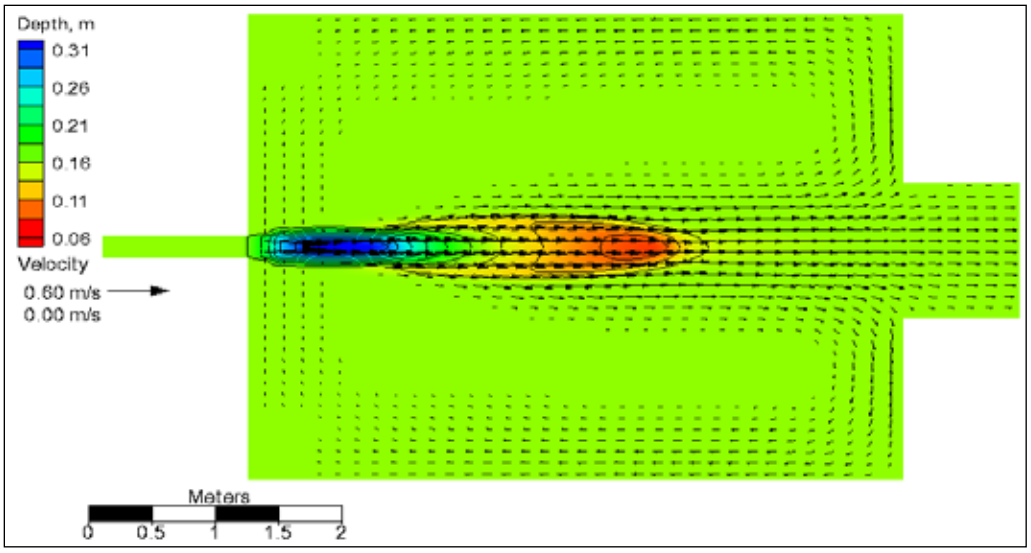

Figure 24. Computed bed elevations and current velocities at 4 hr for the Thuc (1991) test case.

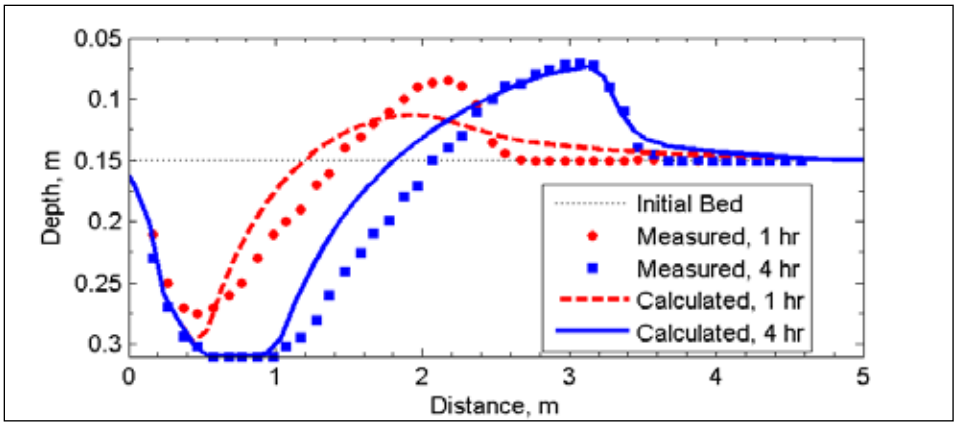

Figure 25. Comparison of calculated and measured bed elevations at 1 and 4 hr for the Thuc (1991) test case.

3.6.5 Conclusions and recommendations

The laboratory experiment of Thuc (1991) was simulated with the CMS. The water depth BSSs calculated at 1 and 4 hr were good and demonstrated excellent model performance, respectively (see Appendix A). The water depth NMAEs were approximately 19 and 6 percent at 1 and 4 hr, respectively. The sediment inflow loading factor was used to apply a clear-water boundary condition. Two important model features were tested, hardbottom and avalanching, both of which performed satisfactorily.

Table 25. Water depth goodness-of-fit statistics* for the Thuc (1991) test case.

Time, hr	BSS	NRMSE, %	NMAE, %	R^2	Bias, m
1.0	0.411	26.95	19.32	0.413	-0.023
4.0	0.941	8.52	5.60	0.956	-0.0012

*defined in Appendix A

3.7 Test C2-Ex6: Bed aggradation and sediment sorting

3.7.1 Purpose

The CMS was applied to three laboratory cases of channel deposition with multiple-sized sediments. The laboratory experiments are useful for testing the non-uniform sediment transport under transcritical flow conditions. The specific model features tested were the multiple-sized sediment transport, bed change, and bed material sorting algorithms.

3.7.2 Experiment setup

Laboratory experiments of bed aggradation and sediment sorting were carried out at the St. Anthony Falls Laboratory (SAFL) by Paola et al. (1992) and Seal et al. (1995). The flume was 45-m long and 0.305-m wide, as shown in Figure 26. A tailgate was used to keep the downstream end at a constant water level. The inflow water flux was 0.049 m^3/sec. The initial bed slope was 0.002. A slightly bimodal mixture of sediments ranging in size from 0.125 to 64 mm was fed into the flume. A summary of the experimental conditions for the three SAFL cases used here is provided in Table 26.

3.7.3 Model setup

The CMS-Flow computational grid for the rectangular flume was 3-cells-wide and 100-cells-long, which were of size 0.5 m by 0.1 m in x- and y-directions, respectively (see Figure 27). A constant flux boundary condition was applied at the upstream end and a constant water level boundary condition was applied at the downstream end of the flume. A 1-hr ramp period was necessary to stabilize the hydrodynamics. During this ramp period, the sediment transport equation was solved but the bed elevation was not updated. In addition, a relatively small time step of 1 sec was necessary to stabilize the flow due to the transcritical flow. A summary of the selected hydrodynamic and sediment transport parameters is presented in Table 27. The laboratory study was simulated as a 1-D problem and the flume wall effects were ignored in the simulation for simplicity and, therefore, wall friction is lumped into the bottom friction. A Manning's roughness coefficient of 0.028 sec/$m^{1/3}$ was estimated based on the measured flow depths and bed slopes.

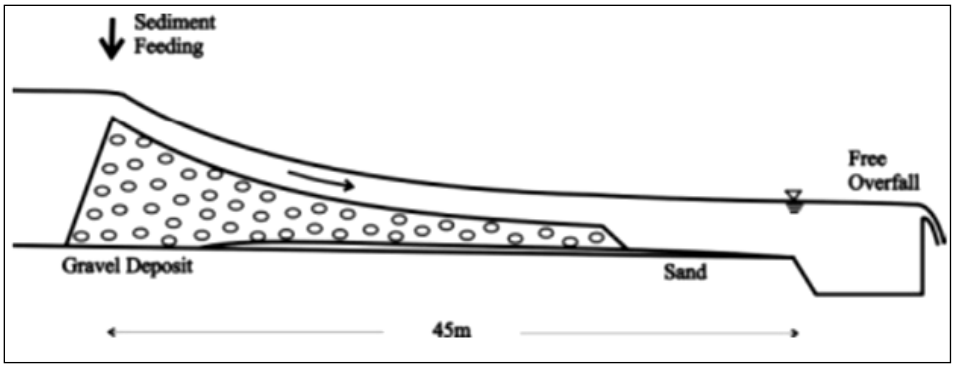

Figure 26.Sketch of the SAFL channel aggradation experiment.

Table 26. Hydrodynamic and sediment conditions for the three simulated SAFL cases.

Variable	Case 1	Case 2	Case 3
Experiment duration, hr	16.83	32.4	64
Inflow discharge, l/sec	49	49	49
Initial bed slope	0.002	0.002	0.002
Downstream water level, m (from bed)	0.4	0.45	0.5
Sediment feed rate, kg/min	11.3	5.65	2.83
Initial d_{50} (50th percentile), mm	5.9	5.9	5.9
Initial d_{90} (90th percentile), mm	33.1	33.1	33.1
Geometric standard deviation, mm	5.57	5.57	5.57

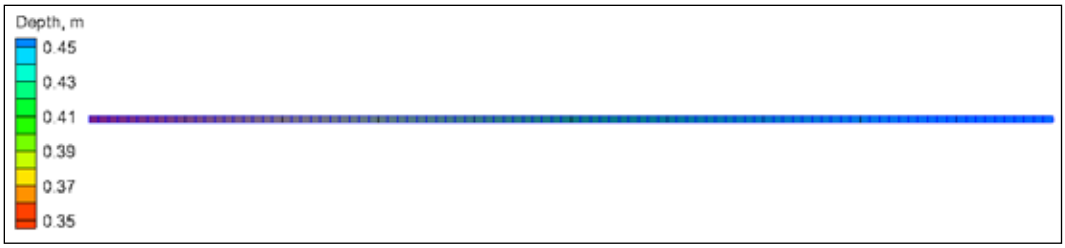

Figure 27.CMS-Flow computational grid for the SAFL test cases.

A fractional sediment transport rate was applied at the inflow boundary using the sediment feeding rate and the grain size distribution shown in Figure 28. The grain size distribution consisted of nine sediment size classes from 0.177 to 45.25 mm. A zero-gradient concentration boundary condition was applied at the downstream end. The initial bed material

Table 27. CMS-Flow settings for the SAFL experiment test case.

Parameter	Value
Time step	1 s
Simulation duration	Case 1: 18 hr Case 2: 34 hr Case 3: 65 hr
Ramp period duration	1 hr
Manning's coefficient	0.028 sec/m$^{1/3}$
Wall friction	Off
Water density	1,000 kg/m^3
Transport formula	van Rijn
Bed slope coefficient	0.0
Number of sediment size classes	9
Porosity	0.3
Sediment density	2,650 kg/m^3
Suspended load scaling factor	1.0
Bed load scaling factor	1.0
Morphologic acceleration factor	1.0
Inflow loading factor	0.9
Morphologic update during ramp period	Off
Total-load adaptation length	0.9 m
Hiding and exposure coefficient	0.2
Minimum bed layer thickness	0.01 m
Maximum bed layer thickness	0.1 m
Number of bed layers	19

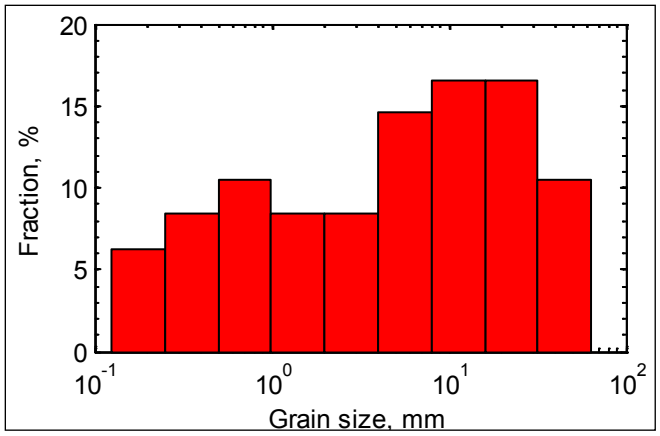

Figure 28.Grain size distribution of the sediment supplied at the upstream end of the flume for the SAFL test cases.

composition was set to the sediment supply distribution. To account for the sediment that rolled backward at the feeding location, an inflow loading factor of 0.9 was applied, meaning 10 percent of the sediment feeding was assumed to role backward. The van Rijn (1984a, b; 2007a, b) transport formula was applied. The transport formula was modified to account for hiding and exposure by multiplying the critical velocity by a correction factor calculated based on Wu et al. (2000).

3.7.4 Results and discussion

Case 2 was chosen for calibration because its hydrodynamic conditions are in between Cases 1 and 3 and is, therefore, the most representative of the group (see Table 26). Cases 1 and 3 were run using the same settings and parameters as Case 2 and serve as model validation.

3.7.4.1 Calibration

Calibration was carried out by first selecting a transport capacity formula and adjusting the bed- and suspended-load transport scaling factors. For simplicity, the same scaling factor was applied to both the bed and suspended load. The van Rijn transport capacity formula with default transport scaling factors of 1.0 was found to provide the best results. Secondly, the total-load adaptation length was adjusted based on the morphology change to 0.9 m, which is very close to other laboratory experiments presented in this report. Lastly, the exponent coefficient used for correcting the critical velocity for hiding and exposure was adjusted to match the measured gain size distribution and was found to be approximately 0.2.

Figure 29 shows a comparison of the calculated and measured bed profiles and water levels for Case 2. The rectangles represent bed layers with colors indicating the median grain size (d_{50}). The corresponding goodness-of-fit statistics are given in Table 28.Calculated bed elevations have normalized errors less than 5 percent and BSSs larger than 0.897. CMS-Flow was able to reproduce the vertical bed aggradation, downstream migration of the depositional fan, the bed slope, and mildly concave bed profile.

The final bed material composition is characterized by coarser (finer) sediments upstream (downstream) and upward (downward) due to selective sediment transport and bed sorting. The water level profile is characterized by a hydraulic jump near the tip of the depositional fan. Calculated water levels were accurate with a NMAE of 3 percent. Interestingly, the bed profile was found to not be significantly sensitive to the hiding and exposure coefficient and was most sensitive to the bed- and suspended-load transport scaling factors, and to lesser extent the total-load adaptation length. The hiding and exposure coefficient did however have a large influence on the bed composition (grain size distribution).

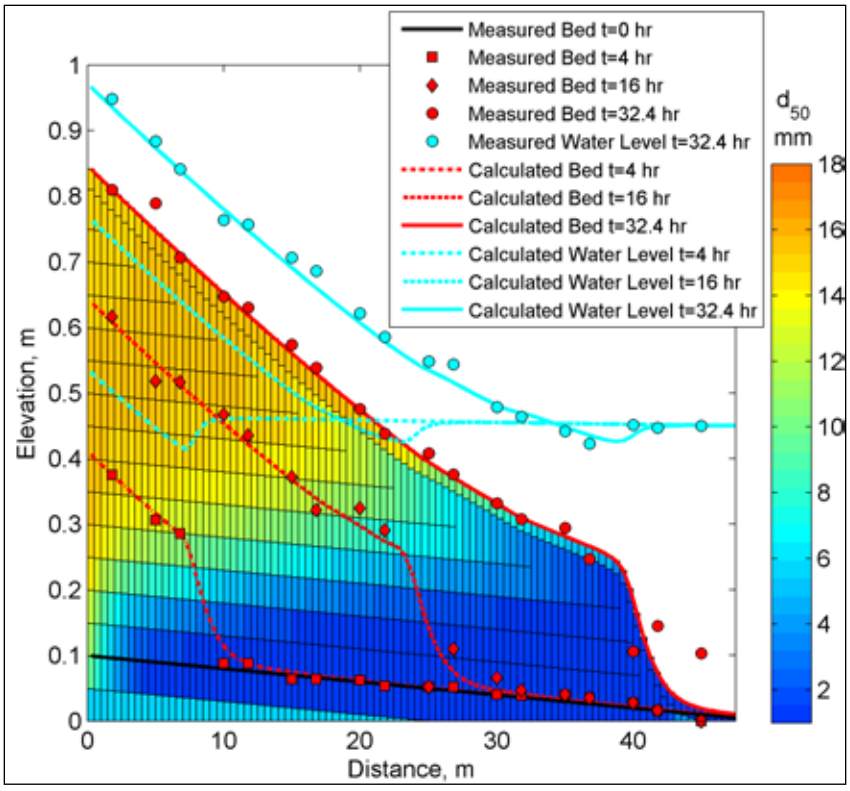

Figure 29. Measured and computed bed elevations and water levels at different elapsed times for the SAFL experiment Case 2. Colored rectangles indicate bed layers with colors corresponding to the median grain size at 32.4 hr.

Table 28. Goodness-of-fit statistics* for the SAFL experiment Case 2.

	Bed level, m			Water Level, m	d_{50}, mm	d_{90}, mm
Time, hr	4	16	32.4	32.4	32.4	32.4
BSS	0.911	0.897	0.920	0.940	0.782	0.067
NRMSE, %	2.28	4.31	4.88	2.58	57.79	35.28
NMAE, %	1.54	2.86	3.02	2.13	53.48	34.04
R^2	0.994	0.984	0.977	0.995	0.549	0.217
Bias	-0.0020	-0.0011	-0.0088	-0.0061	1.1132	4.6798

*defined in Appendix A

Figure 30 compares the calculated and measured bed surface d_{50} and d_{90} at 32.4 hr. There is a noticeable increase in both d_{50} and d_{90} from the initial bed size. Measured d_{50} grain size shows a downstream fining from approximately 16 to 12 mm, while d_{90} shows a larger downstream decrease from approximately 55 to 30 mm. The calculated d_{50} grain size has a NMAE, BSS, and R^2 of approximately 53 percent, 0.78, and 0.55, respectively.

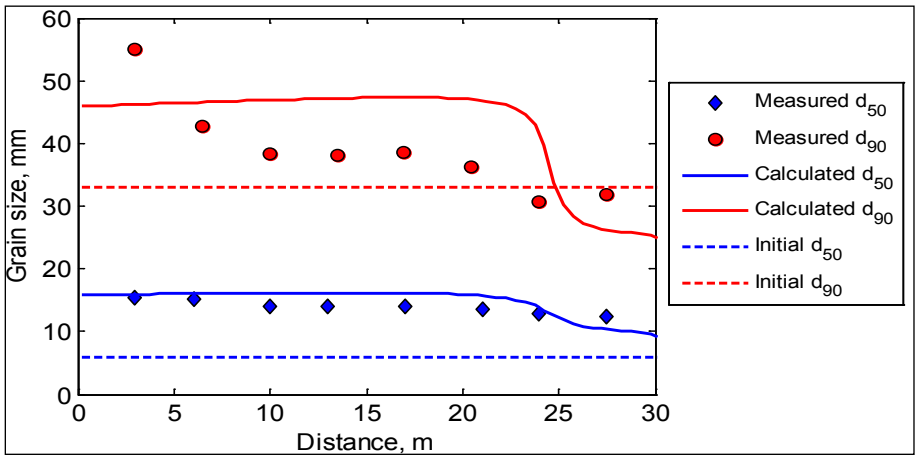

Figure 30. Measured and computed d_{50} and d_{90} grain sizes for the SAFL Case 2.

The d_{50} bias is approximately one third the measure data range. The calculated d_{90} grain size has a lower NMAE of 34 percent compared to d_{50}, but has a lower BSS and R^2 but a smaller NMAE. The d_{90} bias of 4.7 mm is approximately one fifth the measured data range. Both the calculated d_{50} and d_{90} show a slight increase up to about 14 to 16 m downstream followed by a relatively steep decrease. The reason for this is not understood and further investigation is needed. However, it is interesting to note that the measured d_{90} grain size also shows a slight increase from 10 to 17 m. The bed composition however, was sensitive to the hiding and exposure correction factor.

One possible reason why the bed composition was not sensitive to the bed and suspended transport scaling factors is because the same values were applied to all grain sizes. It is expected that improved grain size distributions can be obtained with grain-size-dependant transport scaling factors. However, since no fractional sediment transport rates were available, it was not possible to estimate these factors. For most practical applications, detailed fractional sediment transport rates are not available and, therefore, using constant transport scaling factors is sufficient.

3.7.4.2 Validation

The calculated and measured bed profiles and water levels for the validation Case 1 are presented in Figure 31. Case 1 corresponds to the experiment case with the largest sediment feeding rate and lowest tail gate water level. The corresponding goodness-of-fit statistics are given in Table 29. Similar to Case 2, the calculated bed elevations have normalized errors less than 4 percent and BSSs between 0.87 and 0.924. CMS-Flow was able to reproduce the bed slope and mildly concave bed profile.

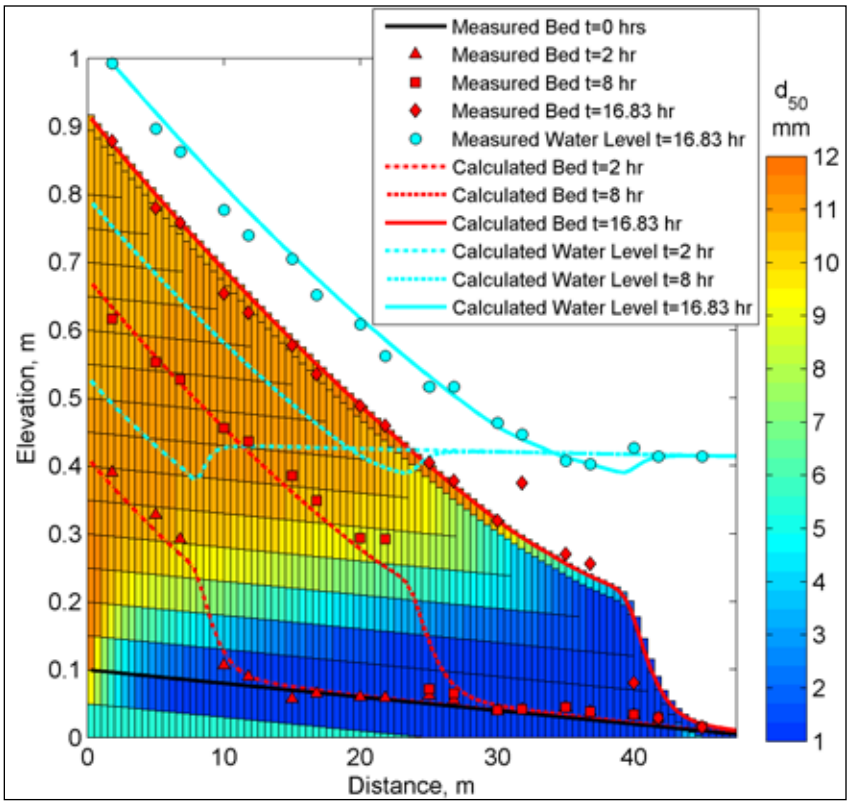

Figure 31. Measured and computed bed elevations and water levels at different elapsed times for the SAFL experiment Case 1. Colored rectangles indicate bed layers with colors corresponding to the median grain size at 16.83 hr.

Table 29. Goodness-of-fit statistics* for the SAFL Case 1.

	Bed level, m			Water Level, m	d50, mm	d90, mm
Time, hr	2	8	16.83	16.83	16.83	16.83
BSS	0.870	0.914	0.924	0.928	-3.78	-0.838
NRMSE, %	3.54	3.74	3.90	3.07	156.19	53.93
NMAE, %	2.90	2.62	2.44	2.36	152.22	47.50
R2	0.990	0.989	0.982	0.995	0.129	0.888
Bias	-0.0058	-0.0031	0.0062	0.0077	5.92	10.14

*defined in Appendix A

The vertical bed aggradation and downstream migration of the depositional fan were slightly over predicted. Similarly to Case 2, the bed material composition is characterized by coarser (finer) sediments upstream (downstream) and upward (downward) due to selective sediment transport and bed material sorting.

The calculated upstream water levels and downstream location of the hydraulic jump were over predicted slightly due to the over predicted bed elevation and deposition fan migration, respectively. However, in general, the water level goodness-of-fit statistics indicate good model performance with a BSS of 0.928, a NMAE of 2.36 percent, and R^2 of 0.995.

The calculated and measured bed surface d_{50} and d_{90} for Cases 1 are shown in Figure 32.The corresponding goodness-of-fit statistics are given in Table 29. Surprisingly, the measured d_{50} is approximately the same as the initial d_{50}. The calculated d_{50} is over predicted, closer to that of Case 2, at around 11 mm, and has a slight increase before decreasing at a distance of approximately 25 m. The calculated d_{90} is within the measured range upstream (x<5 m) but shows an opposite trend to the measurements by increasing downstream. It is possible to improve the grain size distribution by changing the hiding and exposure coefficient, and further tests are needed to test this hypothesis.

The calculated and measured bed profiles and water levels for the validation Case 3 are presented in Figure 33. Case 3 corresponds to the experiment case with the smallest sediment feeding rate and highest tail gate water level. The corresponding goodness-of-fit statistics are given in Table 30. Case 3 has the largest normalized errors of the three cases and range from 1.74 to 7.62 percent. The BSS range from 0.874 to 0.963 which indicate excellent model performance. The upstream vertical bed aggradation was slightly under predicted at 64 hr and led to an under prediction of the water elevation.

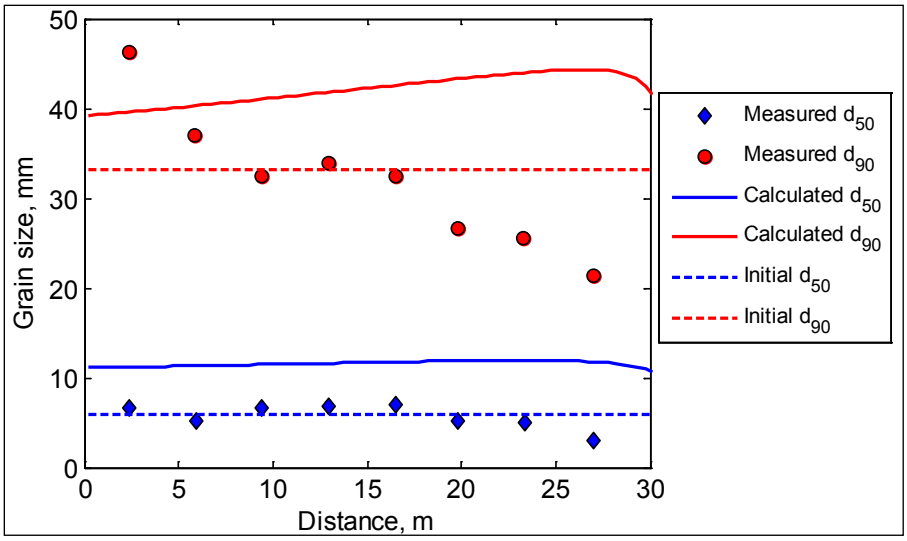

Figure 32. Measured and computed d_{50} and d_{90} grain sizes for the SAFL Case 1.

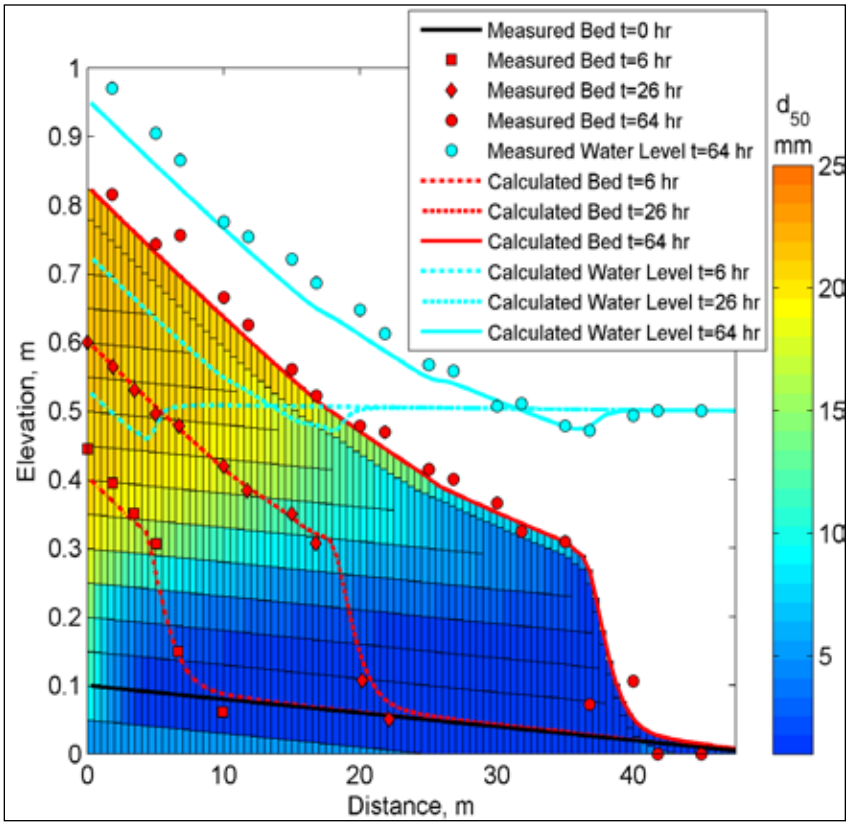

Figure 33. Measured and computed bed elevations and water levels at different elapsed times for the SAFL experiment Case 3. Colored rectangles indicate bed layers with colors corresponding to the median grain size at 64 hr.

Table 30. Goodness-of-fit statistics* for the SAFL Case 3.

	Bed level, m			Water Level, m	d_{50}, mm	d_{90}, mm
Time, hr	6	24	64	64	64	64
BSS	0.874	0.963	0.881	0.867	0.679	0.005
NRMSE, %	7.62	2.35	6.34	5.44	30.41	37.71
NMAE, %	6.67	1.74	3.73	4.26	25.17	31.93
R^2	0.987	0.998	0.961	0.994	0.673	0.699
Bias	-0.0165	0.0071	-0.0033	-0.0188	-1.15	-6.63

*defined in Appendix A

The downstream migration of the depositional fan, bed slope, and mildly concave bed profile were well simulated. Similar to the previous cases, the water level profile is characterized by a hydraulic jump near the tip of the depositional fan. CMS water levels were accurate within approximately 4 percent of the measurements.

The calculated d_{50} for Case 3 on the other hand shows a larger downstream fining while the d_{90} shows a larger downstream decrease from approximately 55 to 30 mm. The calculated d_{50} grain size has a NMAE, BSS, and R^2 of approximately 25 percent, 0.679, and 0.673, respectively. The calculated d_{90} grain size has a lower NMAE of 34 percent compared to d_{50}, but has a lower BSS and R^2 but a smaller NMAE. The d_{90} bias of 4.7 mm is approximately one fifth the measured data range. Similar to the Case 2, the calculated d_{50} and d_{90} for Case 3 exhibit a slight increase up to about 14 to 16 m downstream followed by a relatively steep decrease, the cause of which is unknown. On the other hand, the measured d_{90} grain size also shows a slight increase from 10 to 17 m.

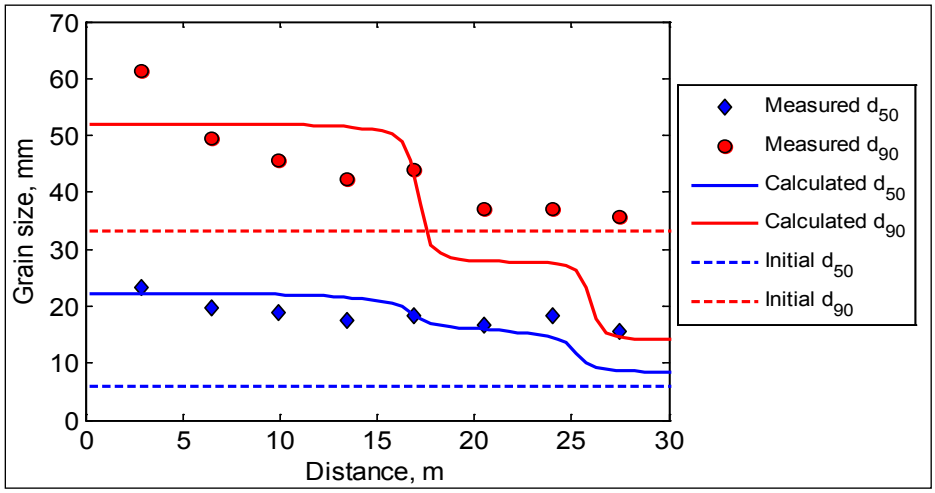

Figure 34. Measured and computed d_{50} and d_{90} grain sizes for the SAFL Case 3.

3.7.5 Conclusions and recommendations

The CMS non-uniform sediment transport model was calibrated and validated using three laboratory experiments of channel aggradation. One experiment was used for calibration and the other two for validation. The experiments are useful for evaluating the performance of the non-uniform sediment transport model under transcritical flow conditions. The upstream increase in bed elevation, downstream migration of the depositional fan, and mildly concave bed profile were well simulated. Bed elevations and water levels were reproduced with a NMAE of approximately 3 and 2 percent, respectively. Results for d_{50} and d_{90} varied but in general the model reproduced the downstream fining. Further analysis is necessary to study the influence of the transport scaling factors, and hiding and exposure coefficient, on the bed composition.

When using the advanced multiple-sized sediment transport option in CMS, it is recommended to calibrate starting with the transport scaling factors and then the total-load adaptation length, as in the case of single-size sediment transport. If measurements of grain size distributions are available, then the hiding and exposure coefficient should be calibrated next. In this study a value of 0.2 for the exponent provided the best results using the van Rijn (1984a, b; 2007a, b) transport formula with a hiding and exposure correction based on Wu et al. (2000).

4 Field Studies

4.1 Overview

Cases presented in this chapter compare CMS calculations to three field studies of non-uniform sediment transport and morphology change: (a) channel infilling at Shark River Inlet, NJ (Test C3-Ex1), (b) ebb shoal morphodynamics at St. Augustine, FL (Test C3-Ex2), and (c) nearshore morphodynamics at Grays Harbor, WA (Test C3-Ex3). Specific model features tested are: (a) inline wave-current-sediment coupling, (b) multiple-sized sediment transport, and (c) non-erodible hardbottom.

4.2 Test C3-Ex1: Channel infilling at Shark River Inlet, NJ

4.2.1 Purpose

This application compares the morphology change calculated with the CMS over a 4-month period to measurements of channel profiles and total infilling volume at Shark River Inlet, NJa dual-jetty coastal inlet system. Because of adjacent beach nourishment that provided a surplus of sand in the littoral system, Shark River had an increasing dredging requirement on time intervals roughly equal to 4-month cycles by 2009. Full documentation of the study is provided by Beck and Kraus (2010). Validation with measured water levels in Shark River Estuary and currents along three inlet channels during a tidal cycle is documented in the companion report Sánchez et al. (2011). This section focuses on model setup and validation to channel infilling, providing insights into CMS morphologic capability on time scales corresponding to dredging cycles.

4.2.2 Model setup

The model domain for the CMS covered a local scale of approximately 11 km centrally located around Shark River Inlet (Figure 35). Two separate grids were used for CMS-Flow and CMS-Wave covering the same alongshore distance with the ocean extending seaward 8.5 km for CMS-Wave and 3.5 km for CMS-Flow. The grid was oriented parallel to the shoreline. A telescoping grid was developed with 8-m cell resolutions within the main throat of the inlet, extending out to 128-m cell size in the ocean. Resolution around the groins and beach was kept to a 16-m cell size. The total of active ocean cells was approximately 20,000.

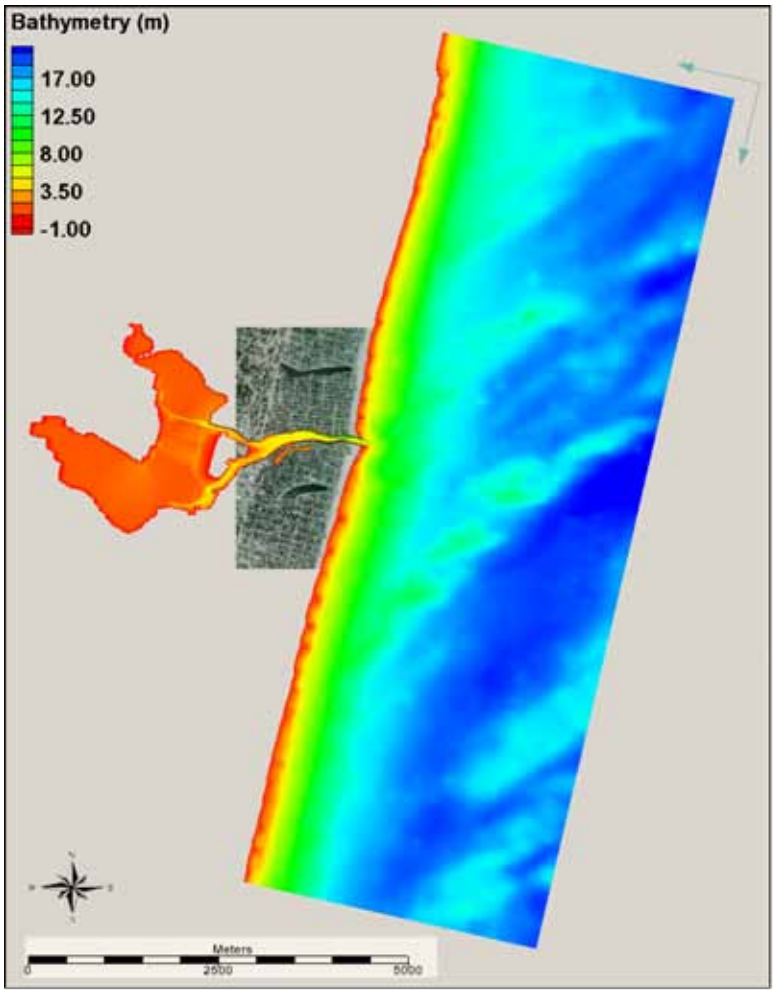

Figure 35. CMS model domain for the Shark River Inlet field case.

Bathymetry needed to develop the backbay, entrance channel, and ocean was assembled from several datasets and converted to mean sea level (MSL) as given by the local tidal datum for Long Branch, NJ (NOAA). Bay bathymetry consisted of data collected by the USACE and State of New Jersey. The nearshore and ocean bathymetric datasets were a combination of 2005 LIDAR (NOAA) and the National Geodetic Data Center's Coastal Relief Model (NOAA).

CMS-Flow was driven with measured open ocean tide (water surface elevation) from a tidal gage at Sandy Hook, NJ, approximately 30 km north of Shark River Inlet. Due to the constricted nature of the main channel for Shark River Inlet from multiple shoals and bridge crossings, Manning's coefficient was modified to account for this increase in flow drag and improved the current velocity calibration. Manning's coefficient was set to 0.02 sec/$m^{1/3}$ in the surfzone.

Wave data from Wave Information Study (WIS) station 129 provided input parameters for generating spectral waves for CMS-Wave. After analyzing the 20-year wave hindcast, a representative year (1990) was chosen to force the model. The wave grid boundary was located at 26 m, the water depth of the hindcast station.

The multiple-sized sediment transport model of CMS was used to represent the various grain sizes being transported, and include the significant impact of sediment hiding and exposure. Five transport grain sizes were used and the initial bed composition was defined by assuming an initial log-normal grain size distribution, and specifying an initial geometric standard deviation σ_g = 1.8 mm and median grain size d_{50} = 0.26 mm. Using the multiple-sized sediment transport reduced scour within the channel thalweg, and accurately represented the spatial distribution of sediment observed in this region.

Bed change was calculated over the same sediment transport time step, which was 15 min, and updated in both the wave and flow models. Bed change was updated in the wave model on the steering interval of 3 hr. An existing condition from a recent January 2009 bathymetry formed the basis to generate a grid for a contemporary representation of the inlet after dredging, and was used to calibrate the model.

Morphologic response was calibrated to the measured change from January - April 2009, a typical recent dredging interval. Empirically derived coefficients for sediment transport were modified within the model to calibrate to sediment transport rates available for the region. The model results for sediment transport are largely dependent on the wave forcing, and therefore the calculated morphology change is driven by the quality of wave input. Because measured wave data are not available for the area, the WIS hindcast waves that were selected do not coincide to the modeled time periods (January - April 2009), but they do represent an average January to April time period. Finally, bed- and suspended-load scaling factors of 2.0 were calibrated to match the channel infilling estimates which are within the generally accepted range of 0.5 to 2.0.

The Non-Equilibrium Total-load sediment transport calculation method (NET) was used in CMS for this test case. Total-load adaptation lengths of 1, 2, 3, 4, 5, 10, and 100 m were tested. A total-load adaptation length of 100 m was selected for the final calculations because it produced the most

realistic patterns and volumetric changes compared to measurements. A summary of the selected CMS setup parameters is shown in Table 31, calibrated using the dredged pit channel infilling rate. Additional details on the model setup for this test case are given by Beck and Kraus (2010).

Table 31. CMS setup parameters for the field case of Shark River Inlet, FL.

Parameter	Value
Solution scheme	Implicit
Simulation duration	4 months
Ramp period	12 hr
Hydrodynamic time step	15 min
Manning's coefficient (flow only)	0.02 – 0.06 sec/$m^{1/3}$
Steering interval	3 hr
Initial median grain size	0.26 mm
Initial geometric standard deviation	1.8 mm
Transport formula	Lund-CIRP
Bed load scaling factor	2.0
Suspended load scaling factor	2.0
Total-load adaptation length	100 m
Morphologic acceleration factor	1.0
Bed porosity	0.3
Bed slope coefficient	0.1

4.2.3 Results and discussion

Figure 36 shows a comparison of actual and calculated morphology changes within the dredged region of the channel after a 4-month simulation. Based on the surveys, channel infilling volume expected for the 4-month simulation is 8,900 m^3 for the entrance channel alone. The 4-month simulation produced a similar channel infilling volume of 9,200 m^3 (NMAE of 3.4 percent) (Table 32). Erosional patterns (blue) along the nearshore to the north and south of the inlet were also captured well by the model.

Even though the model was calibrated to match the measured channel infilling volume, a comparison of measured and calculated water depths along the transects (see Figure 36) showed a high agreement with NMAE values of 7, 11, 2, 4, and 6 percent for transects (arcs) 1 to 5 (see Figures 37 through 41), respectively. Transects 1 and 2 represent the along channel sedimentation patterns in the direction of currents. Both transects extend

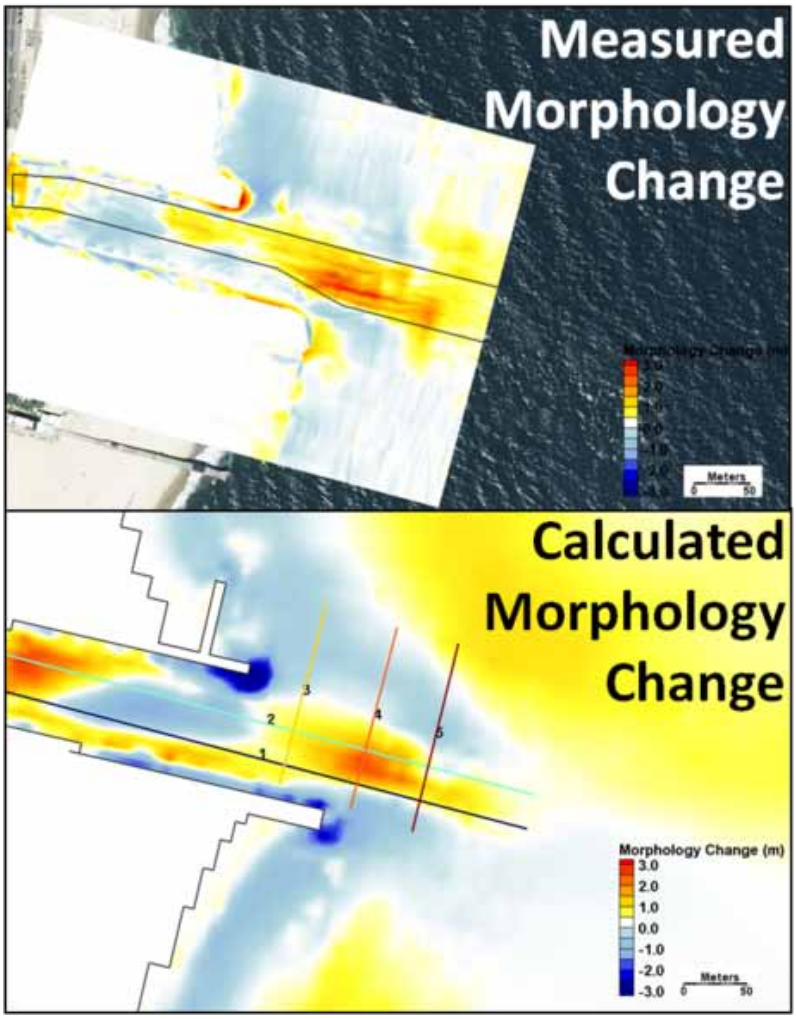

Figure 36. Measured (top) and calculated (bottom) morphology change for a 4-month period (January-April 2009) at Shark River Inlet, FL.

Table 32. Measured and calculated volume changes for dredged channel, Shark River Inlet.

Measured Volume, m^3	Calculated Volume, m^3	NMAE*, %
8,900	9,200	3.4

*defined in Appendix A

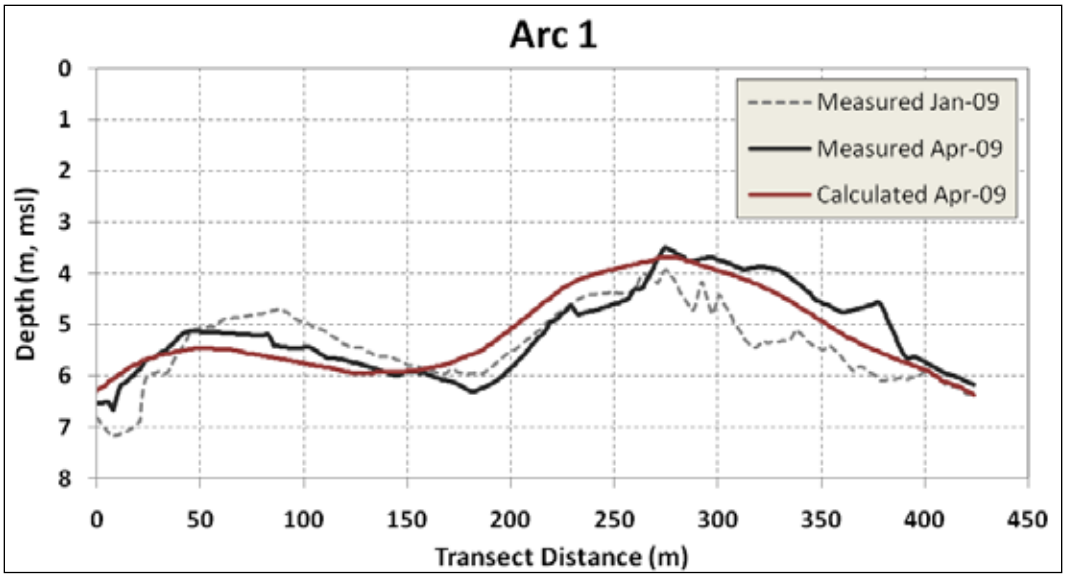

Figure 37. Measured and calculated bathymetry across Arc 1 (transect) at Shark River Inlet, FL; RMAE=7% (see Figure 33 for location of arc). Distance is measured from west to east.

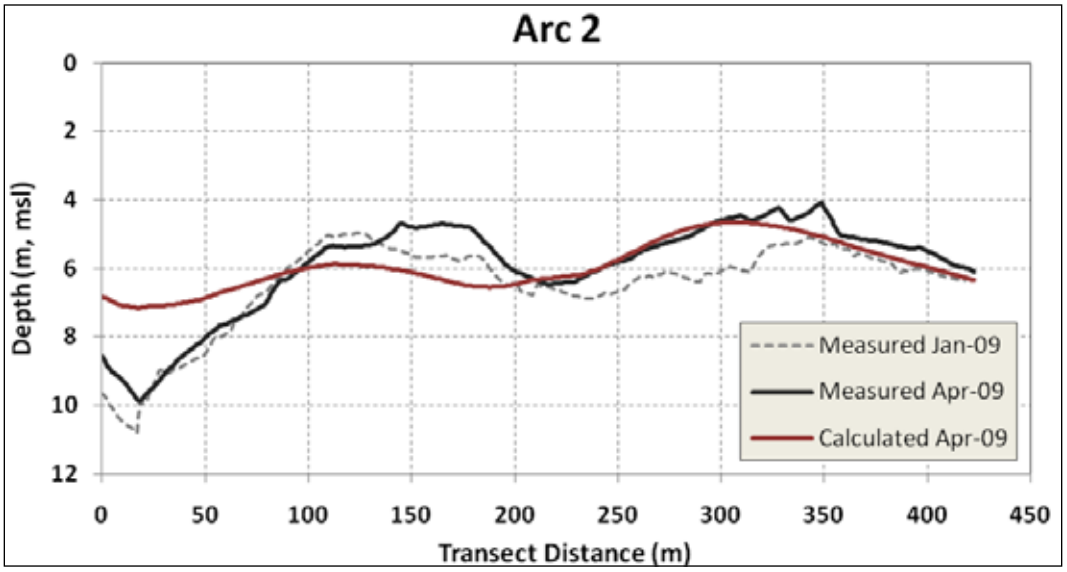

Figure 38. Measured and calculated bathymetry across Arc 2 (transect) at Shark River Inlet, FL; RMAE=11% (see Figure 33 for location of arc). Distance is measured from west to east.

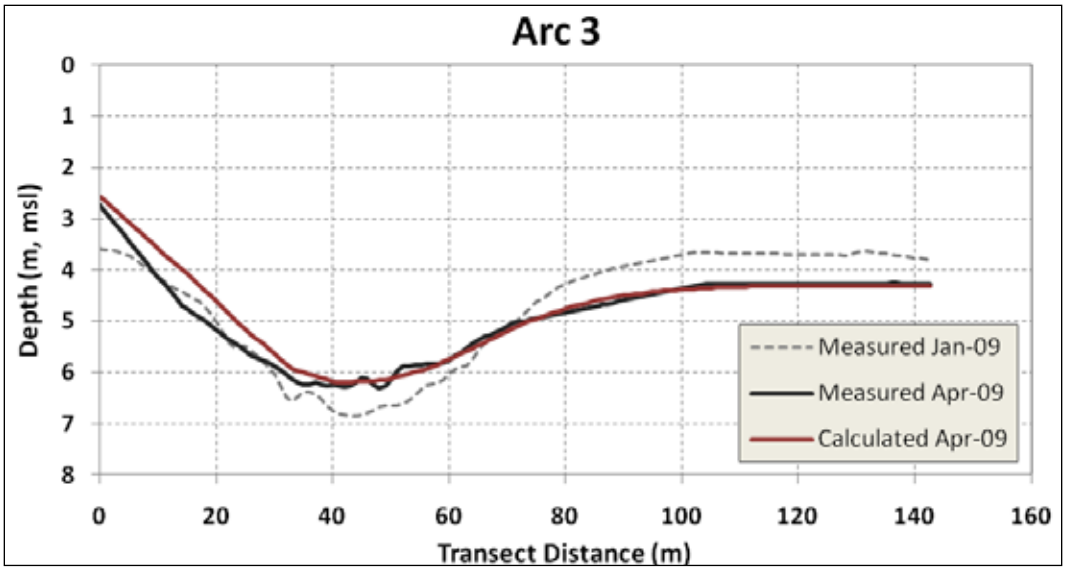

Figure 39. Measured and calculated bathymetry across Arc 3 (transect) at Shark River Inlet, FL; RMAE=2% (see Figure 33 for location of arc). Distance is measured from south to north.

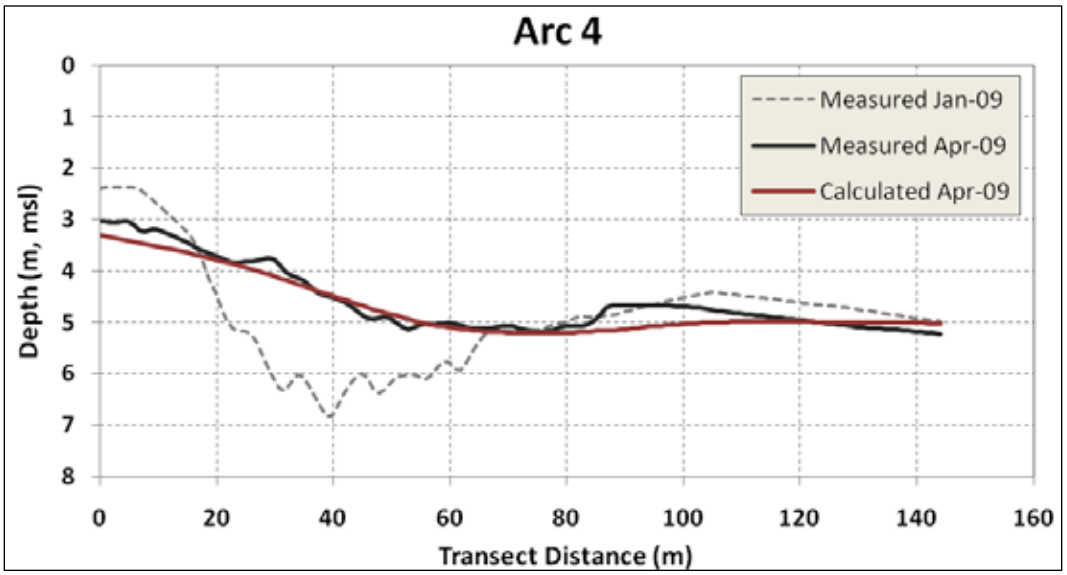

Figure 40. Measured and calculated bathymetry across Arc 4 (transect) at Shark River Inlet, FL; RMAE=4% (see Figure 33 for location of arc). Distance is measured from south to north.

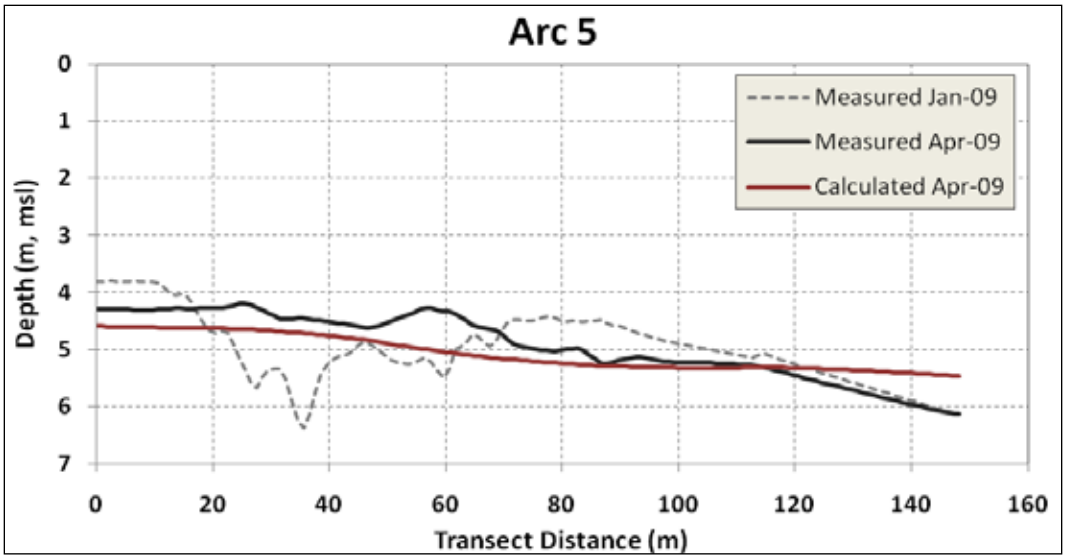

Figure 41. Measured and calculated bathymetry across Arc 5 (transect) at Shark River Inlet, FL; RMAE=6% (see Figure 33 for location of arc). Distance is measured from south to north.

from the bridge pilings eastward toward the ocean, as indicated by the deep thalweg (~20 m transect distance) and the two shoals within the channel. Transect 3 is located within the jettied part of the channel, and illustrates a smaller scale of change in deposition in the center of the channel and some deflation of the northern nearshore area adjacent to the north jetty. Transect 4 best illustrates the model comparison to the measured channel infilling at the location of greatest change. Calculated and measured values were very close and resulted in a good agreement with an NMAE of 4 percent. Transect 5 also had a good agreement demonstrating the model's capability to reproduce natural sedimentation rates over the dredged channel.

The non-uniform sediment is transported and deposited as a function of its grain size through the simulation. The model outputs the changing distribution through a d_{35}, d_{50}, and d_{90}. The median grain size d_{50} is shown in Figure 42, and illustrates the modification of the median grain size from 4 months of simulated selective sediment transport. In areas that experienced the greatest velocities, the inlet throat and main channels, d_{50} values were highest at around 0.4 to 0.5 mm corresponding to regions with thalweg sedimentation patterns. This also included the nearshore areas and around the groin fields and jetties. The smallest d_{50} values are found in areas of low energy or velocities, and tend to be at the distal end of channels. This distribution of sediment agrees with qualitative understanding that coarser sediment tends to remain in higher energy regions, whereas finer sediment is deposited in relatively quiescent areas.

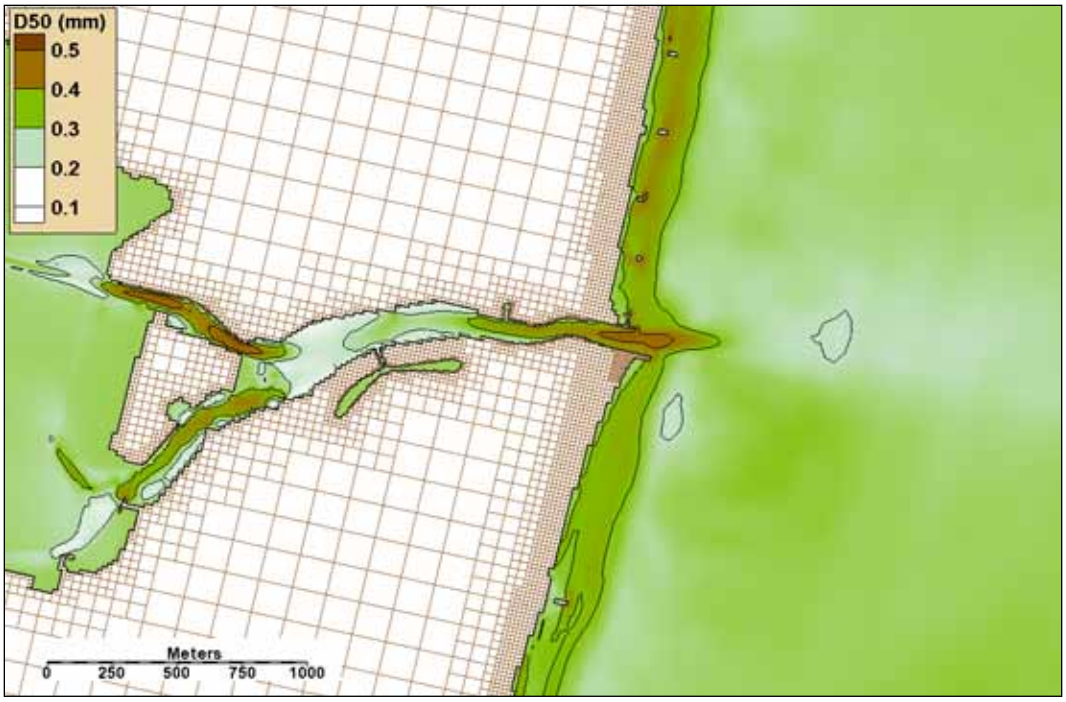

Figure 42. Final median grain size distribution after a 4-month simulation showing general agreement of coarse and fine sediment in high- and lower-energy zones, respectively.

4.2.4 Conclusions

The CMS was applied to a coastal dual-jettied inlet with wave and tidal forcing. Hindcast wave data were provided to CMS-Wave at an offshore station, and tidal forcing was provided from a gage 30 km north of the project site. Calculations presented herein demonstrated the CMS performance and capability in simulating channel infilling under combined wave-tidal forcing. Total infilling volume during a 4-month simulation, the time period between dredging, agreed with the total measured volume with a NMAE of 3.4 percent. The model performance was also tested using the water depth at selected transects. Two transects along the axis of the channel and three transects across-channel agreed with calculated transects with Root Mean Absolute Errors between 2 to 11 percent. Calculation of sediment grain size distribution during the 4-month simulation agreed qualitatively with general knowledge. That is, the CMS calculated armoring of more energetic regions with coarser sediment and deposition of finer sediment in quiescent regions. This application demonstrates the ability of CMS to accurately calculate channel infilling on engineering time scales typical of dredging intervals. Total magnitude and distribution of the shoaled sediment within the coastal navigation channel under the combined influence of waves and currents agreed with measurements with errors less than 11 percent.

4.3 Test C3-Ex2: Ebb shoal morphology change at St. Augustine Inlet, FL

4.3.1 Purpose

The CMS was validated with measured ebb shoal morphology change over a 1.4-year period at St. Augustine Inlet, FL, in a study of ebb tidal shoal evolution in response to mining by the U.S. Army Engineer District, Jacksonville (SAJ 2010). Validation of CMS to measured water level and current speed data is documented in V&V Report 3. This application here demonstrates the capability of CMS to calculate evolution of inlet ebb shoal morphology as forced by combined waves and currents. Full documentation of the study is provided by SAJ (2010).

4.3.2 Model setup

Two CMS grids were developed for representing St. Augustine Inlet; one for CMS-Wave and another for CMS-Flow. The lateral extent of the CMS-Flow grid was determined through initial calibration of the hydrodynamics to resolve the appropriate bay boundaries for comparison to measured tidal prism. Additionally, the lateral extent (23.5 km) of the grids was defined to include several focus areas of shoreline to the north and south of the inlet. The offshore extent (9 km) of the grids was set to the offshore location of the wave forcing data. The finest resolution of the CMS-Flow model grid was 15 m in the inlet throat, and 30 m in the main bay channels, ebb-tidal delta, and nearshore. Maximum cells sizes in the bay reached 120 m over large open bay expanses, and increased to 240 m along the offshore boundary (Figure 43).

Hydrodynamics and sediment transport were solved using the implicit time marching scheme of CMS-Flow. A tidal constituent boundary condition was applied at the offshore CMS-Flow boundary.

Spatially variable sediment grain sizes were incorporated in the CMS where data existed over the beach, nearshore, and ebb-tidal delta. Sediment grain size data presented in a study by PBS&J (2009) were used as a baseline to delineate the general d_{50} values. Though no record exists of sediment grain sizes for the inlet throat, Jacksonville District geologists confirm that the channel thalweg is armored with large shell fragments (typical of Florida tidal inlets). Zarillo (2008) analyzed beach sediment from St. Johns County, FL, and found that grain sizes are generally

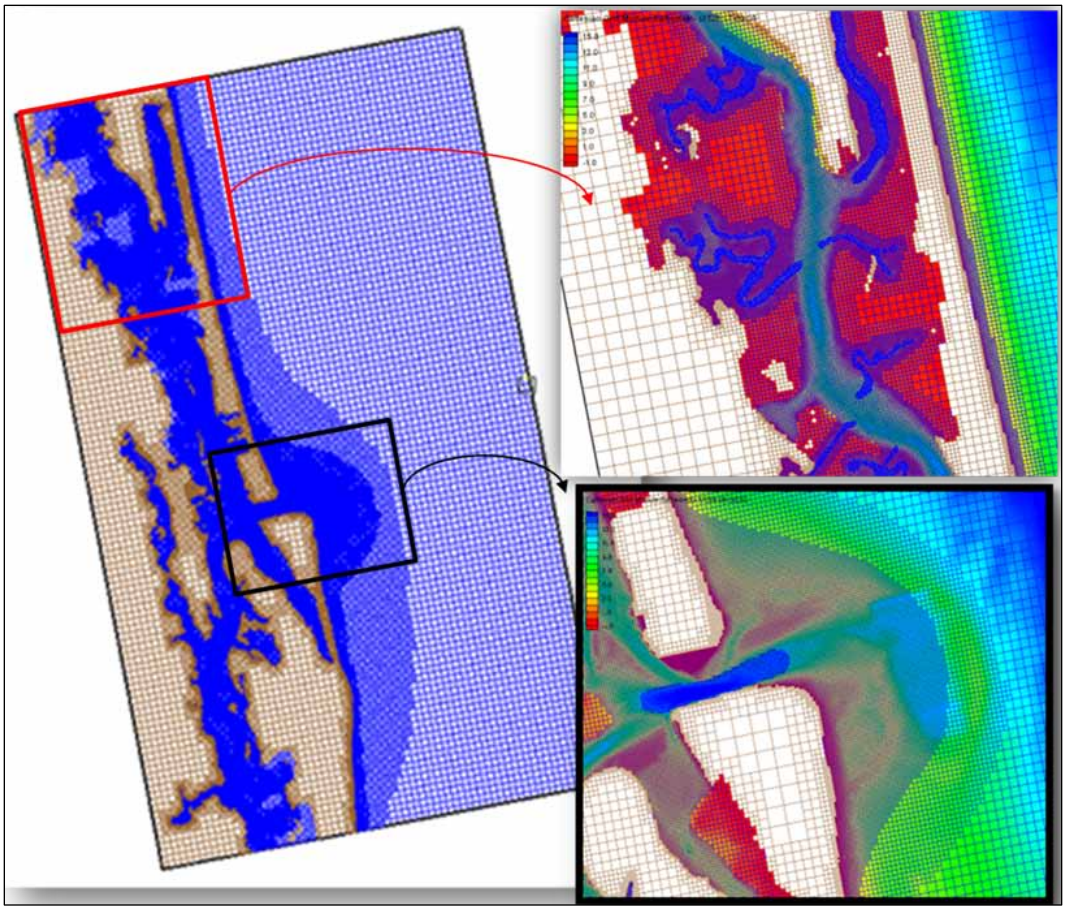

Figure 43. CMS-Flow grid for St. Augustine Inlet, FL (left), zoom-in of the northern part of the bay (top-right), and zoom-in of the entrance (bottom-right).

finest at depths greater than 3 to 5 m and coarsest at the shoreline. Median sediment grain size for the majority of the model domain was set to a constant value of 0.2 mm, representing the average sediment grain size offshore. The inlet channel was represented with d_{50} values ranging from 0.2 to 10 mm (10 mm representing a shell lag for the channel thalweg). The updrift nearshore values ranged between 0.2 to 0.4 mm from offshore to onshore (Zarillo 2008). Finally, the ebb-tidal delta was set to the average mean grain size of 0.16 mm.

The model results for sediment transport are largely dependent on the wave forcing, and therefore the calculated morphology change is driven by the quality of wave input. Wave data from an extensive hindcast study, the Florida Coastal Forcing Project (Dally and Leadon 2003; Leadon et al. 2009), were supplied to CMS-Wave. Of several locations extracted from the hindcast model, one hindcast station was chosen for CMS-Wave. The wave hindcast station lies along the wave grid boundary at 15-m water

depth directly offshore of the inlet (offshore of R-monument 123), outside of the influence of nearshore perturbations such as the ebb-tidal delta. Due to numerous shore-oblique shoals existent along this stretch of coast, a centrally located wave station (82, 448) was chosen along the 15-m water depth contour. Wave bottom friction was represented in CMS-Wave using a Darcy-Weisbach bottom friction factor of 0.005 (default), a typical value applied in coastal inlet studies.

The extent of the grid in the bay was determined by an iterative process to re-create the bay tidal prism. Because the bay system includes a secondary inlet to the south, Matanzas Inlet, there is some uncertainty involved in delineating the boundary for tidal prism between the two inlets. Calibration to both water levels and spatial current velocities was necessary to approximate this delineation of alongshore grid length, which was ultimately selected as 23.5 km. Following this, further calibration of the Manning's coefficient was applied to account for an over prediction of flood currents in the inlet throat. This significantly improved predicted velocity magnitudes and phase spatially through the inlet throat. Winds were not included because they do not generate significant currents or waves in the bay. For CMS-Wave, wind stresses were already incorporated in the generation of the hindcast nearshore waves and, therefore, were not included in the offshore forcing of the wave model. Validation to hydrodynamics is discussed in the companion Report 3.

The model run was set for a ramp period of 24 hr which is more than typically needed for implicit model runs. The hydrodynamic time-step was 15 min, which is reasonable for an implicit model, but not set too high to deviate from capturing the tidal circulation.

The van Rijn (2007a, b) sediment transport formula was used. The bed slope coefficient was set to 0.01 for closer representation to the morphology of channel slopes at St. Augustine. The default CMS suspended-load and bed-load sediment transport scaling factors were used. Bed change was calculated over the same sediment transport time step, which was 15 min, and updated in both the wave and flow models. Bed change was updated in the wave model on the steering interval of 3 hr.

The non-equilibrium total-load sediment transport model was applied with a constant adaptation length. Several total-load adaptation lengths were tested, including from 1 to 100 m, and 10 m was found to produce the

most realistic patterns and trends compared to measurements. Final parameter values were chosen to produce calibration of results to specific regions of interest, such as channel infilling in the dredged pit.

A multi-fraction approach was used to simulate non-uniform sediment transport which considers selective sorting, bed gradation, and hiding and exposure. Five sediment size classes were used to describe the grain size distribution and were defined based on the range of the initial d_{50} and bed sorting. Including hiding and exposure of multiple grain size distributions reduced scour within the channel thalweg, thus accurately representing the shell-hash observed in this region. Also, sediments that are transported over the nearshore and ebb shoal are of the movable grain size and are represented more realistically with the varying grain size distributions. Table 33 summarizes the general setup parameters of CMS-Flow.

Table 33. CMS setup parameters used for the St Augustine, FL field case.

Parameter	Value
Solution scheme	Implicit
Simulation duration	1.4 years
Ramp period	24 hours
Time step	15 min
Manning's coefficient	0.025 – 0.06 sec/m$^{1/3}$
Steering interval	3 hr
Median grain size	0.2 mm (majority of domain) 0.2-10 mm (channel thalweg) 0.16 mm (ebb delta) 0.2-0.4 mm (updrift shoreline)
Transport formula	van Rijn (2007a,b)
Bed load scaling factor	1.0
Suspended load scaling factor	1.0
Total-load Adaptation length	10.0 m
Morphologic acceleration factor	1.0
Bed porosity	0.4
Bed slope coefficient	0.01

Sediment transport calibration was targeted at reproducing both measured transport estimates for the area and measured morphology change with long-term morphologic simulations. Model calibration is discussed here as the comparison of measured and calculated sediment transport and morphology change between the time period extending from the June 2003 post-dredging condition to the pre-dredging condition in November 2004. Measured values of sediment transport rates over the ebb shoal are between 380,000 cu yd (SAJ 1998) to 440,000 cu yd (Walton 1973) toward the south. Calibration of sediment transport to capture these trends in transport rates requires modifications to the sediment transport formula, the bed slope coefficient, and the bed-load and suspended-load scaling factors. Measured morphology change from several ebb-tidal delta and navigation channel surveys were used in part in comparison with calculated morphology change.

4.3.3 Results and discussion

The CMS performance evaluation for St. Augustine Inlet, FL, was completed in two parts: first, through comparison of measured and calculated hydrodynamics, discussed in Report 3, and second through comparison of morphologic end-states, discussed here. The CMS sediment transport and morphology change was evaluated using measured bathymetric surveys for 1.4 yr period from June 2003 (post-dredging condition) to November 2004 (pre-dredging condition). Figure 44 is a comparison of the measured bathymetry for the pre-dredging condition.

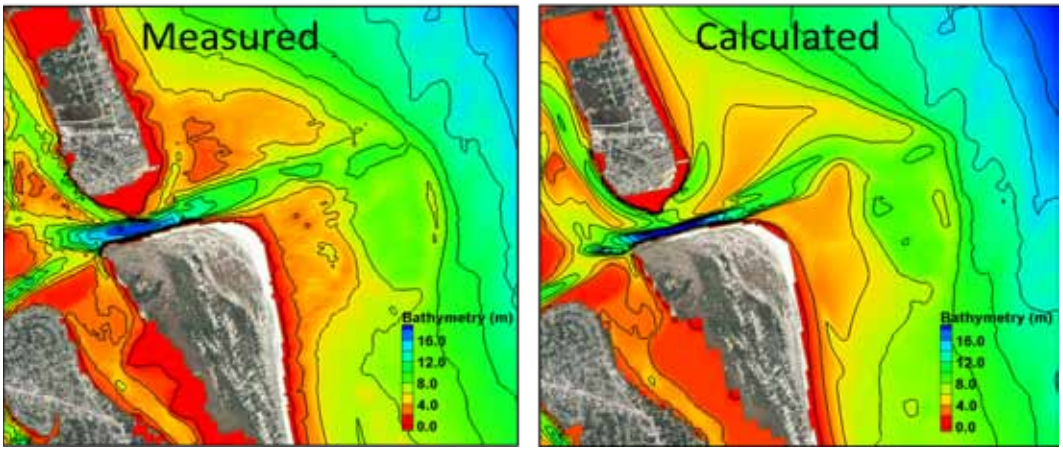

Figure 44. Measured (left) and calculated (right) November 2004 bathymetries (simulation started in June 2003) at St. Augustine Inlet, FL.

Morphology change, illustrated in Figure 45 as red for deposition and blue for erosion, is close in comparison with the volume of channel infilling and

also captures the overall trends of erosion and deposition. Modeled results were filtered for morphology change within a range of ±1 m, which is considered well within the error of morphologic modeling. Therefore, the delineated polygons in Figure 45 are areas with a significant trend of erosion or deposition associated with major morphologic features.

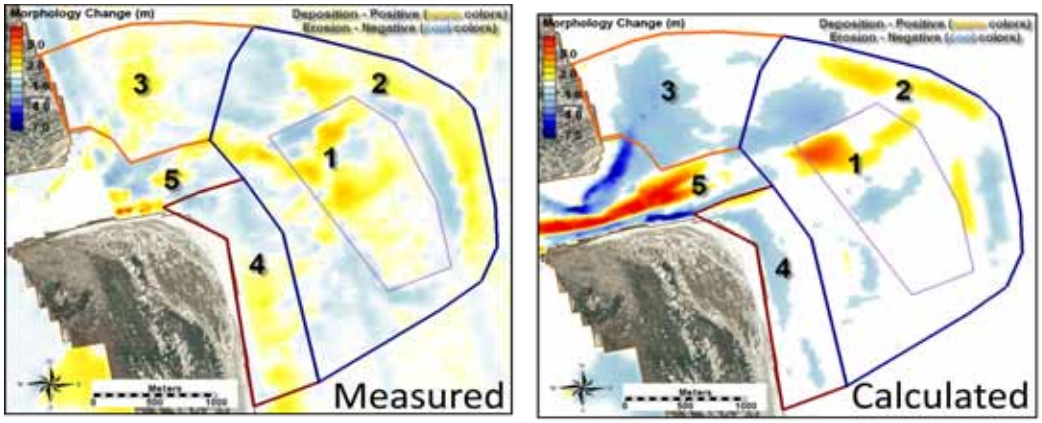

Figure 45. Measured (left) and calculated (right) morphology change (bathymetry difference maps) (from June 2003 to November 2004). Warmer colors indicate deposition and cooler colors are for erosion.

In the present formulation of CMS, cross-shore processes and swash processes are only qualitatively represented. The northern (polygon 3) and southern (polygon 4) sections of the shoal closest to the nearshore beaches show a reduction in offshore platform elevation, which follows the measured trend (Figure 45). The northeast part of polygon 2 shows some erosion in the offshore portion of the updrift ebb shoal, which agrees with the calculation; however, there is a poor correlation closer to the shoreline (polygons 3 and southern part of polygon 4). Eroded sediments in the vicinity of Vilano Beach (nearshore portion of polygon 3) are not modeled properly due to the lack of onshore sediment transport processes in CMS. Because the objective of the calibration of sediment transport and morphology change was to capture the channel infilling and overall ebb shoal morphologic patterns, the nearshore areas were not considered in the final analysis (polygons 3, 4, and 5). The main polygons (1 and 2) representing the ebb tidal shoal were used to compute correlation coefficients for determining model skill in reproducing morphology change. The comparisons of volume change for these two polygons are given in Table 34. Total volume changes for the measured and calculated ebb shoal volumes to the 9.14-m contour are compared are given in Table 35, which show a morphologic error of 3.6 percent.

Table 34. Measured and calculated ebb shoal volume changes for 2 polygons at St. Augustine Inlet, FL.

	Measured, m^3	Calculated, m^3	NMAE*, %
Dredged Pit/Channel (polygon 1)	281,400	292,840	4.1
Remainder of Ebb Shoal (polygon 2)	183,500	97,500	46.8

*defined in Appendix A

Table 35. Measured and calculated ebb shoal volume changes to 9.14-m contour.

	Measured, m^3	Calculated, m^3	NMAE*, %
Dredged Pit/Channel (polygon 1)	24,968,500	24,076,100	3.6

*defined in Appendix A

The van Rijn sediment transport formula chosen for the St. Augustine application provided a good representation of morphology change over the ebb shoal. Transport rates between van Rijn and Lund-CIRP formulas were close in magnitude. Inclusion of the non-uniform sediment transport, and hiding and exposure of the multiple grain sizes, reduced scour within the channel thalweg, thus representing the shell-hash observed in this region accurately. Also, sediments that are transported over the nearshore and ebb shoal are of the movable grain size and are represented more realistically with the varying grain size distributions.

As the non-uniform sediment transport sorts sediments over the domain, the main channel thalweg increases in average grain size, and finer sediments are redistributed. There is little erosion in the deep part of inlet channel, which scours 1 to 2 m, as the hydraulic radius goes to equilibrium with the tidal currents and bottom grain size. Sediments fill in the channel along the northern spit, also called Porpoise Point, which is an active tidal process of re-curved spits in the ebb and flood direction. The representation of sedimentation in this area supports the ability of CMS to reproduce tidally-driven sedimentation and erosion patterns associated with inlet throat processes.

Changes to the updrift shoal platform are a result of initial redistribution of sediments in addition to the model error induced by a lack of appropriate processes in the nearshore. A similar effect is seen along the nearshore portion of the downdrift platform adjacent to St. Augustine Beach. All other offshore ebb shoal attributes, including the main ebb channel and offshore shoals, were well represented in the model. Overall,

there are five areas with significant morphologic change occurring in the modeled results, three of which are the result of a lack of representative processes as described above.

Though analysis of these volume changes can provide insight in to the morphologic behavior, a qualitative analysis of the results bears substantial information about the inlet processes. Some oversight of the initial internal model calibration of morphology to the ambient model conditions and forcing is considered. The CMS reproduced sedimentation patterns and quantities within the area of focus successfully.

4.3.4 Conclusions

The CMS was applied to a coastal inlet with tidal and wave forcing. Validation to hydrodynamics was discussed in V&V Report 3. Calculated morphology change within the primary area of interest in the ebb tidal shoal had a total volume error ranging from 1 to 4 percent. This application demonstrates the ability of CMS to calculate morphology change volumes over a 1.4-yr simulation within a wave-influenced, tidally-dominated inlet system.

4.4 Test C3-Ex3: Non-uniform sediment transport modeling at Grays Harbor, WA

4.4.1 Purpose

The CMS non-uniform sediment transport model was applied to the beaches adjacent to Grays Harbor, WA, to test the model skill in predicting nearshore morphology change. The specific model features tested were bed material hiding, exposure, sorting, stratification, and non-erodible bed surfaces; and transport due to asymmetrical waves, Stokes drift, roller and undertow. The model skill in predicting nearshore morphologic evolution was evaluated with the Brier Skill Score and other goodness-of-fit statistics.

4.4.2 Field study

Grays Harbor inlet, WA is located on the southwest Washington coast at the mouth of the Chehalis River. Between May and July of 2001, the U.S. Geological Survey instrumented six tripods and collected time series of wave height, water surface elevation, near-bottom current velocity, and sediment concentration proxies (Landerman et al. 2004). Weekly

topographic maps and monthly bathymetric surveys along transects spaced 50 to 200 m apart were collected (see Figure 46). In addition, grab samples of surface sediment were collected at several locations. Figure 46 shows the location of the observation stations and monthly nearshore bathymetric profiles.

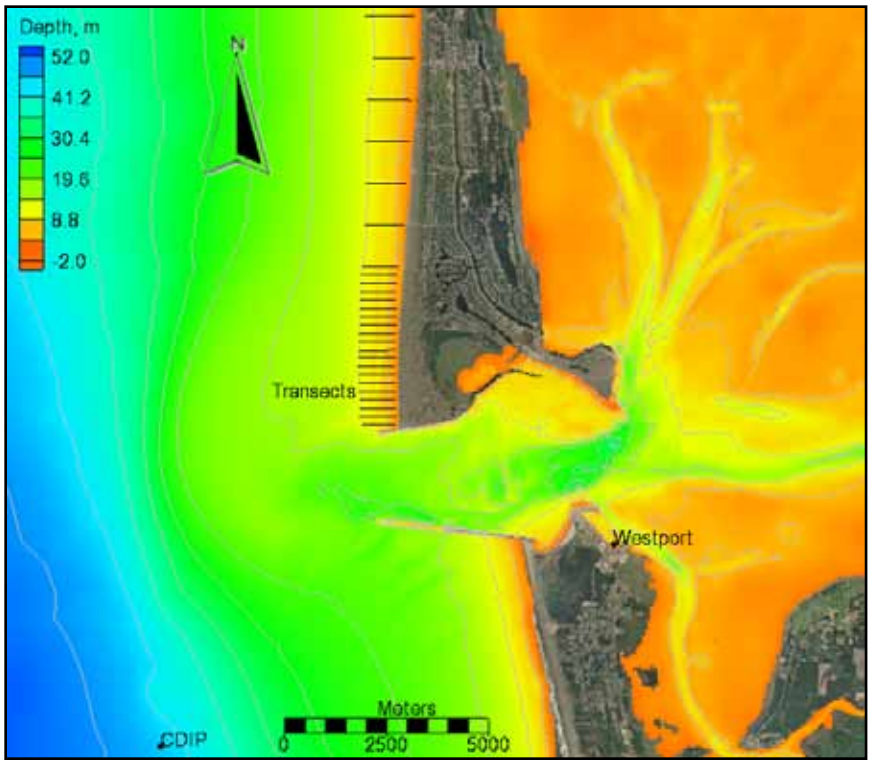

Figure 46. Map of Grays Harbor inlet, WA showing the location of the nearshore bathymetric transects.

4.4.3 Model setup

The first half of the field deployment in 6-30 May 2001 was simulated. The simulation period was characterized by relatively calm conditions, with a few spring storms with significant wave heights on the order of 3 m. The spectral wave transformation model CMS-Wave was run on a ~200,000 cell Cartesian grid with varying grid resolution from 15 to 120 m (see Figure 47). The waves were forced with spectral wave information from the Coastal Data Information Program (CDIP) buoy No. 03601 located southwest of the inlet at a depth of 42 m. For further details see Sánchez and Wu (2011b).

The CMS-Flow was forced with a water level time series from Westport Harbor with a negative 30 min phase lag correction which was obtained by

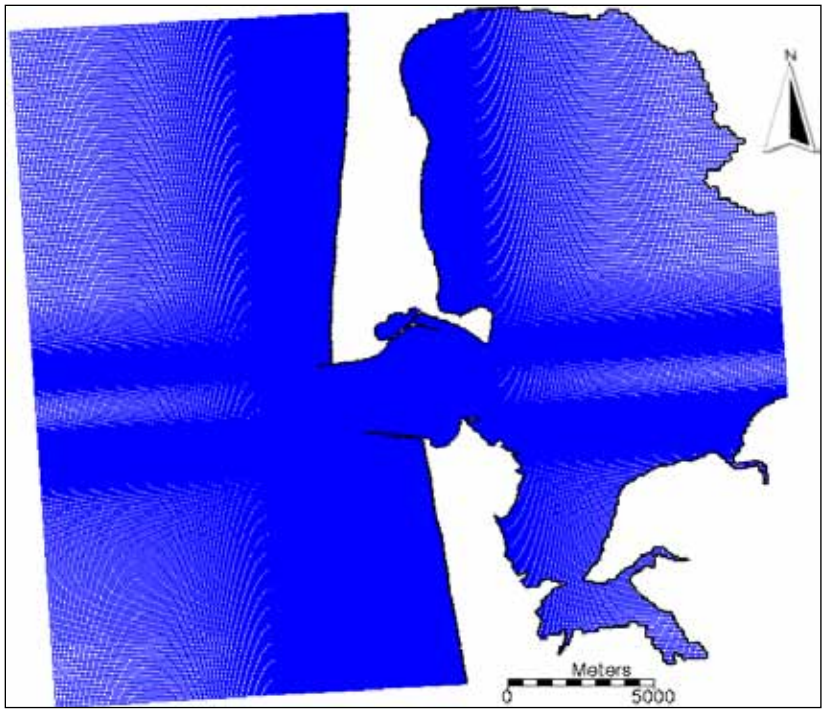

Figure 47. CMS-Wave Cartesian grid used for the Grays Harbor, WA field test case.

comparing with the stations deployed during the field study (see Figure 46). Winds were interpolated from the Blended Sea Winds product of the National Climatic Data Center (Zhang et al. 2006). The Manning's coefficient was calibrated in previous studies as 0.018 sec/$m^{1/3}$ over the whole domain, except on the rock structures where a value of 0.1 was used. A flux boundary condition was applied at the Chehalis River which was obtained from the USGS. The CMS-Flow ~55,000-cell telescoping Cartesian grid is shown in Figure 48 and has six levels of refinement from 20 to 640 m. A variable time step was used with a maximum value of 10 min. The sediment transport and bed change were calculated at every hydrodynamic time step.

A 5-day ramp was implemented based on previous hydrodynamic studies at Grays Harbor (Demirbilek et al. 2010), so that the start of the simulation was 1 May 2001. Waves were calculated at a constant 2-hr interval (steering interval). The significant wave height, peak wave period, wave unit vectors, and wave dissipation were linearly interpolated to the flow grid every steering interval and then linearly interpolated in time at every hydrodynamic time step. Wave variables such as wave length and bottom orbital velocity were updated every hydrodynamic time step for wave-current interaction.

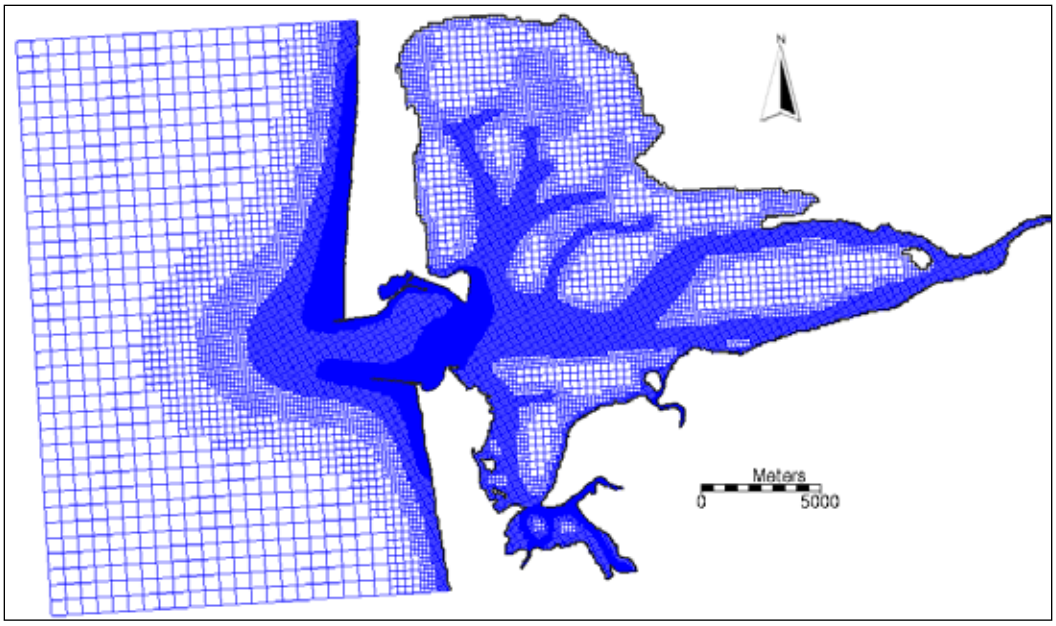

Figure 48. CMS-Flow telescoping grid for the Grays Harbor, WA field test case.

When using such a large steering interval, it is important to consider how the water levels, current velocities, and bed elevations which are passed from the flow to the wave model are estimated. For this application, and for most open coast applications, the nearshore waves are most sensitive to variations in water levels but not currents. Therefore, improved results can be obtained by predicting the water levels at the wave model time step based on a decomposition of the water levels into spatially constant and variable components. The spatially constant component is assumed to be equal to the tidal water surface elevation, and the spatially variable component which includes wind and wave setup is estimated based on the last flow time step. The currents and bed elevations which are passed from the wave to flow grid are simply set to the last time step value. Other types of prediction methods could be used; however, the approach described above has been found to be sufficient for most applications and is simple to calculate. After each wave run, a surface roller model is also calculated on the wave grid and the roller stresses are added to the wave stresses before interpolating onto the flow grid. Even though CMS-Flow and CMS-Wave use different grids, the two models are in a single code which facilitates the model coupling and speeds up the computation by avoiding communication files, variable allocation, and model initialization at every steering interval.

The initial bed material composition was specified by a spatially variable median grain size and constant geometric standard deviation of

1.3 mm based on field measurements. The initial fractional composition at each cell was assumed to be constant in depth and have a log-normal distribution, and represented by six size classes with characteristic diameters of 0.1, 0.126, 0.16, 0.2, 0.25, and 0.31 mm. An example of the initial grain size distribution is shown in Figure 49. Ten bed layers were used with an initial thickness of 0.5 m each. Lund-CIRP transport formulas were used to estimate the transport capacity (Camenen and Larson 2007). The total-load adaptation coefficient is calculated as where is the total-load adaptation length, is the sediment fall velocity, is the depth-averaged current speed, and is the total water dept. Here , where and are the bed- and suspended-load adaptation lengths, respectively. The bed-load adaptation length is set to 10 m, and the suspended-load adaptation length is calculated as where the suspended-load adaptation coefficient is set to 0.5. A constant bed porosity of 0.3 was used in the simulation. For further details the reader is referred to Sánchez and Wu (2011a).

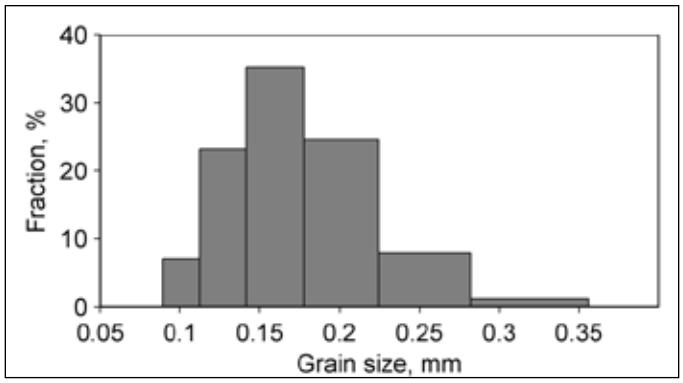

Figure. 49. Example log-normal grain size distribution (d_{50}= 0.16 mm, σ_g= 1.3 mm).

4.4.4 Results and discussion

Calculations were performed on a desktop PC and the 31-day simulation was completed in approximately 10 hr. A comparison of the measured and computed bed changes between 6-30 May 2001 is shown in Figure 50. Selected regions of interest are encompassed by black lines to help visually compare the bed changes. In general, the results show many common features and similar erosion and deposition patterns. More specifically, the bed change is characterized by the erosion of the outer bar, deposition in the inner bar face and outer trough, and erosion of the inner trough face.

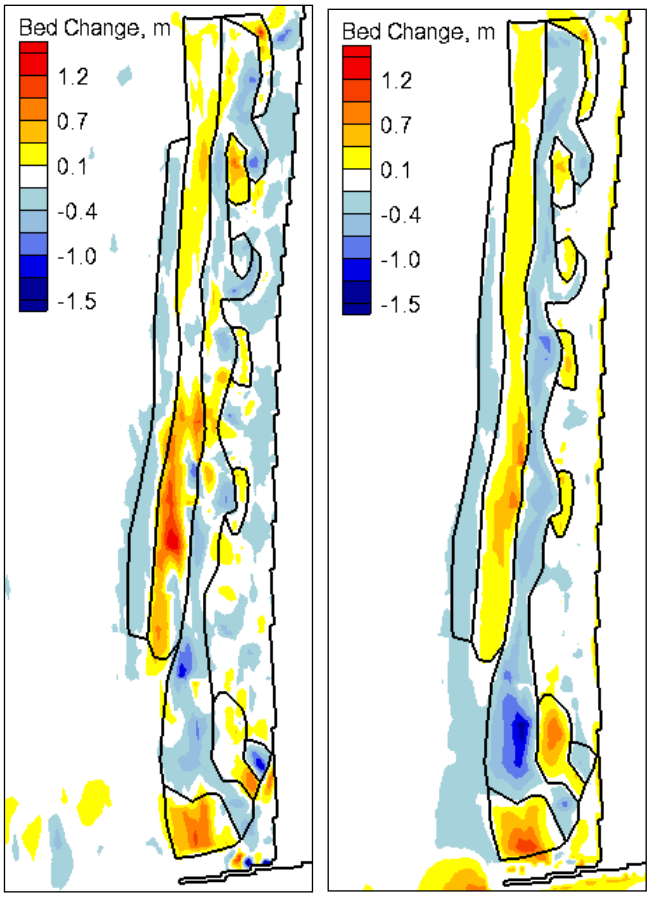

Figure 50. Measured (left) and computed (right) bed changes during May 6 and 30, 2001.

There is a region extending approximately 1 km from the northern jetty where the bed changes are noticeably different from those further to the north. This region is interpreted as being influenced strongly by the presence of the inlet, ebb shoal and northern jetty. Interestingly, both the measurements and model results show that small (200 to 300 m in length) inner bars form adjacent to the trough, which appear to occur at regular 400 to 500 m intervals.

The computed bed changes in the foreshore region (beach face) are relatively small compared to the measurements due to the lack of swash zone processes in the present version of CMS. Swash zone processes enhance transport in the surf zone by increasing the current velocities, transport rates, and mixing at the shoreline. A large portion of the total longshore sediment transport occurs in the swash zone, and without these processes, morphodynamic models tend to underestimate longshore transport rates and bed change in the foreshore region. Walstra et al. (2005) simulated the bed change at transects 9 and 20 using a two-

dimensional vertical (2-DV) profile evolution model and were able to predict the onshore migration of the bar, but also found that the model performance deteriorates in the foreshore region.

The measured and computed water depths and bed changes for Transects 1 and 9 are shown in Figure 51. As observed in Figure 50, most of bed changes occurred from the nearshore bar to the outer beach face. The model was able to predict an onshore bar migration accurately, although it underestimated the nearshore bar height which is also observed in Figure 50. To evaluate the model performance in predicting the nearshore bathymetry, the BSS was applied to the water depths and the correlation coefficient R^2 to the bed change. Other goodness-of-fit parameters were also calculated and showed similar patterns. For simplicity only the previously mentioned parameters are shown in Figure 52. The goodness-of-fit statistics show a wide range of values.

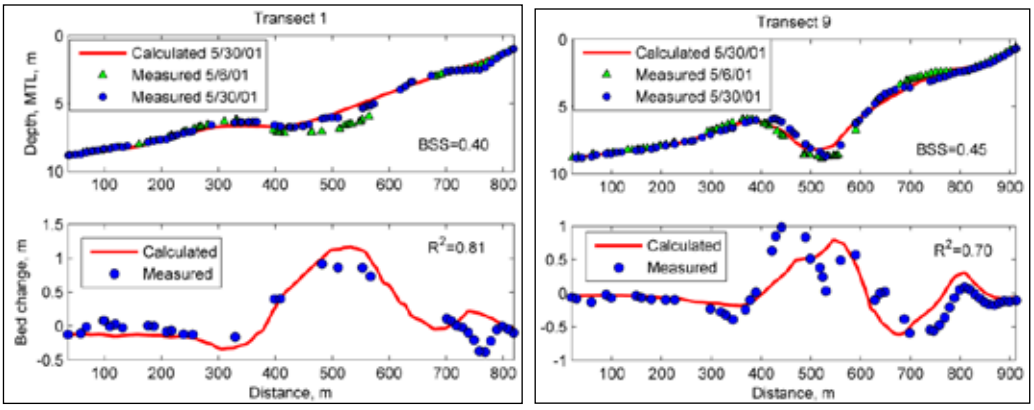

Figure 51. Measured and computed water depths (top) and bed changes (bottom) for Transect 9.

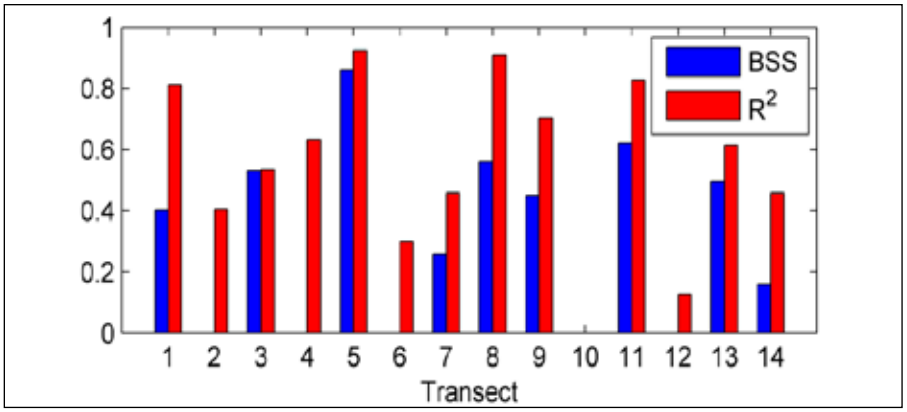

Figure 52. Brier Skill Score for water depths and correlation coefficient for computed bed changes at selected Transects.

The measured bed change shows a larger variation than the modeled bed changes, indicating that morphology change is sensitive to longshore variations in forcing, initial bathymetry, or 3-D processes such as rip currents. As discussed by Walstra et al. (2005), the model results indicate that the waves and currents do in fact vary over the spatial scales (10 to 100 m) of the observed morphological variations.

The computed median grain size on 30 May 2001 is shown in Figure 53. Qualitatively, the results agree well with field measurements and typical findings for most inlets and beaches. Coarser sediments are found in the beach face and breaker line (offshore bar), and finer sediments are found in the trough and offshore of the surf zone. In addition, coarser sediments are found in the inlet entrance and finer sediments are found on the periphery of the ebb shoal. In addition, it is noted that the sea bed around the jetties is highly armored due to the strong currents and large waves present, which were also observed in the field.

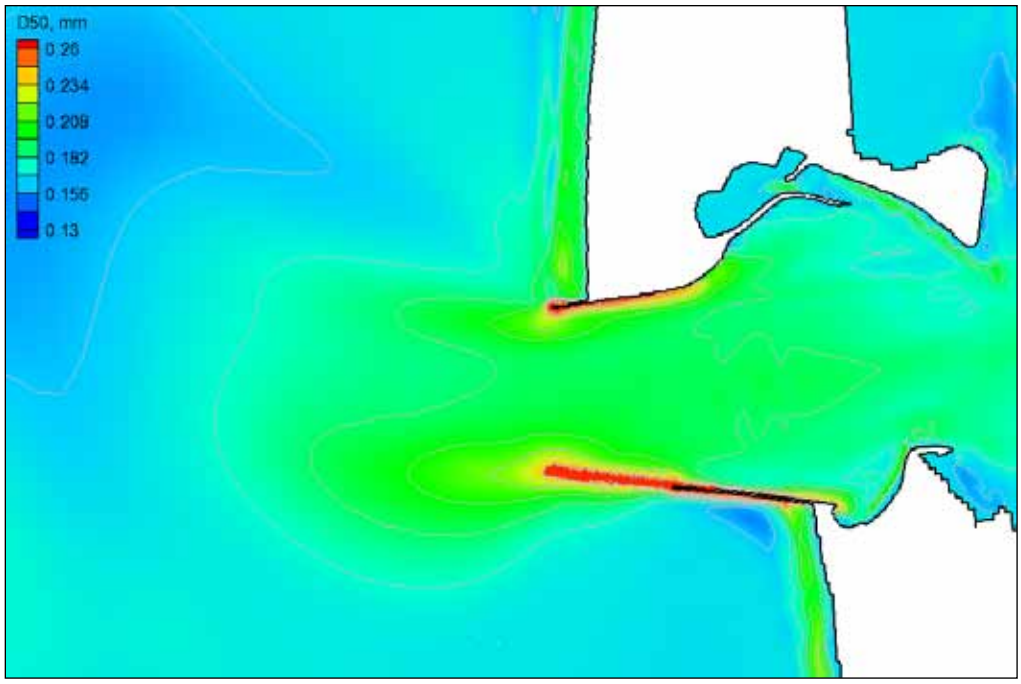

Figure 53. Distribution of median grain size calculated after the 25-day simulation for the Grays Harbor,WA test case.

4.4.5 Conclusion and recommendations

The CMS model has been applied to Grays Harbor, WA. Nearshore measurements of bathymetry were used to validate the model during the period of 6-30May 2001. Goodness-of-fit statistics of water depths and bed

changes indicate generally reasonable-to-good model performance although the model skill varied significantly, especially on the beach face where swash zone processes were likely important and were not represented in the model. The measured bed change shows a larger degree of variability compared to model results, indicating that nearshore morphology is sensitive to longshore variations in forcing and cross-shore processes which are difficult to resolve. Results also show that there is a region adjacent to the north jetty (transition zone) which is influenced strongly by the presence of the inlet due to wave refraction over the ebb-tidal delta, ebb and flood currents including detached eddies, and the north jetty.

5 Summary and Recommendations

The CMS-Flow capabilities for Sediment Transport and Morphology Change modeling were evaluated with analytical, laboratory and field test cases with a wide range of hydrodynamic, wave and sediment conditions. This evaluation provides an in-depth assessment of various features and capabilities of the CMS for sediment transport and resulting morphology change. Types of applications considered in this V&V study included coastal inlets, navigation channels, bays, estuaries, and coastal structures. For each test case, the CMS (Wave and Flow) model setup was described, and recommendations for default values of the model parameters were provided for similar practical applications. Limitations of the CMS models were described in the discussion of results for each test case. A summary of work done and recommendations are:

- Three analytical cases were presented for 1-D scalar (e.g., sediment, salinity) transport: advection only, advection-diffusion, and advection-diffusion-decay.
- The implicit time marching scheme was used to simulate the 1-D scalar advection, diffusion, and decay. The computed results converged to the analytical solution for smaller time steps and grid resolution.
- In the case of advection only, the first-order upwind was found to produce significantly more numerical diffusion than the second-order HLPA scheme. In addition to being more accurate, the HLPA scheme led to shorter run times due to faster solver convergence.
- In the test cases for advection-diffusion, and advection-diffusion-decay, results were found to be much less sensitive to the advection scheme and time step, indicating that the relative importance of numerical dissipation is relatively small compared to the physical diffusion. This partially explains why, for field applications, the differences between first- and second-order advection schemes are relatively small.
- Six laboratory data sets were compared with CMS calculations to investigate channel infilling and migration; the cross-shore distribution of waves, currents, bed- and suspended-sediment transport; erosion of sand over hard bottom; and deposition of non-uniform sediments.

- Channel infilling calculations, one of the major applications of the CMS for CIRP, was shown to give good agreement as compared to laboratory cases except for channels with steep side slopes (1:7 and 1:3), in which flow separation occurred. For cases with flow separation, a three-dimensional model may be required for more accurate estimates.
- The CMS calculated surf zone processes accurately for wave height, current speed (with surface roller activated), and sediment transport from the breaker zone to mid-way through the surf zone. Calculated longshore sediment transport rates may be underestimated near the shoreline due to the lack of swash zone sediment transport, a feature that is presently under development in the CMS.
- Three field measurements of sediment transport and morphology change were compared to CMS calculations, including navigation channel, ebb shoal infilling, and multiple-sized sediment transport on a beach adjacent to a large tidal inlet.
- Infilling of navigation channels and an ebb shoal borrow area with wave, longshore current, and tidal current forcing was well reproduced by the CMS. In two field cases, the calculated total infilling of the channel and borrow site agreed with measurements with errors of less than 11 percent. The CMS application was shown to be representative and useful for evaluating project alternatives such as channel realignment or deepening, ebb shoal mining, and jetty configurations.
- The CMS calculated armoring of more energetic regions with coarser sediment and deposition of finer sediment in quiescent regions. This general sorting of non-uniform sediments in CMS was shown to be reasonable for mid-term (order of months to years) calculations. The natural self-stabilizing of the bed due to sediment sorting increased the model accuracy.
- It should be noted that the V&V study presented in this report was constrained by available measurement data. In several test cases, such as C2-Ex1 and C2-Ex6, the CMS sediment transport model was first calibrated using one set of data and then validated using one or more separate sets of data. This calibration and validation was conducted perfectly. However, only a few cases have such detailed measurement data. In more general cases, such as case C2-Ex5 and C3-Ex1, only one experimental run was conducted, but the data consisted of measurements at multiple times (time periods) or for multiple physical parameters; thus, the model was calibrated using part of the data (e.g., at one time or for one physical quantity) and then validated using the remaining data. In other cases, such as C3-Ex2 and C3-Ex3, the data

were not sufficient to conduct both calibration and validation. Strictly, only calibration was conducted properly and validation was not warranted in these cases. However, these tests demonstrated that the model could reproduce the temporal and spatial variations of the physical quantities of the system reasonably, using the calibrated parameters; thus, to a certain extent, the model was also validated. Overall, the CMS sediment transport model has been verified and validated well, and it has been calibrated in the selected laboratory and field test cases. For future applications of this model, calibration is always preferred if measurement data are available. If no measurement data are available, a sensitivity study is recommended.

- The laboratory and field test cases demonstrated that the sediment transport capacity and adaptation length are two very important parameters in the NET model. Among these two parameters, the sediment transport capacity is more important than the adaptation length. When calibrating for sediment transport, start with the transport formula, then use the transport scaling factor, and finally the adaptation length. Other parameters such as the bed slope coefficient and bed porosity usually do not have a significant effect on the morphologic change. Measurements of bed- and suspended-load transport rates are rarely available for most coastal engineering projects, and the bed and suspended load transport scaling factors are typically calibrated by using estimates of longshore sediment transport or channel infilling rates. If no data are available for estimating transport scaling factors, it is then recommended that the default value of 1.0 should be used and a sensitivity study conducted using the typical range of 0.5-2.0. The CMS provides four formulas for sediment transport capacity under combined currents and waves. As shown in this report, different capacity formulas may produce significantly different results and, therefore, the optimal transport formula for each application should be chosen based on measured morphologic response and sediment transport estimates.
- The total-load adaptation length between 0.5 and 1 m provided good model results for laboratory cases, whereas larger values between 10 and 100 m were used for field application cases. This implies that the adaptation length needs to be calibrated in applications if possible.
- Additional verification (analytical) tests are needed for two dimensional problems with source terms.

- Research is needed to understand how to estimate the adaptation length for coastal applications as a function of forcing conditions and sediment characteristics.
- Further research is needed in determining how to implement swash zone processes within the current 2-D framework to simulate shoreline change and represent longshore sediment transport rates more accurately.
- Further research is needed in representing cross-shore sediment transport processes, primarily wave asymmetry and undertow, to better simulate the onshore and offshore migration of sediments.
- Additional studies are needed to quantify the mechanisms of non-uniform sediment transport, morphology change, bed material hiding, exposure, and armoring.

In summary, Verification and Validation of CMS-Flow will continue with additional comparisons, and future publications will document the findings. As cases are prepared, they will be posted to the CIRP website[1].

[1] The CIRP website is at: http://cirp.usace.army.mil/

References

Armanini, A., and G. di Silvio. 1986. Discussion on the paper 'A depth-averaged model for suspended sediment transport' by Galappattti, G., and Vreugdenhil, C.B. *Journal of Hydraulic Research*. 24(5), 437-441.

Batten, B. K., and N. C. Kraus. 2006. Evaluation of Downdrift Shore Erosion, Mattituck Inlet, New York: Section 111 Study. *Technical Report ERDC/CHL-TR-06-1*. U.S. Army Engineer Research and Development Center, Coastal and Hydraulics Laboratory, Vicksburg, MS. http://cirp.usace.army.mil/pubs/html/batten-kraus-06.html, accessed 7 June 2011.

Battjes, J. A., J. P. F. M. Janssen. 1978. Energy loss and set-up due to breaking of random waves. *Proc. 16th International Conference on Coastal Engineering*, ASCE, 569–588.

Beck, T.M. 2010. Model Application to St. Augustine Inlet. Coastal Inlets Research Program Wiki http://cirp.usace.army.mil/wiki/Model_Application_to_St._Augustine_Inlet, updated 18 November 2010, accessed 5 June 2011.

Beck, T. M. 2011. Morphology Change Validation of CMS at Shark River Inlet. Coastal Inlets Research Program Wiki, http://cirp.usace.army.mil/wiki/Morphology_Change_Validation_of_Shark_River_Inlet, updated 6 June 2011, accessed 7 June 2011.

Beck, T. M., and N. C. Kraus. 2010. Shark River Inlet, New Jersey, Entrance Shoaling: Report 2, Analysis with Coastal Modeling System. *Technical Report ERDC/CHL-TR-10-4*. U.S. Army Engineer Research and Development Center, Coastal and Hydraulics Laboratory, Vicksburg, MS. http://cirp.usace.army.mil/ pubs/html/10-Beck-Kraus_TR-10-4.html, accessed 7 June 2011.

Buttolph, A. M., C. W. Reed, N. C. Kraus, N. Ono, M. Larson, B. Camenen, H. Hanson, T. Wamsley and A. K. Zundel. 2006. Two-dimensional depth-averaged circulation model CMS-M2D: Version 3.0, Report 2: Sediment transport and morphology change. *Technical Report ERDC/CHL TR-06-09*. U.S. Army Engineer Research and Development Center, Coastal and Hydraulics Laboratory, Vicksburg, MS.

Byrnes, M. R., S. F. Griffee, and M. S. Osler. 2010. Channel Dredging and Geomorphic Response at and Adjacent to Mobile Pass, Alabama. *ERDC/CHL-TR-10-8*. U.S. Army Engineer Research and Development Center, Coastal and Hydraulics Laboratory, Vicksburg, MS. http://cirp.usace.army.mil/pubs/html/10-Byrnes_TR-10-8.html, accessed 7 June 2011.

Camenen, B., and M. Larson. 2005. A general formula for non-cohesive bed load sediment transport. *Estuarine, Coastal and Shelf Science*, 63, 249–260.

Camenen, B., and M. Larson. 2007. A unified sediment transport formulation for coastal inlet application. *Technical report ERDC/CHL CR-07-1*. US Army Engineer Research and Development Center, Vicksburg, MS.

Camenen, B., and M. Larson. 2008. A general formula for non-cohesive suspended sediment transport. *Journal of Coastal Research*, 24 (3), 615–627.

Chapra, S.C. 1997. Surface water-quality modeling. McGraw-Hill, New York, 835 p.

Choi, S. K., H. Y. Nam, and M. Cho. 1995. A comparison of higher-order bounded convection schemes. *Computational Methods in Applied Mechanics and Engineering*, 121, 281-301.

Dally, W. R., and M. E. Leadon. 2003. Comparison of Deep-Water ADCP and NDBC Buoy Measurements to Hindcast Parameters. Report submitted to the U.S. Army Corps of Engineers, Jacksonville District.

Demirbilek, Z., L. Lin, J. Smith, E. Hayter, E. Smith, J. Gailani, G. Norwood, and D. Michalsen. 2010. Waves, hydrodynamics and sediment transport modeling at Grays Harbor, WA. *Technical Report ERDC/CHL-TR-10-13*. U.S. Army Engineer Research and Development Center, Coastal and Hydraulics Laboratory, Vicksburg, MS.

Demirbilek, Z., and J. D. Rosati. 2011. Verification and validation of the Coastal Modeling System: Executive Synopsis. *Technical Report ERDC/CHL-TR-11-XX*. U.S. Army Engineer Research and Development Center, Coastal and Hydraulics Laboratory, Vicksburg, MS.

DHL 1980. Computation of Siltation in Dredged Trenches. Delft Hydraulics Laboratory, Storm Surge Barrier Oosterschelde, *Report 1267-V/M* 1570.

Gravens, M. B., and P. Wang. 2007. Data report: laboratory testing of longshore sand transport by waves and currents; morphology change behind headland structures. *Technical Report, ERDC/CHL TR-07-8*. U.S. Army Engineer Research and Development Center, Coastal and Hydraulics Laboratory, Vicksburg, MS. http://cirp.usace.army.mil/pubs/html/gravens-wang-07.html, accessed 7 June 2011.

Landerman, L., C. R. Sherwood, G. Gelfenbaum, J. Lacy, P. Ruggiero, D. Wilson, T. Chrisholm and K. Kurrus. 2004. Grays Harbor Sediment Transport Experiment: Spring 2001 –Data Report. U.S. Geological Survey Data Series.

Leadon, M. E., W. R. Dally, and D. A. Osiecki. 2009. The Florida Coastal Forcing Project. Letter Report Submitted to the U.S. Army Corps of Engineers Jacksonville District.

Li, H., M. E. Brown, T. D. Smith, and J. H. Podoski. 2009. Evaluation of Proposed Channel on Circulation and Morphology Change at Kawaihae Harbor and Pelekane Bay, Island of Hawaii, HI. *Technical Report ERDC/CHL-TR-09-19*. U.S. Army Engineer Research and Development Center, Coastal and Hydraulics Laboratory, Vicksburg, MS. http://cirp.usace.army.mil/pubs/html/09-Li-Brown_TR-09-19.html, accessed 7 June 2011.

Li, H., L. Lin, C. Lu, and A. T. Shak. 2011 In press. Evaluation of Breakwaters and Sedimentation at Dana Point Harbor, CA. *Proceedings Coastal Sediments*. http://cirp.usace.army.mil/pubs/html/CS11_Li-Lin.html, accessed July 2011.

Lin, L., Z. Demirbilek, H. Mase, and J. Zheng. 2008. CMS-Wave: A nearshore spectral wave processes model for coastal inlets and navigation projects. *Technical Report ERDC/CHL TR-08-13*. U.S. Army Engineer Research and Development Center, Coastal and Hydraulics Laboratory, Vicksburg, MS.

MacDonald, N. J., M. H. Davies, A. K. Zundel, J. D. Howlett, Z. Demirbilek, J. Z. Gailani, T. C. Lackey, and J. Smith. 2006. PTM: Particle Tracking Model; Report I: Model theory, implementation, and example applications. *Technical Report ERDC/CHL TR-06-20*. U.S. Army Engineer Research and Development Center, Coastal and Hydraulics Laboratory, Vicksburg, MS.

Mase, H., K. Oki, T. S. Hedges, and H. J. Li. 2005. Extended energy-balance-equation wave model for multidirectional random wave transformation. *Ocean Engineering*, 32(8-9), 961-985.

Militello, A., C. W. Reed, A. K. Zundel, and N. C. Kraus. 2004. Two-dimensional depth-averaged circulation model CMS-M2D: Version 2.0, Report 1, Technical documentation and user's guide. *Technical Report ERDC/CHL TR-04-02*. U.S. Army Engineer Research and Development Center, Coastal and Hydraulics Laboratory, Vicksburg, MS.

Min Duc, B., T. Wenka, and W. Rodi. 2004. Numerical modeling of bed deformation in laboratory channels. *Journal of Hydraulic Engineering*, ASCE, 130(9), 894-904.

Nam, P. T., M. Larson, H. Hanson, and L. X. Hoan. 2009. A numerical model of nearshore waves, currents, and sediment transport. *Coastal Engineering*, 56, 1084-1096.

Paola, C., G. Parker, S. K. Sinha, J. B. Southard, and P. R. Wilcock. 1992. Downstream fining by selective deposition in a laboratory flume. *Science*, 258: 1757-1760.

PBS&J 2009. St. Johns County Shore Stabilization Feasibility Study for South Ponte Vedra and Vilano Beach Regions. Tampa, Florida.

Reed, C. W., M. E. Brown, A. Sánchez, W. Wu, and A. M. Buttolph. 2011. "The Coastal Modeling System Flow Model (CMS-Flow): Past and Present," Journal of Coastal Research, Special Issue, 59, 1-6.

Reed, C. W., and L. Lin. 2011. "Analysis of Packery Channel Public Access Boat Ramp Shoreline Failure," Journal of Coastal Research Special Edition, Coastal Education and Research Foundation, Inc., Special Issue, 59, 150-155.

Rosati, J. R., A.E . Frey, M. E. Brown, and L. Lin. 2011. Analysis of Dredged Material Placement Alternatives for Bottleneck Removal, Matagorda Ship Channel, Texas. *ERDC/CHL-TR-11-2*. U.S. Army Engineer Research and Development Center, Coastal and Hydraulics Laboratory, Vicksburg, MS. http://cirp.usace.army.mil/pubs/html/11-Rosati-Frey-TR-11-2.html, accessed 7 June 2011.

SAJ 2010. Regional Morphology, St. Augustine Inlet, St. Johns County, Florida. Draft Report U.S. Army Engineer Jacksonville District, 156 p.

SAJ 1998. St. Johns County, Florida Shore Protection Project, General Reevaluation Report with Final Environmental Assessment. U.S. Army Engineer District Jacksonville District.

Sánchez, A., and W. Wu. 2011a. A non-equilibrium sediment transport model for coastal inlets and navigation channels. *Journal of Coastal Research*, Special Issue, 59, 39-48.

Sánchez, A., and W. Wu. 2011b. Non-uniform sediment transport modeling and Grays Harbor, WA. *Proceedings Coastal Sediments '11*, [In Press].

Sánchez, A., W. Wu, T. M. Beck, H. Li, J. Rosati, R. Thomas, J. D. Rosati, Z. Demirbilek, M. Brown, and C. Reed. 2011. Validation of the Coastal Modeling System: Report III, Hydrodynamics. *Technical Report ERDC/CHL-TR-11-xx*. U.S. Army Engineer Research and Development Center, Coastal and Hydraulics Laboratory, Vicksburg, MS.

Seal, R., G. Parker, C. Paola, and B. Mullenbach. 1995. Laboratory experiments on downstream fining of gravel, narrow channel runs 1 through 3: supplememtal methods and data. *External Memorandum M-239*, St. Anthony Falls Hydraulic Laboratory, University of Minnesota, Minneapolis.

Soulsby, R. L. 1997. Dynamics of marine sands. A manual for practical applications. Thomas Telford Publications, London, England, 249 p.

Thuc, T. 1991. Two-dimensional morphological computations near hydraulic structures. *Doctoral Dissertation*, Asian Institute of Technology, Bangkok, Thailand.

van Rijn, L. C. 1984. Sediment transport, part I: bed load transport. *Journal of Hydraulic Engineering*, ASCE, 110(10), 1431-1456.

van Rijn, L. C. 1984. Sediment transport, part II: suspended load transport. *Journal of Hydraulic Engineering*, ASCE, 110(11), 1613-1641.

van Rijn, L. C., and F. J. Havinga. 1986. Transport of fine sands by currents and waves. *Journal of Waterway, Port, Coastal, and Ocean Engineering*, 121(2), 123-133.

van Rijn, L. C., and F. J. Havinga. 1995. Transport of fine sands by currents and waves. *Journal of Waterway, Port, Coastal, and Ocean Engineering*, 121(2), 123-133.

van Rijn, L. C. 2007a. Unified View of Sediment Transport by Currents and Waves. I: Initiation of Motion, Bed Roughness, and Bed-load Transport. *Journal of Hydraulic Engineering*, 133(6), 649-667.

van Rijn, L. C. 2007b. Unified View of Sediment Transport by Currents and Waves. II: Suspended Transport. *Journal of Hydraulic Engineering*, 133(6), 668-689.

Walton, T. L. 1973. Littoral drift computations along the coast of Florida by means of Ship Wave Observations. *TR-15*, University Florida, Gainesville, FL.

Walstra, D. R, P. Ruggiero, G. Lesser, and G. Gelfenbaum. 2005. Modeling nearshore morphological evolution at seasonal scale. *Proceedings of the 5th International Conference on Coastal Dynamics*, Barcelona, Spain.

Wamsley, T. V., M. A. Cialone, K. J. Connell, and N. C. Kraus. 2006. Breach History and Susceptibility Study, South Jetty and Navigation Project, Grays Harbor, Washington. *Technical Report ERDC/CHL-TR-06-22*. U.S. Army Engineer Research and Development Center, Coastal and Hydraulics Laboratory, Vicksburg, MS. http://cirp.usace.army.mil/pubs/html/wamsley-cialone-connell-06.html, accessed 7 June 2011.

Wang, P., T. M. Beck, and T. M. Roberts 2011. Modeling regional-scale sediment transport and medium-term morphology change at a dual-inlet system examined with the Coastal Modeling System (CMS): A case study at Johns Pass and Blind Pass, West-central Florida, *Journal of Coastal Research*, Special Issue, 59, 49-60.

Watanabe, A. 1987. 3-dimensional numerical model of beach evolution. *Proceedings Coastal Sediments '87*, ASCE, 802-817.

Wu, W., S. S. Y. Wang, and Y. Jia. 2000. Non-uniform sediment transport in alluvial rivers. *Journal of Hydraulic Research*, IAHR, 38(6), 427-434.

Wu, W. 2004. Depth-averaged 2-D numerical modeling of unsteady flow and non-uniform sediment transport in open channels. *Journal of Hydraulic Engineering*, ASCE, 135(10) 1013-1024.

Wu, W. 2007. Computational River Dynamics. Taylor & Francis, 494 p.

Wu, W., A. Sánchez, and M. Zhang. 2010. An implicit 2-D depth-averaged finite volume model of flow and sediment transport in coastal waters. *Proceeding of the International Conference on Coastal Engineering*, North America, 1 Feb 2011, Available at: http://journals.tdl.org/ICCE/article/view/1431. Date accessed: June 12.

Zarillo, G. A. 2008. Geotechnical Analysis of Native Beach Samples Collected from St. Johns County, Florida. *Scientific Environmental Applications*, Inc. (S.E.A.)

Zhang, H.-M., R. W. Reynolds, and J. J. Bates. 2006. Blended and Gridded High Resolution Global Sea Surface Wind Speed and Climatology from Multiple Satellites: 1987 – Present. *American Meteorological Society 2006 Annual Meeting*, Paper #P2.23, Atlanta, GA, January 29 - February 2, 2006.

Zhu, J. 1991. A low diffusive oscillation-free convection scheme. *Communications of Applied Numerical Methods*, 7, 225-232.

Zundel, A. 2006. "Surface-water modeling system reference manual – Version 9.2," Brigham Young University Environmental Modeling Research Laboratory, Provo, UT.

Appendix A: Goodness-of-Fit Statistics

In this report, the Root Mean Squared Error (RMSE) is defined as

$$\mathrm{RMSE} = \sqrt{\left\langle (x_c - x_m)^2 \right\rangle} \tag{A1}$$

The RMSE has the same units as the measured data. Lower values of RMSE indicate a better match between measured and computed values.

The Normalized Root Mean Squared Error (NRMSE) is defined as

$$\mathrm{NRMSE} = \frac{\mathrm{RMSE}}{\mathrm{range}(x_m)} \tag{A2}$$

The NRMSE is often expressed as percent and in units of data. The measured data range $\mathrm{range}(x_m)$ can be estimated as $\max(x_m) - \min(x_m)$. Lower values of NRMSE indicate a better agreement between measured and computed values.

The Mean Absolute Error (MAE) is defined as

$$\mathrm{MAE} = \left\langle \left| x_c - x_m \right| \right\rangle \tag{A3}$$

Similarly, the Normalized Mean Absolute Error (NMAE) is given by

$$\mathrm{NMAE} = \frac{\mathrm{MAE}}{\mathrm{range}(x_m)} \tag{A4}$$

The NMAE is also expressed as percent quantity and in units of data. Smaller values of NMAE indicate a better agreement between measured and calculated values.

Correlation is a measure of the strength and direction of a linear relationship between two variables. The correlation coefficient R is defined as

$$R = \frac{\left\langle x_m x_c \right\rangle - \left\langle x_m \right\rangle \left\langle x_c \right\rangle}{\sqrt{\left\langle x_m^2 \right\rangle - \left\langle x_m \right\rangle^2} \sqrt{\left\langle x_c^2 \right\rangle - \left\langle x_c \right\rangle^2}} \tag{A5}$$

A correlation of 1 indicates a perfect one-to-one linear relationship and -1 indicates a negative relationship. The square of the correlation coefficient is the variance between two variables as described by a linear fit. The interpretation of the correlation coefficient depends on the context and purposes this statistical measure is used. In the present work, the following interpretations apply to model-to-data comparisons: $0.7<R^2<1$ for a strong correlation, $0.4<R^2<0.7$ for a medium correlation, $0.2<R^2<0.4$ for a weak or small correlation, and $R^2<0.2$ for no correlation.

The Bias is defined as

$$\text{Bias} = \left\langle x_c - x_m \right\rangle \tag{A5}$$

Positive values indicate over-prediction and negative values indicate under-prediction.

The Brier Skill Score (BSS) is defined as

$$\text{BSS} = 1 - \frac{\left\langle (x_m - x_c)^2 \right\rangle}{\left\langle (x_m - x_0)^2 \right\rangle} \tag{A6}$$

where the angled brackets indicate averaging, and subscripts *m*, *c*, and *o* indicate measured, calculated, and initial values, respectively. The BSS ranges between negative infinity and one. A BSS value of 1 indicates a perfect agreement between measured and calculated values. Scores equal to or less than 0 indicate that the mean observed value is as, or more, accurate than the calculated values. The following quantifications of agreement are associated with the BSS values: $0.8<\text{BSS}<1.0$ for excellent, $0.6<\text{BSS}<0.8$ for good, $0.3<\text{BSS}<0.6$ for reasonable, $0<\text{BSS}<0.3$ for poor, and $\text{BSS}<0.0$ indicates bad agreement.

REPORT DOCUMENTATION PAGE

Form Approved
OMB No. 0704-0188

1. REPORT DATE *(DD-MM-YYYY)*	2. REPORT TYPE	3. DATES COVERED *(From - To)*
December 2011	Report 4 of a series	

4. TITLE AND SUBTITLE
Verification and Validation of the Coastal Modeling System, Report 4, CMS-Flow: Sediment Transport and Morphology Change

5a. CONTRACT NUMBER

5b. GRANT NUMBER

5c. PROGRAM ELEMENT NUMBER

6. AUTHOR(S)

Alejandro Sánchez, Weiming Wu, Tanya Marie Beck,
Honghai Li, Julie Dean Rosati, Zeki Demirbilek, and Mitchell Brown

5d. PROJECT NUMBER

5e. TASK NUMBER

5f. WORK UNIT NUMBER

7. PERFORMING ORGANIZATION NAME(S) AND ADDRESS(ES)

U.S. Army Engineer Research and Development Center
Coastal and Hydraulics Laboratory
3909 Halls Ferry Road
Vicksburg, MS 39180-6199

8. PERFORMING ORGANIZATION REPORT NUMBER

ERDC/CHL TR-11-10

9. SPONSORING / MONITORING AGENCY NAME(S) AND ADDRESS(ES)

10. SPONSOR/MONITOR'S ACRONYM(S)

11. SPONSOR/MONITOR'S REPORT NUMBER(S)

12. DISTRIBUTION / AVAILABILITY STATEMENT
Approved for public release. Distribution is unlimited.

13. SUPPLEMENTARY NOTES

14. ABSTRACT

This is the fourth report in the series of four reports, toward the Verification, and Validation (V&V) of the Coastal Modeling System (CMS). This report contains details of a V&V study conducted to assess skills of the CMS sediment transport and morphology change for a wide range of problems encountered in coastal applications. The emphasis is on coastal inlets, navigation channels and adjacent beaches. This evaluation study began by considering simple idealized test cases for checking basic physics and computational algorithms implemented in the model. After these initial fundamental tests, the model was evaluated with several laboratory and field test cases. This report provides description of each test case, model setup, boundary conditions used in different numerical simulations, and assessment of modeling results. The report also includes major findings and provides guidance to users on how to setup and calibrate the model for practical applications of CMS-Flow for sediment transport and bed change modeling.

15. SUBJECT TERMS

Bed Change Modeling
Circulation
Coastal Modeling System
Errors
Field and laboratory tests
Model verification and validation with data
Numerical models
(see reverse)

16. SECURITY CLASSIFICATION OF:			17. LIMITATION OF ABSTRACT	18. NUMBER OF PAGES	19a. NAME OF RESPONSIBLE PERSON
a. REPORT	b. ABSTRACT	c. THIS PAGE			19b. TELEPHONE NUMBER *(include area code)*
UNCLASSIFIED	UNCLASSIFIED	UNCLASSIFIED		98	

15. SUBJECT TERMS (concluded)

Performance of models
Sediment transport
Simulations
Statistics
Verification and validation process
Waves